PREDICTION OF LIMIT CYCLE OSCILLATIONS IN PIECEWISE LINEAR SYSTEMS

A Dissertation
Presented to
The Academic Faculty

By

Yongeun Yoon

In Partial Fulfillment
of the Requirements for the Degree
Doctor of Philosophy in the
School of Aerospace Engineering

Georgia Institute of Technology

May 2019

PREDICTION OF LIMIT CYCLE OSCILLATIONS IN PIECEWISE LINEAR SYSTEMS

Approved by:

Dr. Eric N. Johnson, Co-Advisor
Department of Aerospace Engineering
Penn State University

Dr. Eric M. Feron, Co-Advisor
School of Aerospace Engineering
Georgia Institute of Technology

Dr. Jonnalagadda V. R. Prasad
School of Aerospace Engineering
Georgia Institute of Technology

Dr. Magnus B. Egerstedt
School of Electrical and Computer Engineering
Georgia Institute of Technology

Dr. Federico Bonetto
School of Mathematics
Georgia Institute of Technology

Date Approved: March 14, 2019

Just when the caterpillar thought the world was over, it became a butterfly.

To Seungjae

ACKNOWLEDGEMENTS

I would like to thank my parents and my wife for supporting me both morally and materially throughout my enduring Ph.D. days. In many aspects they provided me a shelter in which to heal my exhausted body and soul, enjoy the zest of life, and restore myself to prepare for the next rush. I would also like to thank my advisor, Professor Eric N. Johnson, for accepting me as one of his graduate students and guiding me through otherwise enigmatic world of flight dynamics and controls. He has been both a guidance light that led me to a worthy research topic, and a crossbeam that supported me to thrive on my own. Whenever my progress is stalled he pointed out the very essence of my problem to help me escape the slump.

The other one of the most memorable acknowledgements is won by Professor Eric M. Feron, my co-advisor at Georgia Tech who showed me an excellence of insight on the control theory. The support that I owe him as well is the understanding of what a Ph.D. is and what it means to me. I especially appreciate the effort of Professor Frank C. Park at Seoul National University for providing me the inspiration and motivation to study in the US as well as helping me to prepare my course of life ever since I was his graduate(master) student back in Korea. I would also like to thank Dr. Liling Ren at the United Technology for the opportunity to experience the state-of-the-art industrial regime and all kinds of benefactions he provided when we worked together.

TABLE OF CONTENTS

LIST OF TABLES

LIST OF FIGURES

NOMENCLATURE

Abbreviation	Full Meaning
DF	Describing Function
EAF	Equivalent Analytic Function
EBM	Energy Balance Method
HBM	Harmonic Balance Method
KYP	Kalman-Yakubovich-Popov
LCO	Limit-Cycle Oscillation
LMI	Linear Matrix Inequality
LTP	Linear Time Periodic
LTV	Linear Time Varying
MH96	Minneapolis-Honeywell Adaptive System
MIMO	Multi-Input Multi-Output
PCM	Primary Characteristic Multiplier
PLS	Piecewise Linear System
PN	Piecewise Nonlinearity
PR	Positive Real
SLS	Space Launching System

SYMBOLS

Symbols	Full Meaning
$\mathbf{A}_{ij}$	Coefficient matrix of the system with i-j switching combination
A,A_1,A_2	Amplitudes of input sinusoidal signal to PNs
A_{LCO}	Amplitude of limit-cycle oscillation
$\mathbf{D}(t)$	Jacobian matrix of a nonlinear system evaluated at its periodic solution.
$EAF(g(u))$	Equivalent analytic function of a piecewise nonlinearity $g(u)$
$\boldsymbol{\eta}(t)$	Periodic solution of a nonlinear system
$\mathbf{F}$	Floquet exponent matrix
$\mathcal{F}$	The F equation
$g(u)$	A piecewise nonlinearity with input u
γ	A large positive real number in the equivalent analytic functions
$h(u)$	Spatial derivative of a piecewise nonlinearity $g(u)$
$\mathbf{H}(t)$	Time-periodic matrix of a linear time periodic system.
k_c	Critical gain
k_p	Pilot gain
$N(A,\omega)$	Describing function of input sinusoidal signal with amplitude A and frequency ω
$\mathbf{P}(t)$	Fundamental matrix of a linear time periodic system.
$\boldsymbol{\phi}(\mathbf{y})$	Nonlinear input to Lur'e type system
$\boldsymbol{\Phi}(t,t_0)$	State transition matrix of a linear time varying system from time t_0 to t
$\mathcal{S}$	The S equation
t_{ij}	Switching time of the system-based index of i-j switching combination
T	Potential period of limit-cycle oscillation
T_{LCO}	Period of limit-cycle oscillation
τ_p	Pilot time constant
τ_i	ith switching time of the phase-driven index
ω_{LCO}	Limit-cycle oscillation frequency

SUMMARY

The mathematical model of most mechanical and electrical systems involves the piecewise linear system, which consists of a linear part and piecewise nonlinearities (PN) or sector-bounded nonlinearities such as saturation, backlash, dead-zone, etc. Many piecewise linear systems inherently possess periodic orbits called a limit-cycle oscillation (LCO) as one of its solutions, which can seriously undermine the system performance depending on its amplitude and frequency. Therefore, how to predict LCO and its parameters, the frequency and the amplitude, is one of the primary concerns for control and system engineers.

To cope with the adverse LCO of the system we need to identify and change the LCO parameters. On top of the well-known piecewise linear system analysis we apply Floquet theory to identify LCO parameters. The introduction of Floquet theory to piecewise linear systems is allowed through the transformation of PNs into corresponding equivalent analytic functions. Together with switching functions based on the exact switching order, the Floquet theory leads to the verification of the stability of LCO as well as the identification of LCO parameters. In addition, the basic approach used to identify the LCO parameters also enables us to determine the least upper bound of the system gain that does not cause any LCO. Furthermore, with the design of appropriate lead compensators we can increase the LCO frequency up to a higher band so that the LCO amplitude would decrease to a desirable level. We take an example of a simple rate saturated feedback system common in aircraft flight control systems to demonstrate the effectiveness of the framework presented above. Also, additional example of the YF-12 flight control system illustrates that this framework works well even in control systems with multiple PNs.

CHAPTER 1
INTRODUCTION

Limit cycle oscillations (LCOs) in adaptive flight control systems has been important since the application of Minneapolis-Honeywell Adaptive System (MH96) to the space launching system (SLS) [1]. MH96 dates back to the 1960's when it was providing high-gain flight controls to the experimental aircraft X15, in which it was designed to avoid a specific band of frequency and make the loop gain as high as possible [2]. The X-15 was an experimental aircraft tested by the US Air Force back in the 1960s, performing 199 successful flight tests. Unfortunately, on November 15, 1967, it ran into a fatal incident that led to a crash. The investigation of the crash of X15 in the 1960's and 1970's tentatively concluded that MH96, the adaptive control law, was partly responsible for the severe LCO that the aircraft showed during its crash, and recent analysis of the accident demonstrated the detailed mechanisms that led X15 to the severe LCO [2], [3]. From the reflection of the MH96, the adaptive law for SLS is designed to tackle the severe LCO issue by incorporating a spectral damper that adjusts the adaptive gain depending on the input frequency band [1]. After all, high gain adaptive control law relies on the presence of LCO.

A limit cycle is defined as an isolated, periodic solution present in the nonlinear system. Thus LCO is a characteristic of nonlinear systems including piecewise linear systems–the systems of interest in this research. A piecewise linear system is a linear system with piecewise nonlinearities (PN) such as a relay, saturation, dead-band, backlash, or any combination of them which are characterized by the sector-bounded linear output. Including the flight control system of the X-15 and the SLS, the exact mathematical model of most mechanical and/or electrical systems involves the piecewise linear system [4]. In the perspective of the control systems design, PN plays an important role in making the system nonlinear and can cause an LCO, especially when we apply high gain to the system. Since

the existence of LCO is an important constraint on raising gains in the system, the need to predict the LCO has entailed a myriad of studies such as describing function (DF) analysis, piecewise linear systems approach, harmonic balance method (HBM) or energy balance method (EBM), and so on [5, 6, 7, 8].

1.1 Previous Work

The analysis of LCO should focus on the identification of the amplitude, frequency, and the stability of any LCO. DF analysis provides a simplified and reasonable approximation of the LCO parameters for the linear systems with PNs [5]. By approximating the input and output signal as a unimodal sinusoidal form, DF of a PN is modeled as a phasor representation to enable the linear steady state frequency response analysis. The simplicity and accuracy of DF analysis has entailed many studies on the piecewise linear systems including the flight control systems involving the LCO analysis [9, 10, 11, 12, 13]. If, however, the frequency of LCO turns out to be relatively low compared to the system bandwidth of the linear part, or if there are more than two PNs in parallel, then the accuracy of the LCO parameter prediction significantly decreases. This lack of accuracy stems from the violation of the two important assumptions on which DF analysis relies.

- Linear transfer functions in the loop work as low-pass filters such that the second or higher order harmonic terms of the Fourier series of the output of DF are ignored
- The input signal to the DF is a unimodal symmetric sinusoidal function

If the system bandwidth is low compared to the LCO frequency then the linear system may not reject the component of higher order harmonics of the LCO signal and this in turn leads to inaccurate LCO predictions. This inaccuracy is more likely to appear in the system with multiple PNs because the bandwidth of each linear transfer function near each PN can be different, while there is only one LCO frequency to be identified.

By piecewise linear systems approach, we can predict the exact frequency of LCO along

with the stability of LCO of the piecewise system in which the system dynamics are divided into a finite number of linear affine systems by the PNs [6, 14]. Assuming the unimodal sinusoidal signal as an input to a PN, this approach calculates half the LCO period based on the switching time between surfaces defined by the PN. The stability of the LCO is also verified by the surface Lyapunov function, and in the example of a linear system with a hysteresis relay, the effectiveness of this framework is demonstrated [14]. However, we virtually cannot apply this approach to the system with multiple PNs, because the switching order between surfaces defined by each PN is, unlike the example of a single hysteresis relay, generally not clear. Therefore, the clarification of the switching order needs to be found in order to successfully apply the piecewise linear approach to the LCO prediction of a general piecewise linear system.

Analysis of LCO for more general nonlinear systems also led to methods that identify and describe the LCO. Harmonic balance method (HBM) and energy balance method (EBM) presents the LCO amplitude-period relationship in a simple and accurate framework [7, 8, 15, 16]. With HBM we can incorporate more accurate modeling including higher order harmonic terms for the periodic solution of LCO. In contrast to EBM which is restricted in terms of the state space dimension, HBM is applicable to general n-dimensional state space [7, 15]. But HBM along with EBM are applicable only to conservative systems, which is not always the case for piecewise linear systems. Furthermore, the solution for each coefficients of harmonic terms are not necessarily feasible and HBM lacks ability to analyze the stability of LCO. Besides HBM and EBM, we also have research studies on the center manifold theorem and its branches for the analysis of the LCO of general nonlinear system of up to three dimensional state space, which yield excellent analytic results only if calculation of Lyapunov exponent is feasible [4, 17, 18].

1.2 Contributions

The main contribution of this thesis is summarized as the establishment of a new framework for LCO analysis in piecewise linear systems. To be more specific, they are the introduction of Floquet theory to piecewise linear systems, the invention of the algorithm to clarify switching order, and the validation of the framework by applying it to existing control systems. The details are as follows in the itemized list.

- Equivalent Analytic Functions (EAF) is designed corresponding to common PNs. The piecewise convergence of EAF to the original PN function is proven.
- The Perturbed Linear Time Periodic (LTP) system evaluated at a periodic solution of piecewise linear systems is established so that Floquet theory may be applied.
- The Primary Characteristic Multiplier (PCM) of the perturbed LTP system is calculated leading to the first necessary condition to predict an LCO, or the $\mathcal{F}$ equation. The numerical methods to calculate the PCM as a state transition matrix of a general LTP are adopted from Friedman's work [19].
- A framework to analyze the switching order of piecewise linear systems is organized. This involves the classification of switching configurations, switching time identification, and the establishment of switching equation.
- The absolute stability of every Lur'e type system corresponding to each switching configuration is proven based on Popov Criteria and KYP lemma [20, 21]. Showing that at least one of the systems is not absolutely stable leads to the construction of a switching equation.
- Switching equations are derived and are applied to the second necessary condition to predict an LCO, or the $\mathcal{S}$ equation.

- From the $\mathcal{F}$ and the $\mathcal{S}$ equations, LCO parameters of a practical system (YF-12) are predicted. Also, the system parameters such as upper limit of system gain and lead/lag compensator paramters are determined with the $\mathcal{F}$ and the $\mathcal{S}$ equations.

- LCO parameters are predicted based on the DF analysis of the piecewise linear system with two PNs.

1.3 Outline of Dissertation

In the following chapter we introduce the background necessary to describe the framework to be presented successively. They are basic concepts on DF, linear time varying system, Floquet theory, and absolute stability of Lur'e type system. Linear time varying systems are a background for Floquet theory, and the absolute stability of Lur'e type system is needed for eliminating switching configurations in which an LCO does not exist. In chapter three, the preparatory works to apply the Floquet theory and the nature of error propagation of numerical integration are introduced. How and why EAF can represent a PN in a piecewise linear system and how it can be incorporated into the Floquet analysis will also be discussed. In addition, the fact that the numerical integration cannot be fully trusted in the LCO analysis will be demonstrated. In chapter four we present the concrete framework to analyze the LCO of piecewise linear system followed by the demonstration with the example of a simple rate saturated loop. We show how the LCO parameters for the rate saturated system are determined and further illustrate how to find out the upper bound of system gain that does not create any LCO in the system. In addition, we show that the adverse oscillation of system output can be significantly attenuated by changing the LCO parameters with the design of a proper lead compensator. The next chapter is about the second example, this time a piecewise linear system with two nonlinearities based on the YF-12 flight control system. In this chapter, a more sophisticated approach will be demonstrated, especially in the analysis of a non-trivial switching order, and how the assumption of multi-modal sinusoidal form for the LCO solution makes a difference in the results. In

the final chapter we present conclusive remarks along with suggestions for future studies.

CHAPTER 2

BACKGROUND

The purpose of this chapter is to introduce some mathematical principles necessary to understand the main results of this research. The discussions in this chapter include the describing function (DF) analysis, the linear time varying system, Floquet theory, and absolute stability for Lur'e type system.

2.1 Describing Function (DF)

Even if we have a PN within an otherwise linear system we still have a way to analyze the system in the framework of the linear control theory, but only if we can approximate the PN in a linear transfer function–DF. A DF is a linearized representation of such nonlinearities subjected to a sinusoidal input. Hence the full name for DF is sinusoidal-input describing function, but it is typically just called as DF. In this section we present the DFs corresponding to PNs such as a relay, saturation, and dead-band.

Definition 2.1.1. Describing function (DF) [5]

The DF of a nonlinearity is the phasor representation of the ratio of the output component at frequency ω to that of the input component at frequency ω, of the nonlinearity.

We usually want the DF associated with a sinusoidal-input DF because we want to

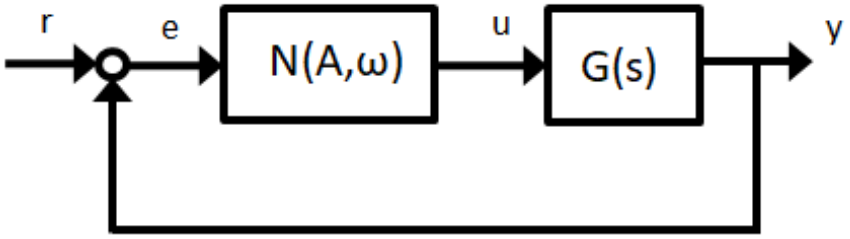

Figure 2.1: A simple feedback loop with a DF N(A,ω).

analyze the frequency response. Other types of DFs such as random-input DF and two sinusoidal-input DF are also available [5].

The expression for DF is derived from the Fourier series form of the output of the DF. Given the input $e(t)$ and output $u(t)$ of the DF, respectively, we assume

$$\begin{aligned} e(t) &= A\sin(\omega t) \\ u(t) &= \frac{a_0}{2} + \sum_{n=1}^{\infty} \big(a_n \cos(n\omega t) + b_n \sin(n\omega t)\big) \end{aligned} \tag{2.1}$$

Since we have a linear transfer function $G(s)$ shown in Figure 2.1., we assume that $G(s)$ functions as a linear low-pass filter that rejects all the higher order harmonic terms except the fundamental one. In addition, by the symmetric property of the unimodal sinusoidal signal, a_0 is equal to zero. Thus, the output $u(t)$ is approximated as follows.

$$u(t) = a_1 \cos(\omega t) + b_1 \sin(\omega t) \tag{2.2}$$

where

$$a_1 = \frac{2}{T}\int_0^T u(\tau)\cos(\omega\tau)\,d\tau, \qquad b_1 = \frac{2}{T}\int_0^T u(\tau)\sin(\omega\tau)\,d\tau \tag{2.3}$$

where $T = \frac{2\pi}{\omega}$. Now, taking the Laplace transform of Equation 2.1 and 2.2 yields

$$N(A,\omega) = \frac{U(i\omega)}{E(i\omega)} = \frac{\frac{a_1 s}{s^2+\omega^2} + \frac{b_1\omega}{s^2+\omega^2}}{\frac{A\omega}{s^2+\omega^2}}\Big|_{s=i\omega} = \frac{1}{A}\big(b_1 + a_1 i\big) \tag{2.4}$$

with the coefficients a_1 and b_1 in Equation 2.3. We may use DF as if it is a linear transfer function based on the following assumptions.

- $G(i\omega)$ functions as a low-pass filter such that the second or higher order harmonic coefficients of the Fourier series of the output ($u(t)$) ot DF are ignored
- the input ($e(t)$) to the DF is a sinusoidal function

the DFs of some common PNs are listed in Table 2.1. Note that all the DFs listed in

this table are just scalar value, while the actual output is not a sinusoidal signal at all, if the input amplitude is more than the saturating quantity. But the argument on the DFs is justified because of the first assumption listed just above, even though the output signal of a DF is not of sinusoidal shape the overall influence of the DF output is equivalent to an otherwise sinusoidal signal with the same amplitude and frequency, because higher order harmonics components are rejected by the following linear transfer functions with sufficient level of bandwidth.

Table 2.1: List of DFs for common PNs [5].

PN	DF (A as the amplitude of the input sinusoidal signal u)
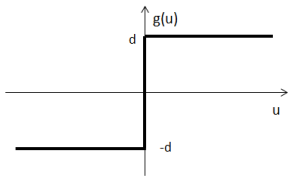 Simple relay	$N = \begin{cases} \frac{4d}{\pi A}, & A > d \\ 1, & A \leq d \end{cases}$
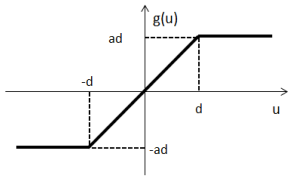 Saturation	$N = \begin{cases} \frac{2a}{\pi}\left[\sin^{-1}\left(\frac{d}{A}\right) + \frac{d}{A}\sqrt{1-(\frac{d}{A})^2}\right], & A > d \\ 1, & A \leq d \end{cases}$
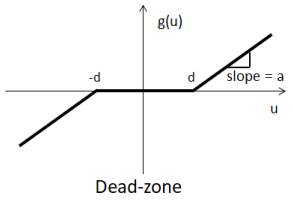 Dead-zone	$N = \begin{cases} a\left(1 - \frac{2}{\pi}\left[\sin^{-1}\left(\frac{d}{A}\right) + \frac{d}{A}\sqrt{1-(\frac{d}{A})^2}\right]\right), & A > d \\ 0, & A \leq d \end{cases}$

2.2 Linear Time Varying System (LTV)

A linear time varying (LTV) system is a linear system of which the system matrix is a function of time. Given the state variables $\mathbf{x}(t) \in \mathbb{R}^n$ and the system input $\mathbf{u}(t) \in \mathbb{R}^m$, the

general state space realization of the LTV system is

$$\begin{aligned} \dot{\mathbf{x}}(t) &= \mathbf{A}(t)\mathbf{x}(t) + \mathbf{B}(t)\mathbf{u}(t), \qquad \mathbf{x} \in \mathbb{R}^n \\ \mathbf{y}(t) &= \mathbf{C}(t)\mathbf{x}(t) \end{aligned} \tag{2.5}$$

but in this chapter we focus on a simpler form of the LTV system

$$\dot{\mathbf{x}}(t) = \mathbf{A}(t)\mathbf{x}(t) \tag{2.6}$$

Given the initial condition $\mathbf{x}_0 = \mathbf{x}(0)$, the solution to the LTV system of Equation (2.6) is

$$\mathbf{x}(t) = \mathbf{\Phi}(t, t_0)\mathbf{x}_0 \tag{2.7}$$

where $\mathbf{\Phi}(t, t_0)$ is the state transition matrix from time t_0 to t, of which a general solution is the Peano-Baker series

$$\mathbf{\Phi}(t, t_0) = I + \int_{t_0}^{t} \mathbf{A}(\sigma_1)d\sigma_1 + \int_{t_0}^{t} \mathbf{A}(\sigma_1) \int_{t_0}^{\sigma_1} \mathbf{A}(\sigma_2)d\sigma_2 d\sigma_1 + \dots \tag{2.8}$$

$\mathbf{\Phi}(t, t_0)$ can also be decomposed as

$$\mathbf{\Phi}(t, t_0) = \mathbf{P}(t)\mathbf{P}^{-1}(t_0)$$

where $\mathbf{P}(t)$ is identified as a fundamental matrix of the system in Equation 2.6, and is defined as the collection of the solution columns ($\boldsymbol{\phi}_i(t)$) of the following differential equations.

$$\mathbf{P}(t) = \begin{bmatrix} | & | & & | \\ \boldsymbol{\phi}_1(t) & \boldsymbol{\phi}_2(t) & \dots & \boldsymbol{\phi}_n(t) \\ | & | & & | \end{bmatrix}$$

where

$$\dot{\boldsymbol{\phi}}_i(t) = \mathbf{A}(t)\boldsymbol{\phi}_i(t), \qquad i = 1, 2, 3, \ldots, n \tag{2.9}$$

thus

$$\dot{\mathbf{P}}(t) = \mathbf{A}(t)\mathbf{P}(t) \tag{2.10}$$

The state transition matrix has the following properties :

1. $\boldsymbol{\Phi}(t, t) = \mathbf{I}$
2. $\boldsymbol{\Phi}^{-1}(t, \tau) = \boldsymbol{\Phi}(\tau, t)$
3. $\boldsymbol{\Phi}(t_1, t_2) = \boldsymbol{\Phi}(t_1, t_0)\boldsymbol{\Phi}(t_0, t_2)$
4. $\frac{d}{dt}\boldsymbol{\Phi}(t, \tau) = \mathbf{A}(t)\boldsymbol{\Phi}(t, \tau)$

with their corresponding proofs

1. $\boldsymbol{\Phi}(t, t) = \mathbf{P}(t)\mathbf{P}^{-1}(t) = \mathbf{I}$
2. $\boldsymbol{\Phi}^{-1}(t, \tau) = [\mathbf{P}(t)\mathbf{P}^{-1}(\tau)]^{-1} = \mathbf{P}(\tau)\mathbf{P}^{-1}(t) = \boldsymbol{\Phi}(\tau, t)$
3. $\boldsymbol{\Phi}(t_1, t_2) = \mathbf{P}(t_1)\mathbf{P}^{-1}(t_0)\mathbf{P}(t_0)\mathbf{P}^{-1}(t_2) = \boldsymbol{\Phi}(t_1, t_0)\boldsymbol{\Phi}(t_0, t_2)$
4. $\frac{d}{dt}\boldsymbol{\Phi}(t, \tau) = \dot{P}(t)\mathbf{P}^{-1}(\tau) = \mathbf{A}(t)\mathbf{P}(t)\mathbf{P}^{-1}(\tau) = \mathbf{A}(t)\boldsymbol{\Phi}(t, \tau)$

Finally, the complete solution to the system of Equation 2.5 is

$$\begin{aligned} \mathbf{x}(t) &= \boldsymbol{\Phi}(t, t_0)\mathbf{x}(t_0) + \int_{t_0}^{t} \boldsymbol{\Phi}(t, \tau)\mathbf{B}(\tau)\mathbf{u}(\tau)\, d\tau \\ \mathbf{y}(t) &= \mathbf{C}(t)\boldsymbol{\Phi}(t, t_0)\mathbf{x}(t_0) + \int_{t_0}^{t} \mathbf{C}(t)\boldsymbol{\Phi}(t, \tau)\mathbf{B}(\tau)\mathbf{u}(\tau)\, d\tau \end{aligned} \tag{2.11}$$

2.3 Floquet Theory

G. Floquet developed a classical result in the analysis of a linear time-periodic (LTP) system in 1883 and this result still remains one of the most important theorems in the area

of LTP systems [22]. An LTP system refers to an LTV system in which the coefficient matrix $\mathbf{A}(t)$ is a time-periodic one, i.e., $\mathbf{A}(t) = \mathbf{A}(t+T)$ with the minimum positive real number T. The essence of Floquet theory is that the fundamental matrix of an LTP system is decomposed as a product of a time-periodic matrix and a matrix exponential, where the latter's eigenvalues reveal characteristics of the periodic solution.

Theorem 2.3.1. [23] In an LTP system whose state space representation is Equation 2.5 with the period of the coefficient matrix $\mathbf{A}(t)$ T, the fundamental matrix $\mathbf{P}(t)$ of this system is decomposed as

$$\mathbf{P}(t) = \mathbf{H}(t)e^{\mathbf{F}t} \tag{2.12}$$

where $\mathbf{H}(t)$ is a T-periodic matrix. Furthermore, the following holds for the state transition matrix of this system $\mathbf{\Phi}(t, t_0)$.

$$\mathbf{\Phi}(T, 0) = e^{\mathbf{F}T} \tag{2.13}$$

Proof. of Theorem 2.3.1

(for the proof of Equation 2.12, refer to the proof of Theorem 3.2.1 in [23])

The proof of Equation 2.13 comes from the basic properties of the state transition matrix introduced above. Without loss of generality, we can choose a solution set of Equation 2.9 $\{\boldsymbol{\phi}_i, i = 1, 2, \ldots, n\}$ such that the initial conditions are $\boldsymbol{\phi}_i(0) = \mathbf{e}_i$, $i = 1, 2, \ldots, n$. Then we obtain

$$\mathbf{P}(0) = \mathbf{I} \tag{2.14}$$

Thus from Equation 2.12,

$$\mathbf{H}(0) = \mathbf{P}(0) = \mathbf{I} \tag{2.15}$$

Finally,

$$\mathbf{\Phi}(T, 0) = \mathbf{P}(T)\mathbf{P}^{-1}(0) = \mathbf{P}(T) = \mathbf{H}(T)e^{\mathbf{F}T} = \mathbf{H}(0)e^{\mathbf{F}T} = e^{\mathbf{F}T} \tag{2.16}$$

□

The matrix $\mathbf{\Phi}(T,0) = e^{\mathbf{F}T}$ is called as the monodromy matrix of the LTP system in Equation 2.5.

Definition 2.3.1. Characteristic multiplier [24]
The characteristic multipliers of an LTP system are the eigenvalues of the monodromy matrix of the LTP system.

The next theorem tells us about the eigenvalues of the monodromy matrix in relation to the properties of the periodic solution of nonlinear systems. Consider an autonomous nonlinear system

$$\dot{\mathbf{x}} = \mathbf{f}(\mathbf{x}), \qquad \mathbf{x} \in \mathbb{R}^n \tag{2.17}$$

Where $\mathbf{f} : \mathbb{R}^n \mapsto \mathbb{R}^n$, $\mathbf{f} \in C^1$ and the autonomous system above has a periodic solution of the least period T. Now we linearize the system above around its periodic solution $\boldsymbol{\eta}(t)$.

$$\dot{\delta\mathbf{x}}(t) = \mathbf{D}(t)\delta\mathbf{x}(t) \tag{2.18}$$

where $\mathbf{D}(t) = \frac{d\mathbf{f}}{d\mathbf{x}}|_{\mathbf{x}=\boldsymbol{\eta}(t)}$ is a Jacobian matrix of the system of Equation 2.17 evaluated at the periodic solution $\boldsymbol{\eta}(t)$. Since $\boldsymbol{\eta}(t)$ is a periodic solution with period T, $\mathbf{D}(t)$ is a T-periodic matrix thus the system of Equation 2.18 is an LTP system. Then the following holds about the LTP system.

Theorem 2.3.2. [24] One of the characteristic multipliers of the LTP system of Equation 2.18 is unity. In addition, if all of the rest of the characteristic multipliers reside within the unit circle in the complex plane, the periodic solution $\boldsymbol{\eta}(t)$ of the system of Equation 2.17 is a stable limit cycle. Otherwise, $\boldsymbol{\eta}(t)$ is an unstable limit cycle.

Proof. of theorem 2.3.2
refer to the proof of Lemma 10.2 and Theorem 11.1 of [24]. □

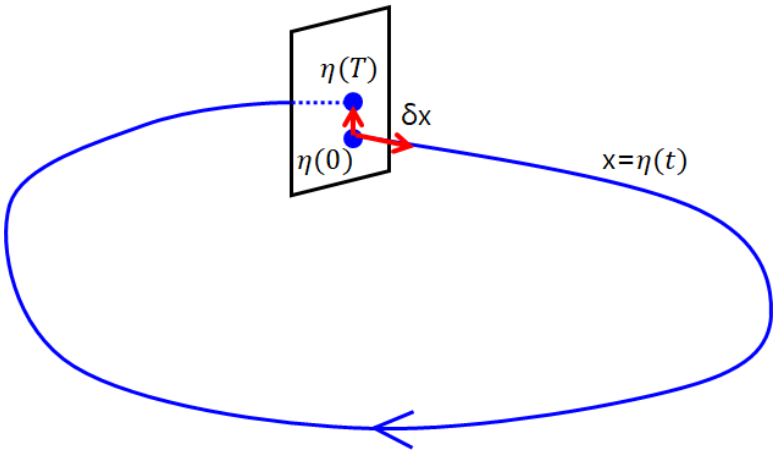

Figure 2.2: A periodic solution $\boldsymbol{\eta}(t)$ passing through a hyperplane.

When one of the characteristic multipliers of the system in Equation 2.18 is unity this implies that any perturbation along the direction of the periodic solution $\boldsymbol{\eta}(t)$ is the same in magnitude exactly after one (or other multiple integer) period of time. In addition, the other characteristic multipliers are the eigenvalues of the Poincaré map in the hyperplane on which $\boldsymbol{\eta}(t)$ passes through periodically, shown in Figure 2.2

2.4 Absolute Stability of Lur'e Type System

The type of piecewise linear system of our interest is also called a Lur'e type system and is defined as below [25].

$$\begin{aligned} \dot{\mathbf{x}} &= \mathbf{A}\mathbf{x} + \mathbf{B}\boldsymbol{\phi}(\mathbf{y}) \\ \mathbf{y} &= \mathbf{C}\mathbf{x} \end{aligned} \tag{2.19}$$

where $\mathbf{x} \in \mathbb{R}^n$, $\mathbf{u} \in \mathbb{R}^m$, and $\boldsymbol{\phi} = [\phi_1, \phi_2, \ldots, \phi_m]^T$, with $\phi_i = \phi_i(y_i) = \phi_i(\mathbf{C}_i\mathbf{x})$, shown in the Figure 2.3. m is the number of the PNs. The nonlinear input function $\boldsymbol{\phi}$ is a certain type of PN, and we say that each PN $\phi_i(y_i)$ is in sector $[0, k_i]$ if it is bounded within the sector bounded by y_i axis and the line of slope $k > 0$, shown in Figure 2.4. In short,

$$0 \leq y_i\phi_i(y_i) \leq k_i y_i^2, \qquad i = 1, 2, \ldots, m \tag{2.20}$$

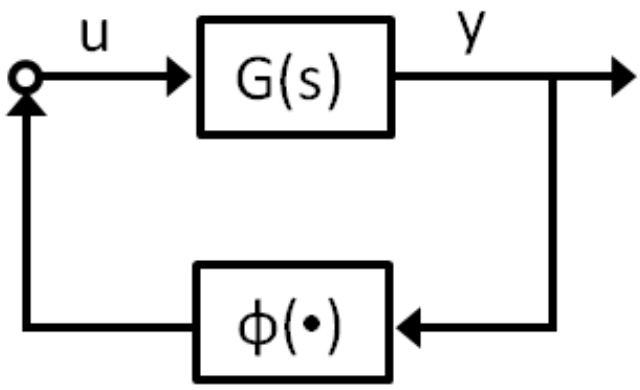

Figure 2.3: A Lur'e system.

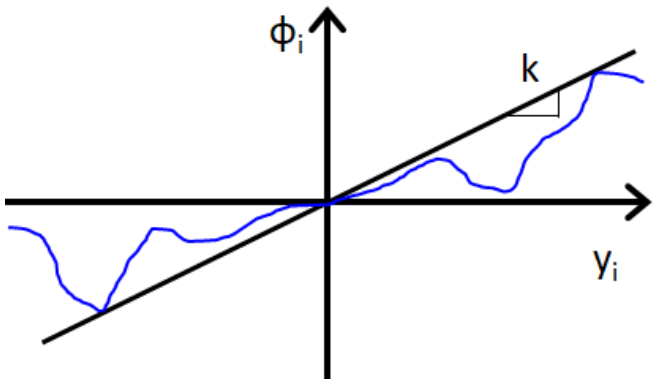

Figure 2.4: A PN of which the output is bounded by a line of slope k.

The notion of absolute stability is introduced to describe the stability of Lur'e type systems.

Definition 2.4.1. Absolute Stability [26, 27]

The system of Equation 2.19 is said to be absolutely stable within the sector $[0, k_i]$ if the system is globally asymptotically stable about its equilibrium $\mathbf{x}_e = 0$.

We can check the absolute stability of the system 2.19 with Popov's criterion as below [20]:

Popov Criterion

System 2.19 in which the nonlinearity is in sector [0,k] is absolutely stable, if this system $G(s) \sim \left[\begin{array}{c|c} \mathbf{A} & \mathbf{B} \\ \hline \mathbf{C} & \mathbf{0} \end{array}\right]$ is asymptotically stable (necessary condition) and if there exists a real number α such that

$$M(i\omega) = Re\big[(1 + i\omega\alpha)G(i\omega)\big] + \frac{1}{k} > 0 \qquad \forall\omega \geq 0 \tag{2.21}$$

In particular, the condition of Equation 2.21 is equivalent to the statement "the transfer function $(1 + i\omega\alpha)G(i\omega) + \frac{1}{k}$ is positive real (PR)". In case there are multiple (m) PNs Equation 2.21 becomes

$$\mathbf{M}(i\omega) = Re\big[(\mathbf{I} + i\omega\mathbf{N})\mathbf{G}(i\omega)\big] + \mathbf{K}^{-1} > 0 \qquad \forall\omega \geq 0 \tag{2.22}$$

where $\mathbf{I} \in \mathbb{R}^m$ is an m-dimensional identity matrix, $\mathbf{N} = \text{diag}(\alpha_1, \alpha_2, \ldots, \alpha_m) \in \mathbb{R}^m$ with $\alpha_i > 0$, $i = 1, 2, \ldots, m$, $\mathbf{G} \in \mathbb{R}^m$ a MIMO transfer function of dimension m, and $\mathbf{K} = \text{diag}(k_1, k_2, \ldots, k_m) \in \mathbb{R}^m$ with k_i, $i = 1, 2, \ldots, m$ in Equation 2.20. The inequality in Equation 2.22 implies entry-wise inequality. Together with Popov's criterion, Kalman-Yakubovich-Popov lemma (KYP lemma) is an essential building block for the absolute stability of Lur'e type systems.

Lemma 2.4.1. *Kalman–Yakubovich–Popov lemma (KYP lemma) [21]*

Let a system $\boldsymbol{G}(s) \sim \left[\begin{array}{c|c} \boldsymbol{A} & \boldsymbol{B} \\ \hline \boldsymbol{C} & \boldsymbol{D} \end{array}\right]$ *is controllable and observable. Then its transfer function* $\boldsymbol{G}(s) = \boldsymbol{C}(s\boldsymbol{I} - \boldsymbol{A})^{-1}\boldsymbol{B} + \boldsymbol{D}$ *is positive real (PR) if and only if there exists a symmetric, positive definite matrix* $\boldsymbol{P}$ *such that*

$$\begin{aligned} \boldsymbol{A}^T\boldsymbol{P} + \boldsymbol{P}\boldsymbol{A} &= -\boldsymbol{L}\boldsymbol{L}^T \\ \boldsymbol{P}\boldsymbol{B} - \boldsymbol{C}^T &= -\boldsymbol{L}\boldsymbol{W} \\ \boldsymbol{D} + \boldsymbol{D}^T &= \boldsymbol{W}^T\boldsymbol{W} \end{aligned} \tag{2.23}$$

where $\boldsymbol{A}$*,* $\boldsymbol{B}$*,* $\boldsymbol{C}$*,* $\boldsymbol{D}$*,* $\boldsymbol{P}$*,* $\boldsymbol{L}$*, and* $\boldsymbol{W}$ *are of appropriate dimensions.*

In other words, if we can find a positive definite matrix $\mathbf{P}$ that satisfies 2.23, the absolute stability of the system 2.19 is guaranteed by the KYP lemma and the Popov criterion. Proof of the absolute stability of the system 2.19 based on the Popov criterion is in references and begins with the construction of so-called a Lur'e–Postnikov Lyapunov function [28, 29].

$$V(\mathbf{x}) = \frac{1}{2}\mathbf{x}^T\mathbf{P}\mathbf{x} + \sum_{i=1}^{m}\alpha_i \int_0^{\mathbf{C}_i\mathbf{x}} \phi_i(y)dy \tag{2.24}$$

where $dim(y) = dim(u) = m$, and $\alpha_i > 0$, $i = 1, 2, \ldots, m$. In addition, each of ϕ_i is in sector $[0, k_i]$. One aspect that we need to be cautious of is that the state space representation in Equation 2.23 is from $\mathbf{M}(i\omega)$, the transfer function of Equation 2.22, not from $\mathbf{G}(i\omega)$. This stems from the course of proof on the absolute stability when dealing with the quadratic part of the Lur'e–Postnikov Lyapunov function above. Assuming that $\mathbf{y}_1$ and $\mathbf{u}_1$ are the output and the input of $\mathbf{M}(s)$ in Equation 2.22, respectively,

$$\begin{aligned} \mathbf{y}_1 &= \mathbf{K}^{-1}\mathbf{u}_1 + \big[\mathbf{G}(s) + \mathbf{N}s\mathbf{G}(s)\big]\mathbf{u}_1 \\ &= \mathbf{K}^{-1}\mathbf{u}_1 + \mathbf{C}\mathbf{x} + \mathbf{N}\mathbf{C}\mathbf{A}\mathbf{x} + \mathbf{N}\mathbf{C}(-\mathbf{B})\mathbf{u}_1 \\ &= (\mathbf{C} + \mathbf{N}\mathbf{C}\mathbf{A})\mathbf{x} + (\mathbf{K}^{-1} - \mathbf{N}\mathbf{C}\mathbf{B})\mathbf{u}_1 \end{aligned}$$

Therefore,

$$\mathbf{M}(s) \sim \left[\begin{array}{c|c} \mathbf{A}_1 & \mathbf{B}_1 \\ \hline \mathbf{C}_1 & \mathbf{D}_1 \end{array}\right] \tag{2.25}$$

where $\mathbf{A}_1 = \mathbf{A}$, $\mathbf{B}_1 = -\mathbf{B}$, $\mathbf{C}_1 = \mathbf{C} + \mathbf{NCA}$ and $\mathbf{D}_1 = \mathbf{K}^{-1} - \mathbf{NCB}$. Hence KYP lemma needs to be in the following form.

$$\begin{aligned} \mathbf{A}_1^T\mathbf{P} + \mathbf{P}\mathbf{A}_1 &= -\mathbf{L}\mathbf{L}^T \\ \mathbf{P}\mathbf{B}_1 - \mathbf{C}_1^T &= -\mathbf{L}\mathbf{W} \\ \mathbf{D}_1 + \mathbf{D}_1^T &= \mathbf{W}^T\mathbf{W} \end{aligned} \tag{2.26}$$

with $\mathbf{A}_1$, $\mathbf{B}_1$, $\mathbf{C}_1$, and $\mathbf{D}_1$ as in Equation 2.25. Furthermore, if the matrix $\mathbf{P}$ satisfies

$$\mathbf{A}_1^T\mathbf{P} + \mathbf{P}\mathbf{A}_1 = -\mathbf{L}\mathbf{L}^T - \beta\mathbf{L}\mathbf{L}^T \tag{2.27}$$

with some $\beta > 0$, then the existence of the solution to $\mathbf{P}$ proves the absolute stability.

CHAPTER 3
PRELIMINARY WORKS

The two major building blocks of the framework to analyze LCO introduced in this thesis are Floquet theory and piecewise linear analysis. However, they are applicable only if preparatory works are ready to support the deployment of the framework. Piecewise nonlinearities (PN) need to be expressed in a function that is differentiable, because Floquet theory is available only for the nonlinear system of which the equation of motion is differentiable. In addition, introducing previous approaches on piecewise linear analysis helps to organize the switching order between a finite number of linear affine systems that constitute the whole piecewise linear system. Finally, we need to narrow down the approximate range of LCO parameters with preliminary LCO analysis with DF analysis and numerical integration.

3.1 DF Analysis

As was discussed in the previous chapter, DF analysis is all about approximating PNs into a phasor representation similar to a linear transfer function under certain assumptions. In other words, we can apply the linear control system theory to the analysis of the linear systems with PNs based on the DF analysis. With a single PN within the loop the analysis is useful. In addition, in the presence of multiple PNs within the loop, if the loop consists of a single feedback DF, analysis yields an approximate prediction of LCO parameters. The most common method is to interpret the system as a quasi-linear one and analyze the eigenvalues of the system. Just as in the linear systems, if the eigenvalue of the quasi-linear system is purely imaginary the entire state space oscillates. Typically we do not call the oscillations in linear systems an LCO, but in the case of the quasi-linear system we can identify such oscillations as an LCO if appropriate analysis is done regarding the stability

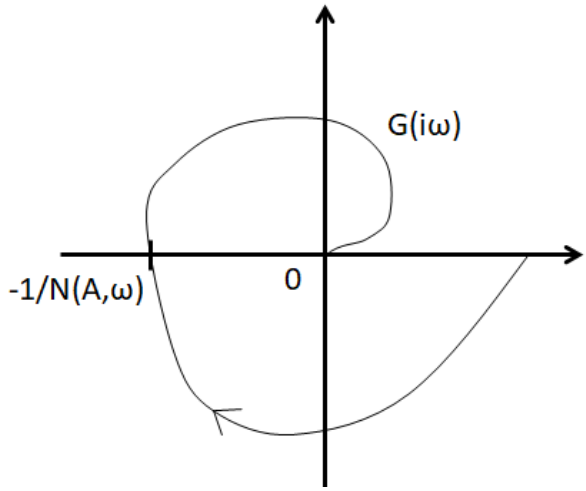

Figure 3.1: Nyquist plot of the system in Figure 2.1.

of LCO.

3.1.1 A Single PN

Analyzing a single PN within an otherwise linear control loop involves a simple test that pertains to the marginal stability of a linear feedback system, shown in Figure 2.1. Given the fact that a DF $N(A,\omega)$ behaves just like a linear transfer function, this system is predicted to have an oscillating behavior when the crossover point of the Nyquist plot of $G(s)$ in the negative real axis is $-\frac{1}{N(A,\omega)}$ as shown in Figure 3.1. This implies that

$$1 + N(A,\omega)G(i\omega) = 0 \tag{3.1}$$

From Equation 3.1, we extract the frequency ω_{LCO} and the amplitude A_{LCO} of LCO.

$$\arg(G(i\omega_{LCO})) = -\pi, \qquad A_{LCO} = |G(i\omega_{LCO})| = \frac{1}{|N(A,\omega_{LCO})|} \tag{3.2}$$

Another interpretation of Equation 3.1 is that we have an LCO in the loop in Figure 2.1. Although the reference input (r) is zero, since all states are oscillating, the inputs to the DF

(e) and the linear system (u) are all non-zero. Hence

$$\begin{aligned} E(i\omega) &= -G(i\omega)U(i\omega) \\ U(i\omega) &= N(A,\omega)E(i\omega) \end{aligned} \tag{3.3}$$

This leads to the following equation with nonzero $E(i\omega)$ and $U(i\omega)$.

$$\begin{bmatrix} N(A,\omega) & -1 \\ a & G(i\omega) \end{bmatrix} \begin{bmatrix} E(i\omega) \\ U(i\omega) \end{bmatrix} = 0 \tag{3.4}$$

Since the vector $[E(i\omega)\, U(i\omega)]^T$ is nonzero, it should belong to the null space of the matrix in Equation 3.4. Therefore the determinant of the matrix should be zero, and Equation 3.1 is verified.

3.1.2 Multiple PNs ([12, 9, 13])

Unlike the single PN case, we need more sophisticated analysis when we have multiple PNs within the system. This is because the two assumptions required for DF analysis (linear system as a low-pass filter, sinusoidal input to DF) no longer hold in the presence of multiple PNs, and the techniques of linear systems theory such as Nyquist plot and Bode diagram would not work. However, since in DF analysis DFs are basically treated as a linear component, we can treat the whole system as one that has its own 'linear' characteristics– eigenvalues. If the eigenvalues of the system are pure imaginary, we can say the states of the system are oscillating with a specific frequency and amplitude.

Consider a single-feedback linear system with multiple nonlinearities shown in Figure 3.2. In this system, $G_1(s)$ and $G_2(s)$ are linear transfer functions and $N_1(A,\omega)$ and $N_2(A,\omega)$ are DFs of corresponding PNs. Given the state space representation of each lin-

ear system,

$$\begin{aligned}
&\dot{\mathbf{x}}_1(t) = \mathbf{A}_1\mathbf{x}_1(t) + \mathbf{B}_1 u_1 = \mathbf{A}_1\mathbf{x}_1(t) - \mathbf{B}_1 N_1(A_1(\mathbf{e}_1), \omega)\mathbf{e}_1, \qquad \mathbf{e}_2 = \mathbf{C}_1\mathbf{x}_1, \\
&\dot{\mathbf{x}}_2(t) = \mathbf{A}_2\mathbf{x}_2(t) + \mathbf{B}_2 u_2 = \mathbf{A}_2\mathbf{x}_2(t) + \mathbf{B}_2 N_2(A_2(\mathbf{e}_2), \omega)\mathbf{e}_2, \qquad \mathbf{e}_1 = -\mathbf{C}_2\mathbf{x}_2 \\
&G_1(s) \sim \left[\begin{array}{c|c} \mathbf{A}_1 & \mathbf{B}_1 \\ \hline \mathbf{C}_1 & \mathbf{O} \end{array}\right], \qquad G_2(s) \sim \left[\begin{array}{c|c} \mathbf{A}_2 & \mathbf{B}_2 \\ \hline \mathbf{C}_2 & \mathbf{O} \end{array}\right]
\end{aligned} \tag{3.5}$$

where A_1 and A_2 are the amplitudes of the input signal to N_1 and N_2, respectively, under the assumption that they are all of unimodal sinusoidal shape. Now we can reconstruct the state space representation of the entire system as follows.

$$\begin{aligned}
&\dot{\mathbf{x}} = \mathbf{A}\mathbf{x}, \qquad \mathbf{x} = \begin{bmatrix} \mathbf{x}_1 \\ \\ \mathbf{x}_2 \end{bmatrix}, \qquad \text{where} \\
&\mathbf{A} = \begin{bmatrix} \mathbf{A}_1 & 0 \\ 0 & \mathbf{A}_2 \end{bmatrix} + \begin{bmatrix} -\mathbf{B}_1 N_1(A_1(\mathbf{C}_2\mathbf{x}_2), \omega)\mathbf{C}_1 & 0 \\ 0 & \mathbf{B}_2 N_2(A_2(\mathbf{C}_1\mathbf{x}_1), \omega)\mathbf{C}_2 \end{bmatrix}
\end{aligned} \tag{3.6}$$

However, this is not a linear state space representation in a strict sense because the coefficient matrix $\mathbf{A}$ contains state variables, and therefore we cannot calculate the eigenvalues of this system just as we do for pure linear systems. Instead, in corresponding references they adopted numerical methods such as a gradient-based function minimization algorithm [12, 13], or an algorithm driving the least damped eigenvalues to the imaginary axis based on a generalized Newton-Raphson method [9]. For the stability of LCO, the perturbation the LCO parameters is introduced to develop the algorithms to inspect the stability. However, solving for the specifications of LCO could practically lead to significant errors due to the approximations including, but not limited to, the design of DFs themselves and the calculation of the system eigenvalues.

Alternatively, we can rely on the singularity of 'the system state flow' matrix in the

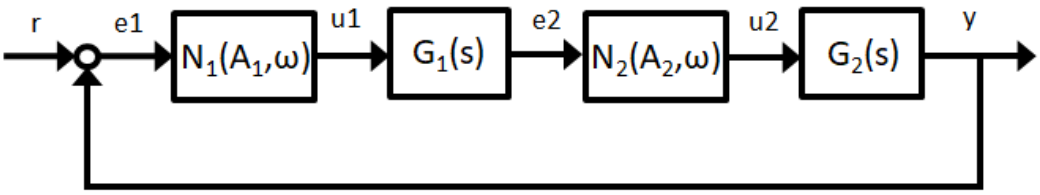

Figure 3.2: A simple feedback loop with multiple DFs.

Equation 3.4 [5].

$$\begin{bmatrix} N_1 & -1 & 0 & 0 \\ 0 & G_1 & -1 & 0 \\ 0 & 0 & N_2 & -1 \\ 1 & 0 & 0 & G_2 \end{bmatrix} \begin{bmatrix} E_1 \\ U_1 \\ E_2 \\ U_2 \end{bmatrix} = 0 \tag{3.7}$$

by the singularity condition, we obtain

$$1 + N_1(A_1, \omega)G_1(i\omega)N_2(A_2, \omega)G_2(i\omega) = 0 \tag{3.8}$$

However, this argument is based on the assumption that PNs are transformed into a completely linear component. Therefore this could lead to the violation of either of the two assumptions on which the validity DF analysis holds. Nevertheless, DF analysis can still provide an estimation of the LCO parameters with reasonable accuracy.

3.2 Piecewise Linear System (PLS) Approach

A PN usually consist of a finite number of input-output characteristics. For example, a saturation has three disparate outputs: positive saturated value, output signal proportional to the input, and negative saturated value. In case of a relay, there are only two possible outputs values. This means that considering only one of the input-output characteristics, a PN can be replaced by a purely linear component or a constant one. Therefore, if we correctly interpret the switching order between each of PN's output, we can utilize the principles and techniques of the linear systems theory. Based on this observation, PLS

enables us to analyze linear systems with PNs and their potential LCO. Unlike the DF analysis, PLS approach produces exact results on the analysis of LCO. This is possible by assuming the linear systems with PNs is one with multiple purely linear state space representations and analyzing them with the linear systems theory.

J. M. Gonalves developed the idea of impact maps on the switching surface in PLS and analyzed the period and the local/global stability of LCO with the introduction of the surface Lyapunov function [6]. An impact map is a generalization of the Poincaré map, and is defined as a map from one switching surface to the other. For example, in a linear system with a relay with hysteresis ($R_d(e(t))$),

$$R_d(e(t)) = \begin{cases} -1, & \text{if } e(t) < -d, \text{ or } e(t) \in (-d, d] \text{ and } u(t-0) = -1 \\ 1, & \text{if } e(t) > d, \text{ or } e(t) \in [-d, d) \text{ and } u(t-0) = 1 \end{cases} \tag{3.9}$$

consider a simple feedback system in Figure 2.1 with the PN $N(A, \omega)$ replaced by $R_d(e(t))$. Then switching surfaces for this system are defined as

$$\begin{aligned} S_0 &= \{\mathbf{x} \in \mathbb{R}^n : \mathbf{C}\mathbf{x} = \mathbf{d}\} \\ S_1 &= \{\mathbf{x} \in \mathbb{R}^n : \mathbf{C}\mathbf{x} = -\mathbf{d}\} \end{aligned} \tag{3.10}$$

Now let S_0^d be some subset of S_0 where any trajectory starting at S_0^d satisfies $\mathbf{x}(t) \in S_1$, for some finite $t \geq 0$. Let also $S_1^a \subset S_1$ be the set of those points $\mathbf{x}_1 = \mathbf{x}(t)$. The set S_1^a can be seen as the image set of S_0^d. We call S_0^d the departure set in S_0 and S_1^a the arrival set in S_1 (Figure 3.3).

Now let $\mathbf{x}_0 \in S_0^d$ and $\mathbf{x}_1 \in S_1^a$. By parameterizing both $\mathbf{x}_0$ and $\mathbf{x}_1$ as follows, respectively,

$$\mathbf{x}_0 = \mathbf{x}_0^* + \Delta_0$$

$$\mathbf{x}_1 = \mathbf{x}_1^* + \Delta_1$$

where $\mathbf{x}_0^* \in S_0$, $\mathbf{x}_1^* \in S_1$, and Δ_0, Δ_1 are any vectors such that $\mathbf{x}_0\Delta_0 = \mathbf{x}_1\Delta_1 = 0$. Defining

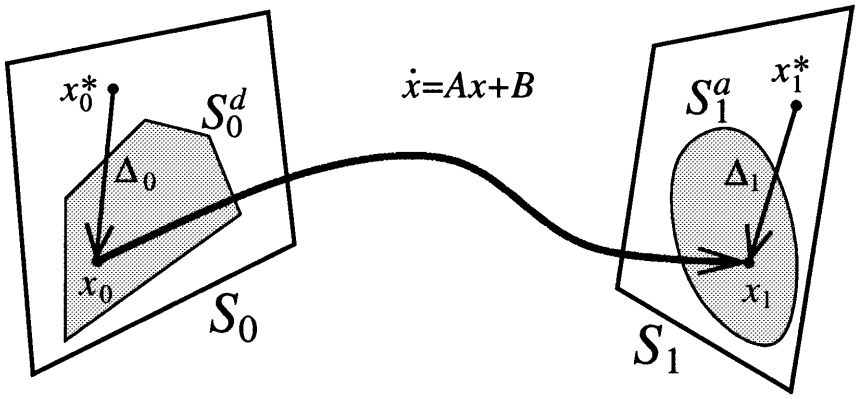

Figure 3.3: Impact map from $\Delta_0 \in S_0^d - \mathbf{x}_0^*$ to $\Delta_1 \in S_1^a - \mathbf{x}_1^*$ [6].

$\mathbf{x}_0^*(t)$ as the trajectory of the linear time invariant system $\dot{\mathbf{x}} = \mathbf{Ax} + \mathbf{Bd}$ starting at $\mathbf{x}_0^*$ for all $t \geq 0$, the impact map is defined as the map from Δ_0 to Δ_1, as shown in Figure 3.3. Or equivalently,

$$\Delta_1 = \mathbf{H_I}(t)\Delta_0$$

where H_I is the impact map from Δ_0 to Δ_1. The surface Lyapunov function is defined on each switching plane as a function of $\mathbf{x}(t) \in S_i$, $i = 0, 1$. Usually the surface Lyapunov function is of a quadratic form in order to guarantee the stability of the impact map such that

$$V_1(\Delta_1) < V_0(\Delta_0), \qquad \forall \Delta_0, \Delta_1 \neq 0 \tag{3.11}$$

where V_0 and V_1 are the surface Lyapunov functions on switching planes S_0 and S_1, respectively.

We assume that the LCO in the PLS with a relay with hysteresis d is symmetric and unimodal, as are defined in [14]. Then the following conditions hold for the LCO in the PLS [14].

$$\begin{aligned} g(\frac{T}{2}) &= \mathbf{C}(e^{\mathbf{A}\frac{T}{2}} + \mathbf{I}_n)^{-1}(e^{\mathbf{A}\frac{T}{2}} - \mathbf{I}_n)\mathbf{A}^{-1}\mathbf{B} - d = 0 \\ z(t) &= \mathbf{C}\big[e^{\mathbf{A}t}(\mathbf{x}^* - \mathbf{A}^{-1}\mathbf{B}) + \mathbf{A}^{-1}\mathbf{B}\big] \geq -d \qquad \text{for } 0 \leq t < \frac{T}{2} \end{aligned} \tag{3.12}$$

where $\mathbf{x}^* = (e^{\mathbf{A}\frac{T}{2}} + \mathbf{I}_n)^{-1}(e^{\mathbf{A}\frac{T}{2}} - \mathbf{I}_n)\mathbf{A}^{-1}\mathbf{B}$

where T is the period of the LCO. To check the stability of LCO, we utilize the stability condition extracted from the surface Lyapunov function, as in Equation 3.11. Since Equation 3.11 can be reduced to a finite number of linear matrix inequality (LMI) problems

$$\mathbf{P}_i - \mathbf{H}_{\mathbf{I}i}^T(t)\mathbf{P}_i\mathbf{H}_{\mathbf{I}i}(t) > 0, \qquad i = 1, \ldots, n$$

For some positive definite matrices $\mathbf{P}_i$ and possible switching time t, we can check the stability by solving those LMI problems above. This is done by dividing the switching time into n-subdivision as $t_0 < t_1 < \cdots < t_n$ and assuming constant $\mathbf{H}_{\mathbf{I}i}(t)$ for $t \in [t_{i-1}, t_i]$ so that we can check if the minimum eigenvalues of the matrices $\mathbf{P}_i - \mathbf{H}_{\mathbf{I}i}^T(t)\mathbf{P}_i\mathbf{H}_{\mathbf{I}i}(t)$ is positive on $[t_0, t_n]$.

Inspired by this work, the framework in this thesis includes similar piecewise linear analysis. While maintaining the feature that enables the accuracy in the analysis of LCO, complementing the arguments on the feasible switching configuration and the switching order enriches this piecewise linear analysis to be introduced in the following chapter.

3.3 Nonlinear Equivalent Analytic Functions for PNs

Since PNs usually consist of multiple sections, they are potentially discontinuous. For example, a relay with hysteresis has three sections as shown in Equation 3.9 and a continuous functions can not approximate the parts between sections. Therefore, a piecewise linear system with PNs are, in fact, also a Lur'e type system as in the equation below [30].

$$\begin{aligned} \dot{\mathbf{x}} &= \mathbf{A}\mathbf{x} + \mathbf{B}\boldsymbol{\phi}(\mathbf{y}) \\ \mathbf{y} &= \mathbf{C}\mathbf{x} \end{aligned} \tag{3.13}$$

The sector property of a PN plays a critical role in preventing Floquet theory from being used in the analysis of LCO for piecewise linear systems. This is because PNs are non-differentiable with respect to both space and time. If there is a way to treat PN as

a differentiable function, then Equation 3.13 turns into a general, differentiable nonlinear equation of motion $\dot{\mathbf{x}} = \mathbf{f}(\mathbf{x})$. Fortunately, the equivalent analytic function (EAF) exists for PN to enable this. The construction of EAF starts from a simple observation that a proper arrangement of infinite quantities in both nominator and denominator reproduces a signal identical to a simple relay.

$$\lim_{\gamma\to\infty} \frac{\gamma u}{\sqrt{1+(\gamma u)^2}} = \begin{cases} 1, & u > 0 \\ 0, & u = 0 \\ -1, & u < 0 \end{cases}$$

Hence we define the EAF for a simple relay as follows.

$$EAF(r(u)) = g(u) = \lim_{\gamma\to\infty} \frac{\gamma u}{\sqrt{1+(\gamma u)^2}} \tag{3.14}$$

where $r(u)$ is a simple relay.

$$r(u) = \begin{cases} 1, & u > 0 \\ 0, & u = 0 \\ -1, & u < 0 \end{cases}$$

Note that as γ grows larger, $g(u)$ becomes closer to $r(u)$ as shown in Figure 3.5. We claim that $g(u)$ converges to $r(u)$ point-wisely, but not uniformly.

Theorem 3.3.1. Convergence of $g(u)$ to $r(u)$ in Equation 3.3

$g(u)$ converges to $r(u)$ point-wise, while $g(u)$ does not converge to $r(u)$ uniformly on $u \in (-\infty, \infty)$

Proof. If $u = 0$, $g(u)$ = $r(u)$ = 0. If $u \neq 0$ and $u \in (0, \infty)$, then $\lim_{\gamma\to\infty} g(u)$ = $r(u)$ = 1. Likewise, if $u \in (-\infty, 0)$ $\lim_{\gamma\to\infty} g(u)$ = $r(u)$ = -1. Hence $g(u)$ converges to $r(u)$ point-wise

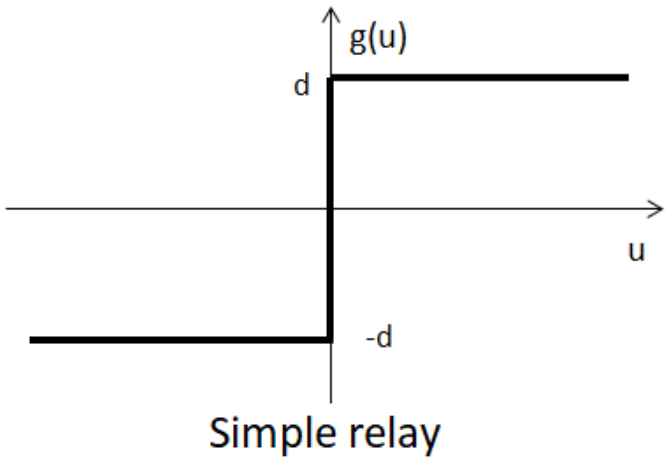

Figure 3.4: A simple relay that corresponds to $r(u)$ in Equation 3.3.

on $u \in (-\infty, \infty)$.

Now assume that $g(u) \to r(u)$ uniformly almost everywhere on $u \in (-\infty, \infty)$. Then

$$\sup_{u \in (-\infty,\infty) \setminus E} |g(u) - r(u)|_{\mathcal{L}} = 0 \tag{3.15}$$

where $|\cdot|_{\mathcal{L}}$ is Lebesgue measure and E is a set whose (Lebesgue) measure is zero [31]. Now define a set F as

$$F = [\frac{1}{n+1}, \frac{1}{n}]$$

then there exists a natural number n such that $F \notin E$. In this case,

$$\sup_{u \in (-\infty,\infty) \setminus E} |g(u) - r(u)|_{\mathcal{L}} \geq |g(\frac{1}{n}) - r(\frac{1}{n})|_{\mathcal{L}} = |\frac{\frac{\gamma}{n}}{\sqrt{1 + (\frac{\gamma}{n})^2}} - 1|$$

by letting $n \to \infty$ we show that

$$\sup_{u \in (-\infty,\infty) \setminus E} |g(u) - r(u)|_{\mathcal{L}} \geq |0 - 1| = 1$$

Thus it is a contradiction to Equation 3.15. □

Although $g(u)$ does not converge to $r(u)$ uniformly, it converges to $r(u)$ point-wise.

Furthermore, with γ finitely large enough $g(u)$ becomes close enough to $r(u)$ in a practical sense, as demonstrated in Figure 3.5. By similar arguments, we could also express a saturation in a similar way. Observing that the input derivative of the saturation looks like a combination of reversed relays shown in Figure 3.6, the saturation function is obtained by integrating the input derivative function.

$$\begin{aligned} h(u) &= \frac{1}{2}\Big(1 - \frac{\gamma(|u| - d)}{\sqrt{1 + (\gamma(|u| - d))^2}}\Big) \\ g(u) &= \frac{1}{2}\Big(u - \text{sign}(u)\frac{\sqrt{1 + (\gamma(|u| - d))^2} - \sqrt{1 + (\gamma d)^2}}{\gamma}\Big) \end{aligned} \tag{3.16}$$

where $h(u) = \frac{dg}{du}$. Next, we check the differentiability of this EAF for saturation in the equation above. By the appearance of Equation 3.16, the most dubious point is where $u = 0$ due to the presence of the 'sign(u)' term. Checking the differentiability at $u = 0$ gives us

$$\begin{aligned} \frac{dg}{du}^+ &= \lim_{\Delta u \to +0} \frac{g(\Delta u) - g(0)}{\Delta u} \\ &= \lim_{\Delta u \to +0} \frac{1}{2}\frac{\Big(\Delta u - \frac{\sqrt{1+(\gamma(\Delta u - d))^2} - \sqrt{1+(\gamma d)^2}}{\gamma}\Big) - \Big(-\frac{\sqrt{1+(\gamma d)^2} - \sqrt{1+(\gamma d)^2}}{\gamma}\Big)}{\Delta u} \\ &= \lim_{\Delta u \to +0} \frac{1}{2}\Big(1 - \frac{\gamma(\Delta u - 2d)}{\sqrt{1 + \big(\gamma(\Delta u - d)\big)^2} + \sqrt{1 + (\gamma d)^2}}\Big) = \frac{1}{2}\Big(1 + \frac{\gamma d}{\sqrt{1 + (\gamma d)^2}}\Big) \end{aligned}$$

from above. On the other hand, from below

$$\begin{aligned} \frac{dg}{du}^- &= \lim_{\Delta u \to -0} \frac{g(\Delta u) - g(0)}{\Delta u} \\ &= \lim_{\Delta u \to -0} \frac{1}{2}\frac{\Big(\Delta u + \frac{\sqrt{1+(\gamma(-\Delta u - d))^2} - \sqrt{1+(\gamma d)^2}}{\gamma}\Big) - \Big(-\frac{\sqrt{1+(\gamma d)^2} - \sqrt{1+(\gamma d)^2}}{\gamma}\Big)}{\Delta u} \\ &= \lim_{\Delta u \to +0} \frac{1}{2}\Big(1 + \frac{\gamma(\Delta u + 2d)}{\sqrt{1 + \big(\gamma(\Delta u - d)\big)^2} + \sqrt{1 + (\gamma d)^2}}\Big) = \frac{1}{2}\Big(1 + \frac{\gamma d}{\sqrt{1 + (\gamma d)^2}}\Big) \end{aligned}$$

Since $\frac{dg}{du}^+ = \frac{dg}{du}^-$, Equation 3.16 is differentiable with respect to u at zero, we might

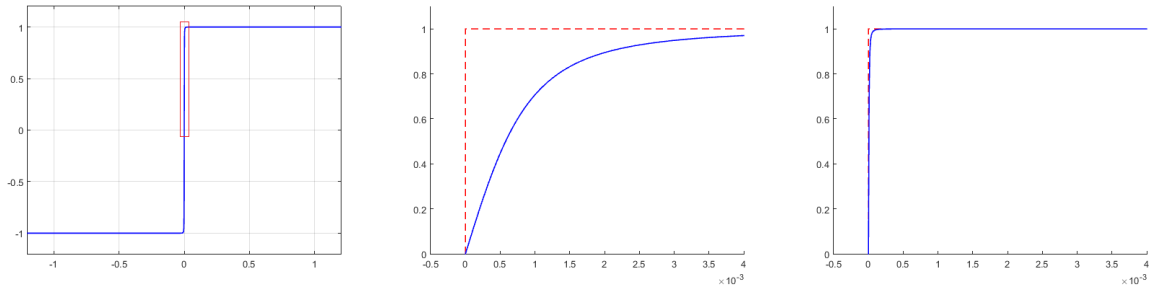

Figure 3.5: (a) (left) An EAF of a simple relay with d=1 and γ=1,000. The part in the thin red rectangle is zoomed in and depicted in (b) and (c) with different γ values. (b) (middle) Zooming in figure (a) by a thousand times along x axis with γ=1,000. (c) Zooming in figure (a) by a thousand times along x axis with γ=100,000. Note that the scaling of x axis of (b) and (c) is 10^{-3}.

conclude that $g(u)$ is differentiable with respect to t(time) as well, only if $u = u(t)$ is differentiable in time. Based on the observation that most PNs are a combination of linear segments just like a saturation, we can construct an EAF corresponding to PNs that are common in control systems in a similar way to a relay or a saturation. Listed in Table 3.1 are the EAFs of the common PNs in control systems. Although the proof of point-wise convergence and differentiability of each EAFs are not presented here, the proof can be done in a similar way to that of Theorem 3.3.1 and differentiability can be verified as above. The construction of each EAF in Table 3.1 is shown in Appendix A.

3.4 Numerical Integration

Numerical integration is the most straightforward and convenient way to track the propagation of the state trajectory of even a quite complicated differential equation used to describe motion. The same argument is applied to the analysis of LCO because propagation of the state variables of the system for a sufficient amount of time may include the convergence to a periodic solution. However, numerical integration has a variety of sources of error including, but not limited to, machine error, mathematical truncation error, noise in function evaluation, under or overflow errors in calculation, and so on [32]. Furthermore,

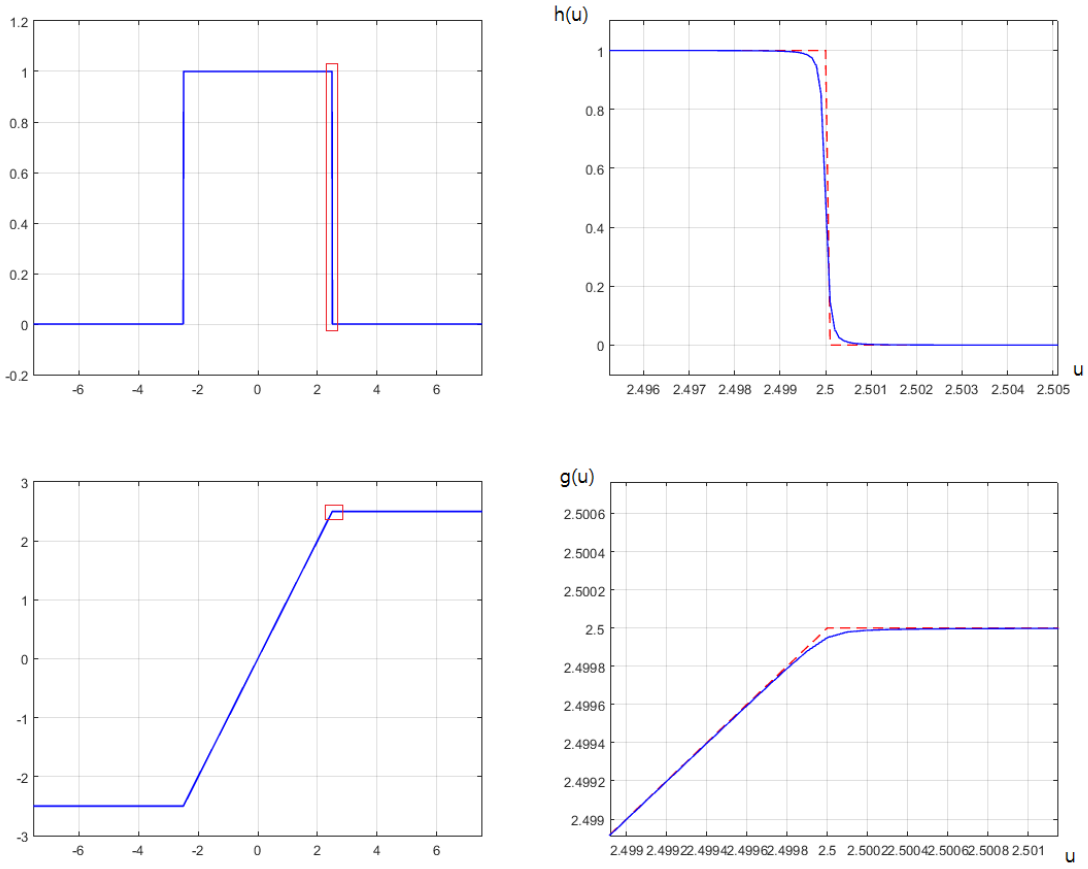

Figure 3.6: (a) (upper left) The EAF of an input derivative ($h(u)$) of a saturation with d=2.5 and γ=10,000. The part in the thin red rectangle is zoomed in and depicted in (b). (b) (upper right) Zooming in figure (a) by about a thousand times along x axis. Red dashed line is the original $h(u)$ and blue solid line is the corresponding EAF. (c) (below left) The EAF of a saturation ($g(u)$) with d=2.5 and γ=10,000. The part in the small red rectangle is zoomed in and depicted in (d). (d) (below right) Zooming in figure (c) by about a thousand times along both axes. Red dashed line is the original $g(u)$ and blue solid line is the corresponding EAF.

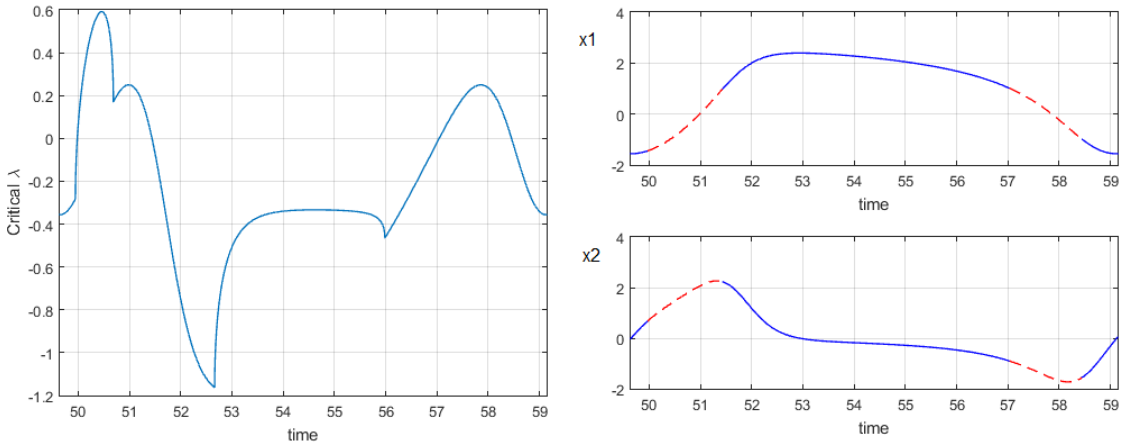

Figure 3.7: Numerical integration of Van der Pol oscillator in time domain for one period(about 9.5 seconds) near the periodic solution. (a)(left)The largest real part of eigenvalues of Jacobian matrix around integrated solution trajectory. Note that from time 50 to 51.45 and from 57 to 58.4 the Jacobian has positive value as its real part of eigenvalue. (b)(right)Solid blue lines indicate the part of trajectory in which the real part of the eigenvalues of Jacobian are all negative (stable numerical integration), and dashed red lines are part of trajectory in which the largest real part of the eigenvalues is positive (unstable numerical integration).

in the course of integrating the state space representation of the system equation of motion in forward direction–i.e., in a direction in which time increases as integrating steps go by, errors stemming from various sources mentioned just above can positively propagate, depending on situations, only to deteriorate the reliability of the numerical integration. One of the most influential factors that determines the numerical integration error to propagate or to diminish is the property of Jacobian of the system [33, 34].

The example of how error propagates with numerical integration is shown in Figure 3.7. Unlike the solid blue trajectory, the dashed red one in the right hand side of Figure 3.7 indicates that the largest real part of eigenvalue is positive, thus it is not very reliable because the numerical integration is unstable during this segment. This implies that even though we might be able to numerically integrate any piecewise linear system and observe an LCO, we cannot fully trust the LCO parameters observed from the numerical integration, because usually there exist unreliable parts such as the red dashed part in Figure 3.7. Fundamentally, the oscillating trajectory obtained with the numerical integration is not an

LCO, but a trajectory that is at best converging to an LCO. Notwithstanding, we might still utilize the numerical integration as a useful tool to approximately locate the LCO parameters if we integrate for a sufficient length of time for the oscillatory trajectory to converge to LCO within the limitation of numerical integration.

Table 3.1: List of PNs and corresponding EAFs.

PN	EAF ($\gamma \gg 1$)
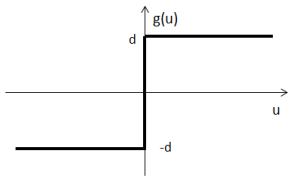 Simple relay	$g(u) = \dfrac{d\gamma u}{\sqrt{1+(\gamma u)^2}}$
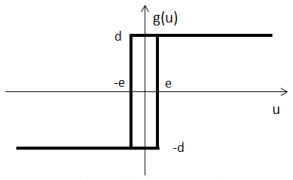 Relay with hysteresis	$g(u) = \dfrac{d\gamma(u-\text{sign}(ui_c)e)}{\sqrt{1+(\gamma(u-\text{sign}(ui_c)e))^2}}$ $u_c =$ the latest critical input(u=e or -e)
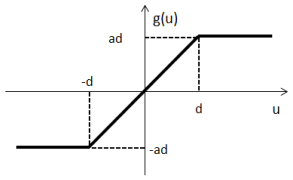 Saturation	$g(u) = \dfrac{a}{2}\left(u - \text{sign}(u)\dfrac{\sqrt{1+(\gamma(\lvert u\rvert - d))^2} - \sqrt{1+(\gamma d)^2}}{\gamma}\right)$
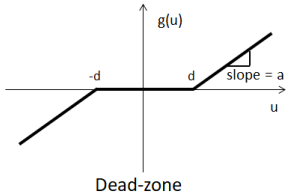 Dead-zone	$g(u) = \dfrac{a}{2}\left(u + \text{sign}(u)\dfrac{\sqrt{1+(\gamma(\lvert u\rvert - d))^2} - \sqrt{1+(\gamma d)^2}}{\gamma}\right)$
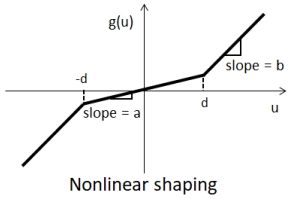 Nonlinear shaping	$g(u) = \frac{1}{2}\left((b+a)u + (b-a)\text{sign}(u)\dfrac{\sqrt{1+(\gamma(\lvert u\rvert - d))^2} - \sqrt{1+(\gamma d)^2}}{\gamma}\right)$
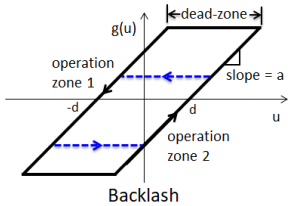 Backlash	$g(u) = av + \frac{a}{2}\left((u-v) + \text{sign}(u-v)\dfrac{\sqrt{1+(\gamma(\lvert u-v\rvert - d))^2} - \sqrt{1+(\gamma d)^2}}{\gamma}\right)$ $v = \begin{cases} u_c + d, & u_c \in \text{ operation zone one,} \\ u_c - d, & u_c \in \text{ operation zone two} \end{cases}$ $u_c =$ the latest critical input from either of two operating zones

CHAPTER 4
A FRAMEWORK FOR DETERMINATION OF LCO PARAMETERS AND ITS APPLICATION

With all the preliminary work developed in the previous chapter, now we are ready to analyze the LCO of a piecewise linear system in detail. Identification of an LCO implies the determination of the LCO parameters– LCO period and LCO amplitude based on the framework provided in this chapter. Numerical integration and/or DF analysis can provide approximate results on LCO parameters, but we may need additional advanced approaches entailing more accurate and reliable analysis. More importantly, we can make use of the framework of the LCO analysis to determine major system parameters, such as the upper bound of a feedback gain in a flight control system, to ensure that any LCO is no longer generated. The basic premise is that we are only allowed to raise any gain until an unacceptable LCO starts to appear in the system, thus an LCO is often the source of upper limits on gains or control bandwidth. Furthermore, based on the same framework we can change the LCO frequency (LCO period) into a specific band of frequency so that we may maintain the LCO amplitude at a desirable level. Normally we need to raise the LCO frequency so that the following linear system can reject the LCO frequency component sufficiently.

The basic framework to analyze the LCO is as follows. First, we express the system both in state space representation and a cascaded series of linear transfer functions and nonlinearities. Sometimes it is convenient to express in state space representation first and cascaded transfer functions later or vice versa. In the end we need to have both representations of the system in hand in order to apply techniques discussed in the previous chapter and the ones discussed in this chapter. Secondly, select the approximate range of LCO parameters with numerical integration and DF analysis. Both of them have limitations in refining the results into accurate LCO parameters, but it is important to narrow the search

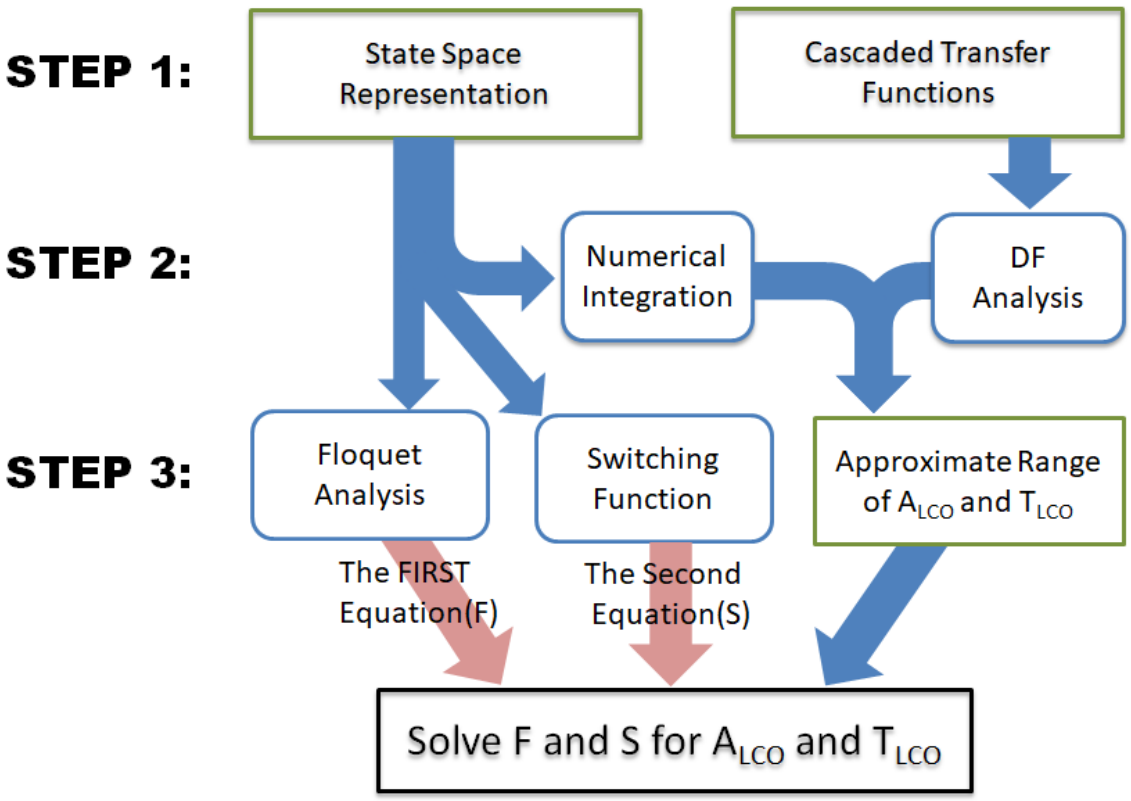

Figure 4.1: Framework to identify LCO parameters. Rectangles represent the system characteristics and the rectangles with round vertices are analytic or arithmetic methods to produce results.

space for the true LCO parameters. This is because our technique based on Floquet theory and switching analysis, narrowing down the range of the candidates of LCO period and LCO amplitude can greatly speed up the process. Then we establish the necessary conditions on the LCO parameters. Since there are two unknowns–LCO period and LCO amplitude, we also need two algebraic equations, one of which we obtain from Floquet analysis and the other from a switching equation. We call the equation built on Floquet analysis the $\mathcal{F}$ equation and the one from switching equation the $\mathcal{S}$ equation. However, the two algebraic equations are not necessarily solved in closed form, so we need to iterate those equations in a certain range of the unknowns in order to find the answer numerically. That is why we needed the range of the two parameters with the preliminary work. The illustrative diagram about this procedure is in Figure 4.1.

In this chapter, we take an example of a simple rate saturated loop, common in flight

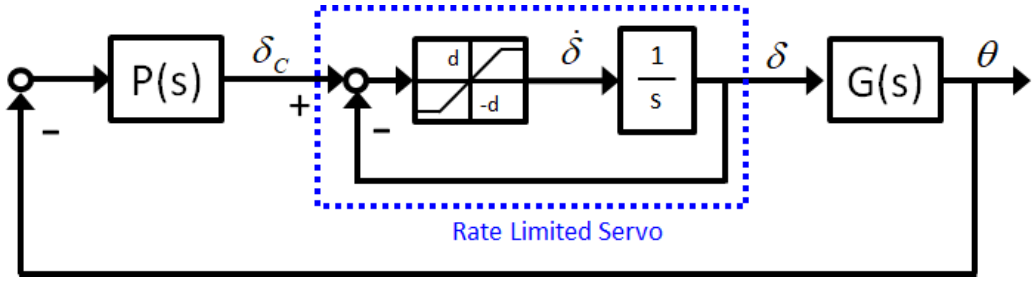

Figure 4.2: A simple rate saturation feedback loop [10].

control systems, to verify the proposed framework to analyze and manipulate the LCO parameters. We first identify the LCO period and LCO amplitude and then determine the upper bound of a pilot gain that does not cause LCO. Additionally, we change the LCO period of the simple rate saturated loop to a desirable quantity based on the proposed framework.

4.1 Simple Rate Saturated Loop

In an aircraft control system, control surface dynamics often include rate limited feedback because of the physical and operational upper bound of performance of the actuator. This rate saturated feedback in the loop that appears in fighter jets such as YF-22 and JAS-39 may lead to a phenomena called as pilot-induced oscillation (PIO) because right in front of the rate saturated loop there is a pilot model whose excessive input can lead to oscillatory behavior [10].

PIO is essentially an LCO because it is a stable periodic solution predicted in a nonlinear system which is a combination of linear transfer function and PN. In addition, the mechanism of PIO generation is not much different from that of LCO. One of the main factors that causes PIO is known to be the pilot gain into the loop [10]. However, the pilot input can be interpreted as a signal that sends the system to a certain set that is eventually attracted to a stable periodic solution, therefore the basic mechanism of generation is similar. This simple rate saturated loop consists of the following components; $P(s)$ is a pilot model with pilot gain k_p and time constant τ_p, $G(s)$ is the airframe dynamics model

based on the short-period mode linearized equation of motion. The rate saturated loop for the control surface is depicted in Figure 4.2. For convenience, we reconstructed $G(s)$ from Klyde's as follows, along with the pilot model $P(s)$ for pitch attitude control of an airplane in level flight [10].

$$G(s) = \frac{6s+5}{s(s^2+2s+5)}, \qquad P(s) = \frac{k_p}{\tau_p s + 1} \tag{4.1}$$

Since the input to the airframe dynamics is δ, an elevator deflection, and the output is θ, the pitching angle, the state space representation of $G(s)$ is as follows.

$$\begin{gathered} \dot{\mathbf{x}} = \mathbf{A}\mathbf{x} + \mathbf{B}\delta, \qquad \theta = \mathbf{C}\mathbf{x}, \qquad \mathbf{x} \in \mathbb{R}^3 \\ \mathbf{A} = \begin{bmatrix} 0 & 1 & 0 \\ 0 & 0 & 1 \\ 0 & -5 & -2 \end{bmatrix}, \qquad \mathbf{B} = \begin{bmatrix} 0 \\ 0 \\ 1 \end{bmatrix}, \qquad \mathbf{C} = \begin{bmatrix} 5 & 6 & 0 \end{bmatrix} \end{gathered} \tag{4.2}$$

Likewise, the state space representation of the pilot model $P(s)$ is as follows.

$$\dot{\delta}_c = -\frac{k_p}{\tau_p}\mathbf{C}\mathbf{x} - \frac{1}{\tau_p}\delta_c$$

where δ_c is the reference command of the elevator deflection from the pilot. Now, the input-output relationship of the saturation is

$$\dot{\delta} = g(\dot{\delta}_r) = g(\delta_c - \delta) \tag{4.3}$$

where $g(u)$ is the EAF of a simple saturation, $\dot{\delta}_r$ is a reference elevator deflection rate, and k_v is a constant proportional gain. For simplicity, we choose k_v as one.

$$g(u) = \frac{1}{2}u\Big(1 - \frac{\sqrt{1+(\gamma(|u|-d))^2} - \sqrt{1+(\gamma d)^2}}{\gamma|u|}\Big) \tag{4.4}$$

where d=1 and the slope of the linear part is one for simplicity. Let $\mathbf{x}_1 = [x^T\, \delta_c\, \delta]^T \in \mathbb{R}^5$ a state vector of the system. Then by Equation 4.2, 4.1 and 4.3, we obtain the overall nonlinear state space realization of the system.

$$\dot{\mathbf{x}}_1 = \mathbf{f}(\mathbf{x}_1) = \begin{bmatrix} \mathbf{A}\mathbf{x} + \mathbf{B}\delta \\ -\frac{k_p}{\tau_p}\mathbf{C}\mathbf{x} - \frac{1}{\tau_p}\delta_c \\ g(\delta_c - \delta) \end{bmatrix} \tag{4.5}$$

where we assume $k_p = 10$ and $\tau_p = 0.1$ as an initial design.

4.2 Approximate Range of the LCO parameters

As explained in the previous chapter, the necessary conditions of T_{LCO} and A_{LCO}, the LCO period and LCO amplitude respectively, need an approximate range for them. In other words, for a specific range of T_{LCO} and A_{LCO} we calculate the $\mathcal{F}$ and the $\mathcal{S}$ equation and find the common solution. To this end we utilize the DF analysis and the numerical integration.

4.2.1 DF Analysis

We begin from checking the basic assumptions for applying the DF method. Those assumptions are repeated here for convenience.

- The linear function following the DF of a PN should function as a low-pass filter.
- The input signal to the DF is a unimodal sinusoidal shape.

The first assumption implies that the bandwidth of the linear transfer function should truncate the higher harmonic frequency component from the output of DF, since the output signal of DF is virtually a multi-harmonic one. The second assumption naturally follows if the first one is satisfied. The bode diagram of the serial of linear transfer functions, i.e. $-P(i\omega)G(i\omega)$, suggests that if the LCO frequency is lower than 3.5(rad/s) (or 1.795

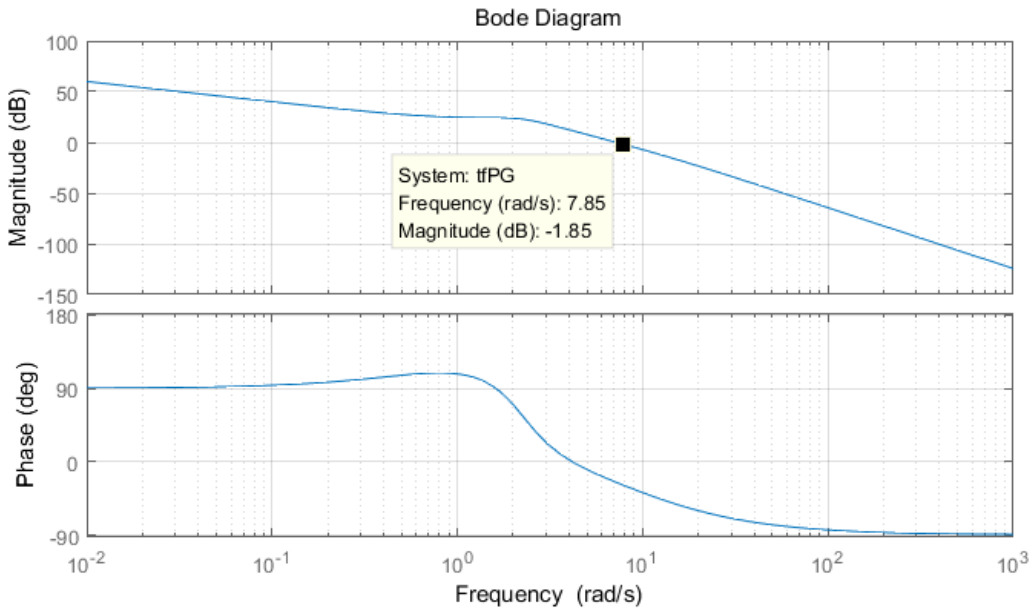

Figure 4.3: A bode diagram of the linear transfer function($-P(i\omega)G(i\omega)$) of a simple rate saturated loop. The bandwidth or the gain crossover frequency is at about 7 (rad/s).

seconds of period)–half the open loop bandwidth, then the accuracy of LCO parameter identification with DF analysis would be lower than expected due to the chance that the second harmonic component might not have died out in the input signal to DF (Figure 4.3). The second assumption leads to the assumption about the input to the PN and the definition of the LCO amplitude–i.e., the amplitude of the signal $\dot{\delta}_r(t)$.

$$\dot{\delta}_r(t) = k_v\big(\delta(t) - \delta_c(t)\big) = A\sin(\frac{2\pi}{T}t) \tag{4.6}$$

Given this, the DF of the saturation PN is as follows. Since LCO takes place only when $A > d = 1$, the DF of the saturation is

$$N(A,\omega) = \frac{2}{\pi}\Big(\sin^{-1}(\frac{d}{A}) + \sqrt{1-(\frac{d}{A})^2}\Big) \tag{4.7}$$

Now we establish the following LCO condition based on the argument in Equation 3.1.

$$1 + \frac{N(A,\omega)}{i\omega + N(A,\omega)}P(i\omega)G(i\omega) = 0 \tag{4.8}$$

where $P(i\omega)$ and $G(i\omega)$ are from Equation (4.1), and $\omega = \frac{2\pi}{T}$. For $\tau_p = 0.1$ and $k_p = 10$, we are able to solve the equation above because there are two unknowns (A and ω) and two equations (real and imaginary parts). The result is 3.7046 (sec) for T_{LCO} and 12.375 (rad/s) for A_{LCO} , respectively.

4.2.2 Numerical Integration

Although numerical integration is not perfect either, we may use it in obtaining the approximate range of the LCO parameters together with DF analysis. Given an appropriate initial point, the numerical integration eventually attracts the state trajectory to an LCO (Figure 4.4). In an effort to minimize the error we used the fourth order implicit Runge-Kutta instead of forward Euler method. The initial condition was $[0, -0.2, 0.3, 0.1, 0]^T$ and the integration leads to the approximate LCO parameters: T_{LCO} =3.7338 (sec), A_{LCO} =12.495 (rad/s).

4.3 Floquet Analysis

Since the exact analytic expression of piecewise nonlinearities are available with corresponding EAFs as in Equation 4.4, we can model the control system with PNs as a nonlinear differential equation of a general, closed form of Equation 2.17. Since the existence of LCO suggests that the control system with PNs has a periodic solution, Floquet theory is applicable. By incorporating the LCO parameters in question into the expression of the characteristic multipliers of the system, we extract a necessary condition through which to establish the $\mathcal{F}$ equation to determine the LCO parameters. As described in Chapter 2, Theorem 2.3.2 implies that a periodic solution to the system guarantees one of the characteristic multipliers is unity (one). Since this specific characteristic multiplier defines the relationship between the LCO parameters, it is useful to define a name for this specific characteristic multiplier here.

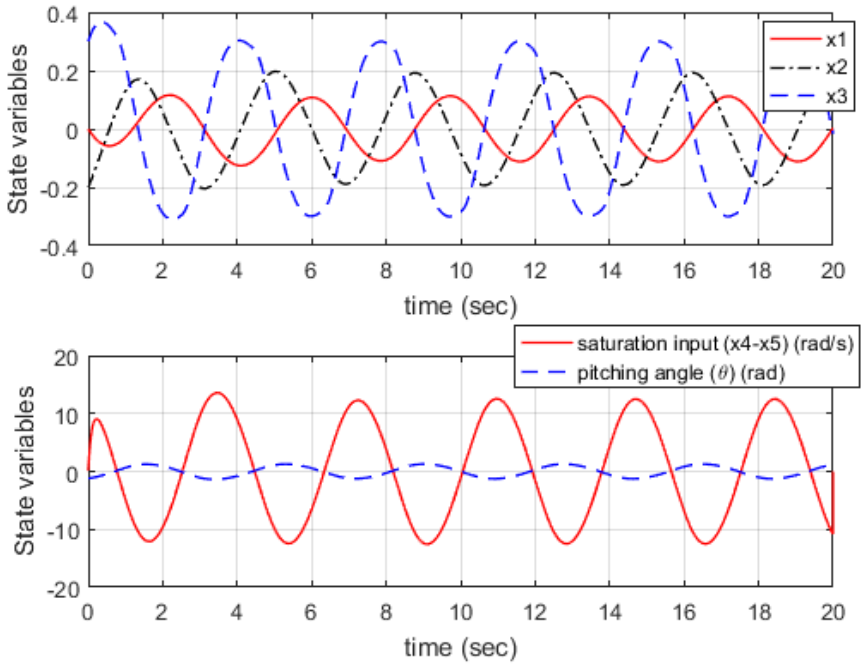

Figure 4.4: The integrated simulation of LCO of the rate saturated feedback system. Although the pitching angle (θ) seems to be a good fit to the LCO amplitude, we choose the amplitude of $\delta - \delta_c$ (or, $\mathbf{x}_4 - \mathbf{x}_5$) as the LCO amplitude instead because it is the input to the saturation PN. After all, the amplitude of the pitching angle can be obtained from the LCO amplitude.

Definition 4.3.1. Primary Characteristic Multiplier (PCM)

The primary characteristic multiplier is a characteristic multiplier of an LTP system of which the real part is the greatest among all of the LTP's characteristic multipliers.

The calculation of PCM is important especially for the system with a stable LCO because, according to Theorem 2.3.2, PCM should be equal to a unity for a stable LCO. PCM for the simple rate saturated system is obtained after we derive corresponding LTP system from the original nonlinear equation of motion in Equation 4.5. Therefore, the next step is to linearize Equation (4.5) around the hypothetical periodic solution $\boldsymbol{\eta}(t)$ to obtain the corresponding LTP system.

$$\dot{\delta\mathbf{x}} = \mathbf{D}(t)\delta\mathbf{x}, \qquad \delta\mathbf{x} \in \mathbb{R}^5 \tag{4.9}$$

where $\delta\mathbf{x} \in \mathbb{R}^5$ is a perturbation around a periodic solution $\boldsymbol{\eta}(t)$, $\mathbf{D}(t) = \frac{\partial \mathbf{f}}{\partial \mathbf{x}}$ is a Jacobian matrix evaluated at $\boldsymbol{\eta}(t)$. Since $\mathbf{D}(t)$ is a function of the periodic solution $\boldsymbol{\eta}(t)$, $\mathbf{D}(t) = \mathbf{D}(\eta(t))$ is potentially periodic as well. Assuming that the period of $\boldsymbol{\eta}(t)$ is T, $\mathbf{D}(t) = \mathbf{D}(t+T)$, $T > 0$, $T \in \mathbb{R}$, therefore Equation (4.9) is an LTP system. Now we need to obtain the expression for the characteristic multipliers of the LTP system of Equation (4.9). Before that, however, the expression for $\boldsymbol{\eta}(t)$ should be determined because $\boldsymbol{\eta}(t)$ appears explicitly in $\mathbf{D}(t)$. Considering that the input to the EAFs usually are the output of the series of linear transfer functions $-P(i\omega)G(i\omega)$, we assure once again the input signal to the saturation $\delta_c(t) - \delta(t)$, or $\dot{\delta}_r(t)$ is a unimodal sinusoid signal. It is obvious from the frequency response of $-P(i\omega)G(i\omega)$ that second or higher order harmonic terms are negligible compared to the fundamental one.

$$\frac{L(i2\omega_{LCO})}{L(i\omega_{LCO})} = -8.3\,(dB), \qquad \frac{L(i3\omega_{LCO})}{L(i\omega_{LCO})} = -16.8\,(dB)$$

where $L(i\omega) = -P(i\omega)G(i\omega)$, and ω_{LCO}=1.683 (rad/s) is the LCO frequency predicted

from the numerical integration. Thus, we repeat Equation 4.6 for clarification.

$$\dot{\delta}_r(t) = k_v\big(\delta(t) - \delta_c(t)\big) = A\sin(\frac{2\pi}{T}t)$$

where k_v is equal to one. We may assume the phase angle to be zero without loss of generality. Then, from the state space representation of the simple rate saturated system in Equation 4.5, we obtain $\mathbf{D}(t)$ as follows.

$$\mathbf{D}(t) = \frac{\partial \mathbf{f}(\mathbf{x}_1)}{\partial \mathbf{x}_1}\,|_{\mathbf{x}_1=\eta(t)} = \begin{bmatrix} \mathbf{A} & \mathbf{O}_{3\times 1} & \mathbf{B} \\ -\frac{k_p}{\tau_p}\mathbf{C} & -\frac{1}{\tau_p} & 0 \\ \mathbf{O}_{1\times n} & \frac{\partial g}{\partial \delta_c} & \frac{\partial g}{\partial \delta} \end{bmatrix} = \begin{bmatrix} 0 & 1 & 0 & 0 & 0 \\ 0 & 0 & 1 & 0 & 0 \\ 0 & -5 & -2 & 0 & 1 \\ -5\frac{k_p}{\tau_p} & -6\frac{k_p}{\tau_p} & 0 & -\frac{1}{\tau_p} & 0 \\ 0 & 0 & 0 & h(t) & -h(t) \end{bmatrix} \tag{4.10}$$

where **A**, **B**, and **C** are from the state space representation of the system in Equation 4.5, and $h(t)$ and $-h(t)$ are spatial derivatives of $g(\delta_c - \delta)$ with respect to δ_c and δ, respectively, so that

$$h(t) = \frac{\partial g(\delta_c - \delta)}{\partial \delta_c} = \frac{1}{2}\Big(1 - \frac{\gamma(|\delta_c(t) - \delta(t)| - d)}{\sqrt{1 + (\gamma(|\delta_c(t) - \delta(t)| - d))^2}}\Big)$$

Now that $\delta_c - \delta$ contains both T and A and so on, $\mathbf{D}(t)$ also contains them.

Since the closed form solution of the fundamental matrix does not generally exist for LTVs, we need to turn to a numerical approach [35]. The basic idea of this numerical calculation of PCM is that the state transition matrix is a product of 'small' transition matrices over small time. In such a small time integral, the corresponding state transition matrix may well be approximated as just the matrix exponential of the LTP system coefficient matrix multiplied by the time gap, i.e., $e^{\frac{1}{\Delta t}\int_{t_{i-1}}^{t_i}\mathbf{D}(\tau)d\tau}$. The idea of dividing into infinitesimally small multiple intervals to calculate the state transition matrix comes from P. Friedmann

[19].

$$\mathbf{\Phi}(T,0) = \Pi_{i=1}^{N} e^{\Delta \mathbf{D}_i}, \qquad \mathbf{D}_i = \frac{1}{\Delta}\int_{t_{i-1}}^{t_i} \mathbf{D}(\tau)\, d\tau \tag{4.11}$$

where N is the number of intervals, $\Delta = \frac{T}{N}$, and $t_i = i\Delta$. Now applying the equation above we can calculate the characteristic multipliers by obtaining the eigenvalue of $\mathbf{\Phi}(T,0)$. Since $\mathbf{D}(t)$ contains T and A, $\mathbf{\Phi}(T,0)$ is a function of them. The requirement that the PCM should be equal to a unity and $\mathbf{\Phi}(T,0)$ is a function of A_{LCO} and ω_{LCO} leads to

$$\text{PCM}(\mathbf{\Phi}(T,0)) = \max_{T,A}\big(\text{Re}(\mathbf{\Phi}(T,0))\big) = 1$$

By definition PCM is not the greatest real part of all the characteristic multipliers, but making PCM the greatest one guarantees stable LCO, if one exists. This leads to the $\mathcal{F}$ equation

$$\mathcal{F}(T,A) - 1 = 0 \tag{4.12}$$

where $F(T,A)$ stands for PCM as a function of the expected LCO period ($T = \frac{2\pi}{\omega}$) and LCO amplitude (A). With preliminary analysis based on the numerical integration and DF analysis we have narrowed down the feasible range of T and A to about 3.0 to 4.5 seconds, and 10 to 15, respectively. The $\mathcal{F}$ equation for the simple rate saturated loop is in the right hand side of Figure 4.5. In addition, all the characteristic multipliers beyond the PCM are depicted in Figure 4.6 when PCM is equal to one. Since they are all within a unit circle in a complex plane, we may say that the T-A pairs in the PCM curve are all candidates for stable LCO parameters.

4.4 Switching Equation

As discussed in the previous chapter, Floquet analysis only provides one of the necessary conditions–the $\mathcal{F}$ equation 4.12, and this is inevitable because Floquet analysis is applied only to the perturbed linearized equation of motion evaluated at the periodic solution

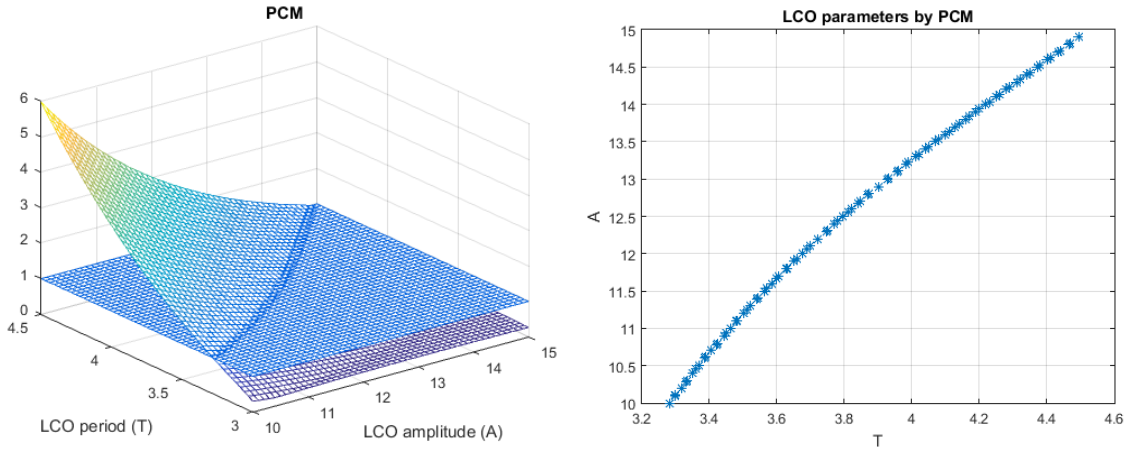

Figure 4.5: (a)(left)The PCM surface of a simple rate saturated loop along with a plane of height one. Each height of PCM surface stands for the PCM with respect to each pair of T and A. (b)(right)The curve of PCM in T-A plane obtained from the figure in the left hand side by collecting the intersection of PCM surface with a horizontal plane with height one.

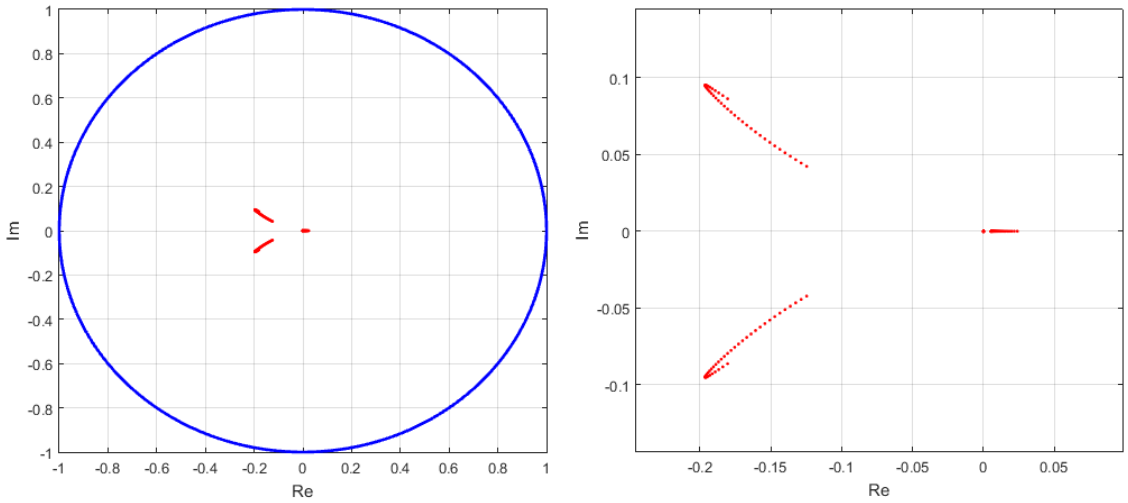

Figure 4.6: (a)(left)The characteristic multipliers other than PCM along the PCM curve of the right hand side figure of Figure 4.5. Note that they are all within a unit circle in a complex plane. (b)(right)The characteristic multipliers zoomed in around the origin.

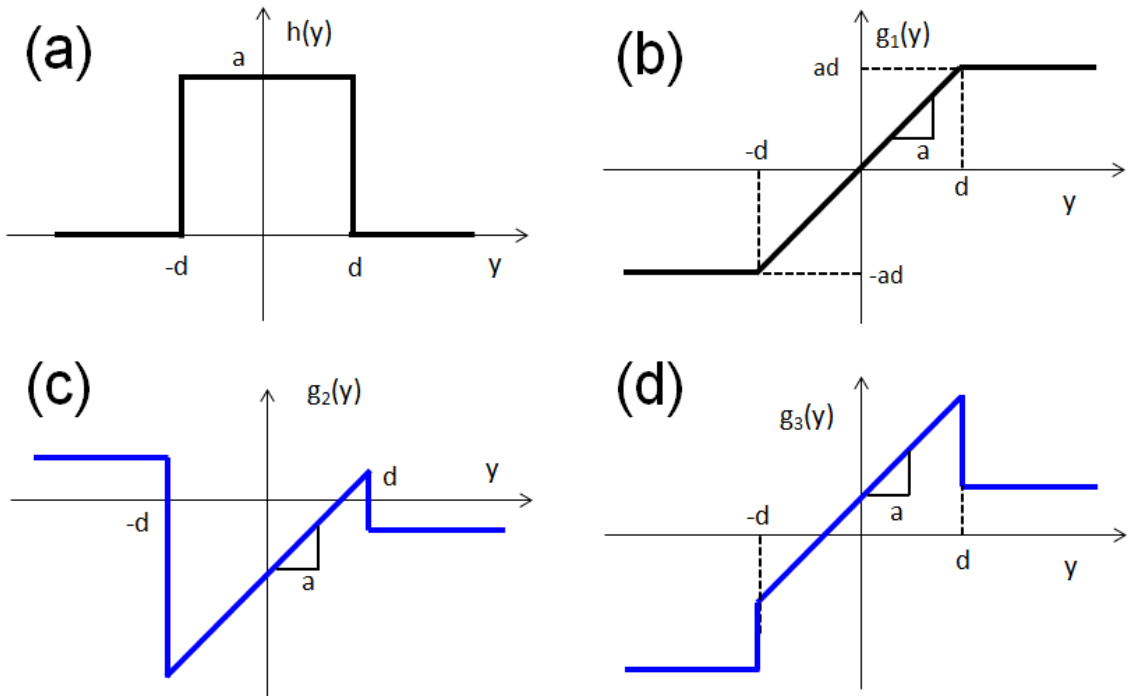

Figure 4.7: The nature of ambiguity in the reconstruction of a PN from its corresponding spatial derivative. In case of a saturation, the original PN g_1 of a spatial derivative h of figure (a) is in figure (b). However, the spatial derivatives of g_2 in (c) and g_3 in (d) are all identical to h as well.

$\boldsymbol{\eta}(t)$. To be more specific, $h(y)$, the spatial derivative of $g(y)$ contained in the coefficient matrix $\mathbf{D}(t)$ of Equation 4.10 of the perturbed LTP system 4.9 can possibly correspond to countlessly many different shapes of $g(y)$, because it is only a spatial derivative of $g(y)$ (Figure 4.7).

Therefore, another necessary condition needs to be one that describes the piecewise nonlinear behavior of PN in the original system. Although the simple rate saturated system can be analyzed as a general smooth nonlinear system as in Equation 4.5, it can also be modeled as a combination of linear systems, because depending on the input amplitude of

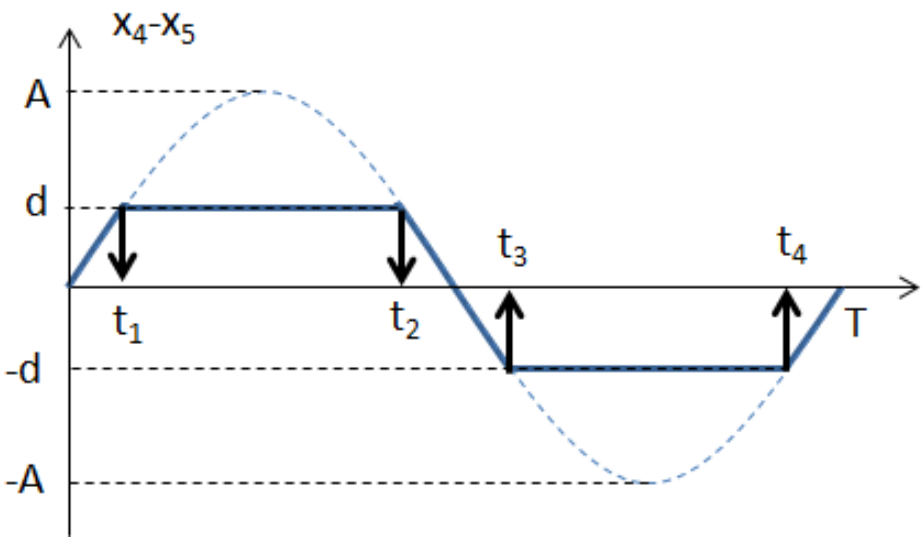

Figure 4.8: Input (dotted thin sinusoidal) and output (solid thick, and broken sinusoidal) of saturation in system of Fig.4.2. Sections $[t_1, t_2)$, $[0, t_1) \cup [t_2, t_3) \cup [t_4, T]$, and $[t_3, t_4)$ belong to the first, the second, and the third linear affine system in Equation 4.13, respectively.

the rate saturation the entire system is divided into three linear affine systems as follows.

$$\begin{aligned} \dot{\mathbf{x}_1}(t) &= \mathbf{A}_1\mathbf{x}_1(t) + \mathbf{D}_5, && g(\delta_c - \delta) = d \\ \dot{\mathbf{x}_1}(t) &= \mathbf{A}_2\mathbf{x}_1(t), && g(\delta_c - \delta) = \delta_c - \delta \\ \dot{\mathbf{x}_1}(t) &= \mathbf{A}_1\mathbf{x}_1(t) - \mathbf{D}_5, && g(\delta_c - \delta) = -d \end{aligned} \tag{4.13}$$

where

$$\mathbf{A}_1 = \begin{bmatrix} 0 & 1 & 0 & 0 & 0 \\ 0 & 0 & 1 & 0 & 0 \\ 0 & -5 & -2 & 0 & 1 \\ -5\frac{k_p}{\tau_p} & -6\frac{k_p}{\tau_p} & 0 & -\frac{1}{\tau_p} & 0 \\ 0 & 0 & 0 & 0 & 0 \end{bmatrix}, \mathbf{A}_2 = \begin{bmatrix} 0 & 1 & 0 & 0 & 0 \\ 0 & 0 & 1 & 0 & 0 \\ 0 & -5 & -2 & 0 & 1 \\ -5\frac{k_p}{\tau_p} & -6\frac{k_p}{\tau_p} & 0 & -\frac{1}{\tau_p} & 0 \\ 0 & 0 & 0 & 1 & -1 \end{bmatrix}, \mathbf{D}_5 = \begin{bmatrix} 0 \\ 0 \\ 0 \\ 0 \\ d \end{bmatrix} \tag{4.14}$$

Given that the input to the rate saturation is assumed to be approximately a plain sinusoidal signal as in Equation (4.6), the switching order between the linear systems is straightforward so that it yields the following.

Claim: The Switching Equation

$$\mathbf{x}_1(0) = -(\mathbf{E}+\mathbf{I})^{-1} e^{\mathbf{A}_2 t_d} \int_0^{\frac{T}{2}-2t_d} e^{\mathbf{A}_1 \tau} d\tau \mathbf{D}_5 \tag{4.15}$$

where $t_d = \frac{T}{2\pi} \sin^{-1}(\frac{d}{A})$ and

$$\mathbf{E} = e^{\mathbf{A}_2 t_d} e^{\mathbf{A}_1 (\frac{T}{2}-2t_d)} e^{\mathbf{A}_2 t_d}$$

Equation (4.15) is derived as follows. With Equation 4.13 and Figure 4.8, it is clear that

$$\begin{aligned}
\dot{\mathbf{x}_1}(t) &= \mathbf{A}_1 \mathbf{x}_1(t) + \mathbf{D}_5, && t \in [t_1, t_2) \\
\dot{\mathbf{x}_1}(t) &= \mathbf{A}_2 \mathbf{x}_1(t), && t \in [0, t_1) \cup [t_2, t_3) \cup [t_4, T] \\
\dot{\mathbf{x}_1}(t) &= \mathbf{A}_1 \mathbf{x}_1(t) - \mathbf{D}_5, && t \in [t_3, t_4)
\end{aligned}$$

Therefore,

$$\begin{aligned}
\mathbf{x}_1(t_1) &= e^{\mathbf{A}_2 t_1} \mathbf{x}_1(0) = e^{\mathbf{A}_2 t_d} \mathbf{x}_1(0), \\
\mathbf{x}_1(t_2) &= e^{\mathbf{A}_1 (t_2 - t_1)} \mathbf{x}_1(t_1) + \int_{t_1}^{t_2} e^{\mathbf{A}_1 (t_2 - \tau)} \mathbf{D}_5 d\tau \\
&= e^{\mathbf{A}_1 (\frac{T}{2} - 2t_d)} e^{\mathbf{A}_2 t_d} \mathbf{x}_1(0) + \int_{t_d}^{\frac{T}{2}-t_d} e^{\mathbf{A}_1 (\frac{T}{2} - t_d - \tau)} \mathbf{D}_5 d\tau, \\
\mathbf{x}_1(t_3) &= e^{\mathbf{A}_2 (t_3 - t_2)} \mathbf{x}_1(t_2) \\
&= e^{\mathbf{A}_2 2t_d} e^{\mathbf{A}_1 (\frac{T}{2} - 2t_d)} e^{\mathbf{A}_2 t_d} \mathbf{x}_1(0) + e^{\mathbf{A}_2 2t_d} \int_{t_d}^{\frac{T}{2}-t_d} e^{\mathbf{A}_1 (\frac{T}{2} - t_d - \tau)} \mathbf{D}_5 d\tau, \\
\mathbf{x}_1(t_4) &= e^{\mathbf{A}_1 (t_4 - t_3)} \mathbf{x}_1(t_3) - \int_{t_3}^{t_4} e^{\mathbf{A}_1 (t_4 - \tau)} \mathbf{D}_5 d\tau \\
&= e^{\mathbf{A}_1 (\frac{T}{2} - 2t_d)} e^{\mathbf{A}_2 2t_d} e^{\mathbf{A}_1 (\frac{T}{2} - 2t_d)} e^{\mathbf{A}_2 t_d} \mathbf{x}_1(0) + e^{\mathbf{A}_1 (\frac{T}{2} - 2t_d)} e^{\mathbf{A}_2 2t_d} \int_{t_d}^{\frac{T}{2}-t_d} e^{\mathbf{A}_1 (\frac{T}{2} - t_d - \tau)} \mathbf{D}_5 d\tau \\
&\quad - \int_{\frac{T}{2}+t_d}^{T-t_d} e^{\mathbf{A}_1 (T - \tau)} \mathbf{D}_5 d\tau
\end{aligned}$$

Finally,

$$\begin{aligned}\mathbf{x}_1(T) &= e^{\mathbf{A}_2(T-t_4)}\mathbf{x}_1(t_4) \\ &= e^{\mathbf{A}_2 t_d}e^{\mathbf{A}_1(\frac{T}{2}-2t_d)}e^{\mathbf{A}_2 2t_d}e^{\mathbf{A}_1(\frac{T}{2}-2t_d)}e^{\mathbf{A}_2 t_d}\mathbf{x}_1(0) \\ &+ e^{\mathbf{A}_2 t_d}e^{\mathbf{A}_1(\frac{T}{2}-2t_d)}e^{\mathbf{A}_2 2t_d}\int_{t_d}^{\frac{T}{2}-t_d} e^{\mathbf{A}_1(\frac{T}{2}-t_d-\tau)}\mathbf{D}_5 d\tau - e^{\mathbf{A}_2 t_d}\int_{\frac{T}{2}+t_d}^{T-t_d} e^{\mathbf{A}_1(t_4-\tau)}\mathbf{D}_5 d\tau\end{aligned}$$

Let's define $\mathbf{E} \equiv e^{\mathbf{A}_2 t_d}e^{\mathbf{A}_1(\frac{T}{2}-2t_d)}e^{\mathbf{A}_2 t_d}$, and since

$$\int_{t_d}^{\frac{T}{2}-t_d} e^{\mathbf{A}_1(\frac{T}{2}-t_d-\tau)}\mathbf{D}_5 d\tau = \int_{\frac{T}{2}+t_d}^{T-t_d} e^{\mathbf{A}_1(t_4-\tau)}\mathbf{D}_5 d\tau = \int_0^{\frac{T}{2}-2t_d} e^{\mathbf{A}_1\tau}d\tau\mathbf{D}_5,$$

And from the fact that $\mathbf{x}_1(T) = \mathbf{x}_1(0)$,

$$\mathbf{x}_1(0) = \mathbf{E}^2\mathbf{x}_1(0) + (\mathbf{E}-\mathbf{I})e^{A_2 t_d}\int_0^{\frac{T}{2}-2t_d} e^{\mathbf{A}_1\tau}d\tau$$

Because $\mathbf{E} = \mathbf{E}(A,T)$, $\mathbf{E} \neq \mathbf{I}$. Hence,

$$\mathbf{x}_1(0) = -(\mathbf{E}+\mathbf{I})^{-1}e^{\mathbf{A}_2 t_d}\int_0^{\frac{T}{2}-2t_d} e^{\mathbf{A}_1\tau}d\tau\mathbf{D}_5$$

Equation (4.15), along with the fact that $\mathbf{x}_{1,4}(0) - \mathbf{x}_{1,5}(0) = 0$, lead to another necessary condition on the LCO parameters, because $t_d = t_d(A, T(\omega))$.

$$\mathcal{S}(T,A) - 0 = 0 \tag{4.16}$$

where $S(T,A)$ stands for $\mathbf{x}_{1,4}(0) - \mathbf{x}_{1,5}(0)$ as a function of the expected LCO period ($T = \frac{2\pi}{\omega}$) and LCO amplitude (A). With preliminary analysis based on the numerical integration and DF analysis we have narrowed down the feasible range of T and A to about 3.0 to 4.5 seconds, and 10 to 15, respectively. The $\mathcal{S}$ equation for the simple rate saturated loop is in the right hand side of Figure 4.9.

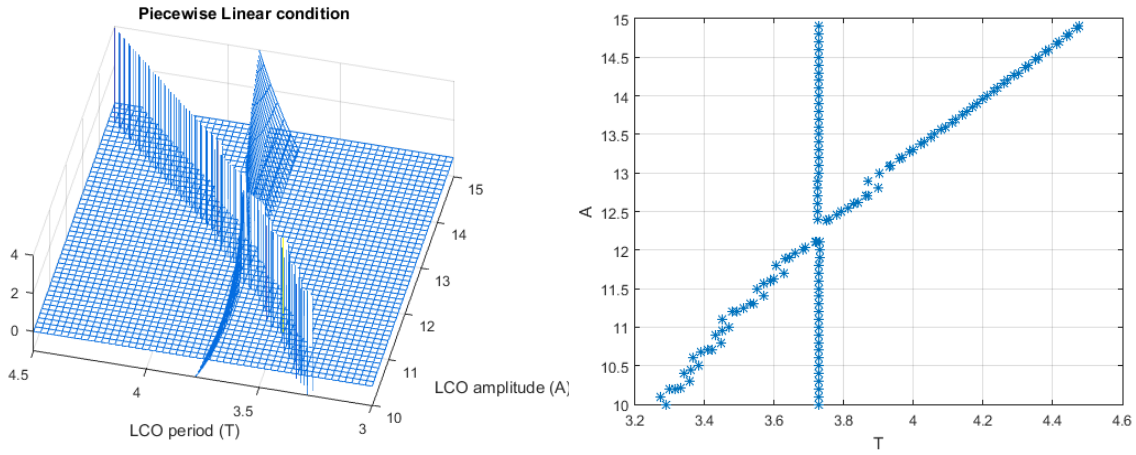

Figure 4.9: (a) (left) The $\mathbf{x}_{1,4}(0) - \mathbf{x}_{1,5}(0)$ surface of a simple rate saturated loop along with a plane of height zero. Each height of $\mathbf{x}_{1,4}(0) - \mathbf{x}_{1,5}(0)$ surface stands for the evaluation of $\mathbf{x}_{1,4}(0) - \mathbf{x}_{1,5}(0)$ with respect to each pair of T and A. (b) (right) The curve of $\mathbf{x}_{1,4}(0) - \mathbf{x}_{1,5}(0)$ in T-A plane obtained from the figure in the left hand side by collecting the intersection of the surface with a horizontal plane with height zero. The uneven curve that crosses T-A plane corresponds to the uneven surface in the left hand side figure, which shows a singular behavior between very large positive and negative values. Therefore the uneven curve is not reliable because of the inherent instability of its source–the singular curve.

4.5 Solving for T_{LCO} and A_{LCO}

Now we are ready to identify the LCO parameters. The two necessary conditions of F in Equation (4.12) and S in Equation (4.16) lead to the conclusion: $T_{LCO} = 3.7269$(sec) and $A_{LCO} = 12.216$. The results are depicted in $T - A$ plane shown in Fig.4.10, where T_{LCO} and A_{LCO} are the intersection between the two equations. In addition, since characteristic multipliers other than the PCM are all within unit circle, this LCO is stable (Table 4.1). For comparison, LCO parameters obtained from this chapter along with preliminary works are listed in Table 4.2. In addition, pros and cons of each method to detect the LCO parameters are listed in Table 4.3, although numerical integration and DF analysis are preliminary works.

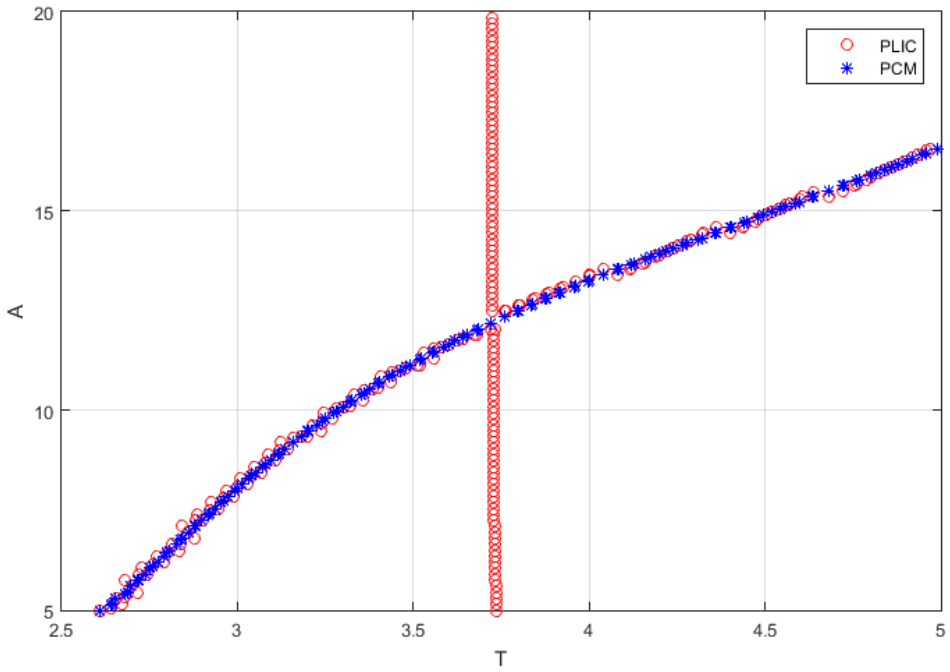

Figure 4.10: Equation (4.12) (blue stars) and Equation (4.16) (red circles) in A-T plane. The coordinates of the intersection between the two trajectories is T_{LCO} and A_{LCO}, respectively.

Table 4.1: Characteristic multipliers for the simple rate saturated system

1st	2nd	3rd	4th	5th
1.000	-0.195+0.093i	-0.195-0.093i	0.944e-2	9.794e-17

Table 4.2: LCO parameter identifications

	T_{LCO}	A_{LCO}
DF analysis	3.7045	12.375
Numerical Integration	3.7338	12.495
Floquet theory and Switching Function	3.7269	12.216

4.6 Application of LCO Analysis

4.6.1 The Least Upper Bound for Pilot Gain without LCO

A primary interest of control system designers lies in how to stabilize the system. Specifically, if it is a system with LCO such as the simple rate saturated loop, then we

Table 4.3: Comparison of methods to predict LCO

Methods	Pros	Cons
DF analysis	· Simple implementation · Reasonably accurate	· Inaccuracy in presence of multiple PNs · Inability to handle multi-harmonic terms
Numerical Integration	· Simple implementation · Intuitive to recognize LCO	· Inaccuracy due to various sources of error · Dependency on initial condition
Floquet theory and Switching Function	· Ability to analyze systems with multiple PNs · Simple stability analysis · Insights into switching sequence	· Complicated and time-consuming

typically would like to maintain the loop gain as high as possible while not inducing any adverse LCO or any instability. Therefore, the least upper bound of the loop gain, or the pilot gain (k_p) in case of the simple rate saturated loop, should be the one that is the largest with which the system is attracted to its stable equilibrium. With the state space representation of the rate saturated system in Equation 4.5 it is straightforward to find out that the only equilibrium is zero, but the stability of this equilibrium depends on k_p. In other words, up to a certain level of k_p the zero equilibrium is stable, but it becomes unstable beyond that.

In other words, the critical k_p that determines the stability of the zero equilibrium is about 1.5607 as shown in Figure 4.11. This suggests that even though there is no LCO the system can become unstable with k_p larger than 1.5607. Therefore 1.5607 is at least one of the upper bounds for the pilot gain k_p.

$$k_{c1} = 1.5607 \tag{4.17}$$

On the other hand, another upper bound of k_p can be determined through reasonings based

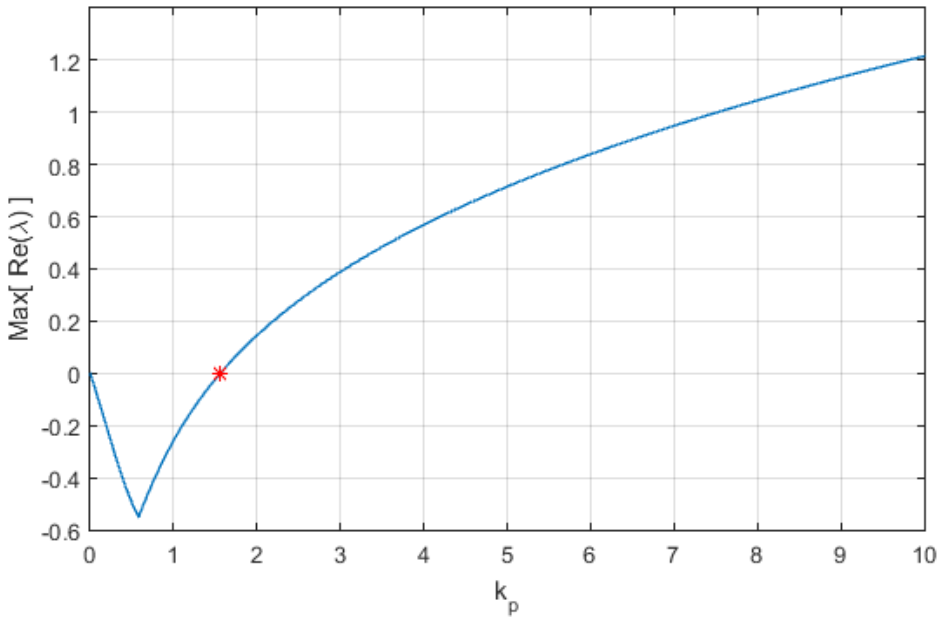

Figure 4.11: The maximum real part among the eigenvalues of Jacobian matrix evaluated at the zero equilibrium of the rate saturated system. The zero-crossing point(red star) is at $k_p = 1.560715$.

on the LCO analysis. We observe that, if the amplitude of the input signal to the saturation is less than the saturation value d, then LCO does not exist. As mentioned before, the absence of LCO does not necessarily mean that the system is stable, but at least this condition on the input amplitude leads to another upper bound of k_p. In other words, another upper bound or the critical gain k_{c2} for k_p should be the highest pilot gain that makes the system stay within a pure linear system of $\dot{\mathbf{x}}_1(t) = \mathbf{A}_2\mathbf{x}_1(t)$, or one that makes the amplitude of the input sinusoidal to the saturation equal to $d = \pm 1$, beyond which switching takes place. Hence, k_{c2} should satisfy

$$k_{c2} = \underset{k}{argmin}\big[\mathcal{F}_k(T,k) - 1 = 0\big] \tag{4.18}$$

The equation above is established from the $\mathcal{F}$ equation 4.12 with one of the unknown A replaced by k, since this time A is known ($A = A_c = d$). Similarly, another $\mathcal{S}$ equation is obtained from the switching equation 4.16 with A replaced by k. Since switching needs

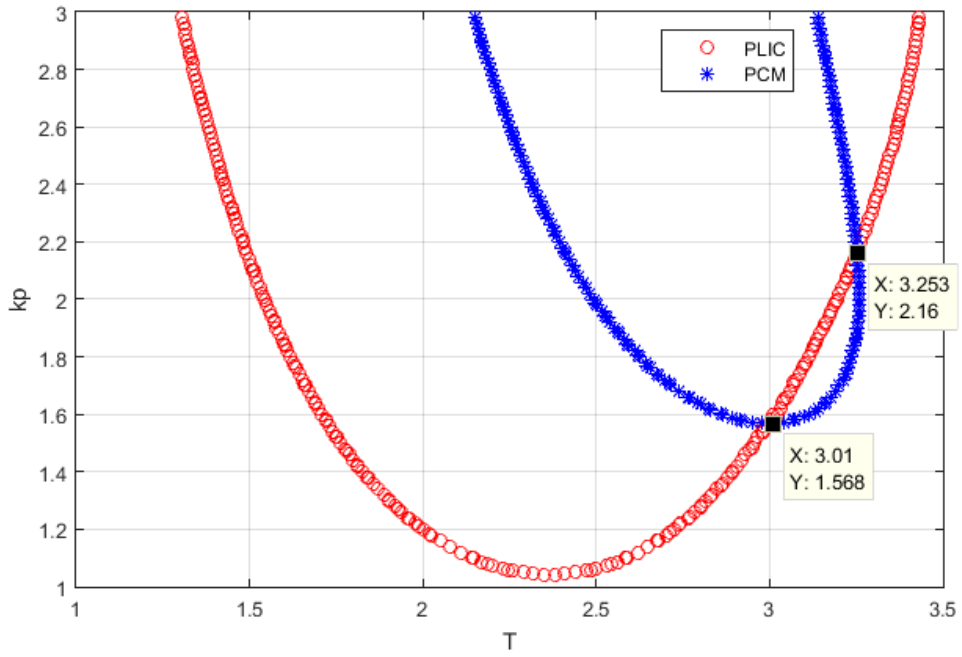

Figure 4.12: Equation (4.18) (blue stars) and Equation (4.19) (red circles) in T-k_p plane. The coordinates of the intersection between the two trajectories are k_c and T, respectively. Since k_c is the least upper bound, it is chosen to be about 1.568, not 2.16.

to take place, we assume $A_{LCO} = 1 + \epsilon_A$ where ϵ_A a very small positive real number.

$$k_{c2} = \underset{k}{argmin}\big[\mathcal{S}_k(T,k) - 0 = 0\big] \tag{4.19}$$

The result is shown in Figure 4.12. Considering that this figure depicts the condition in which LCO just exists, the true upper bound may be slightly lower than 1.568 for no LCO. Numerical integration results suggest that k_c is around 1.554, as shown in the Figure 4.13, since k_p slightly bigger than this would lead the system into an LCO. This holds even when we increase the simulation time to several thousand seconds.

$$k_{c2} = 1.568 \tag{4.20}$$

Therefore $k_c = k_{c1} = 1.5607$. However, considering very little difference between k_{c1} and k_{c2} we may conclude that the LCO begins to appear when the zero equilibrium becomes unstable.

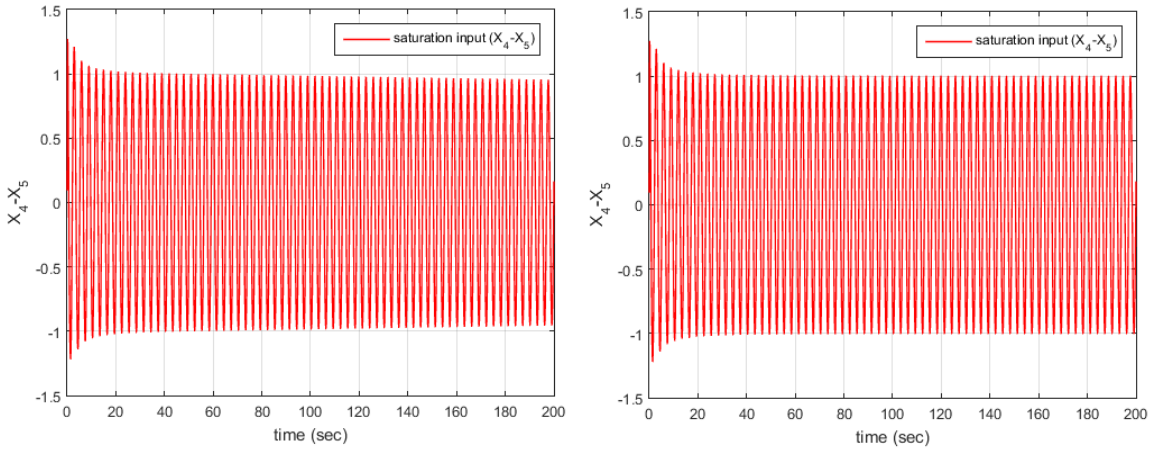

Figure 4.13: Numerical integration of a simple rate saturation loop with (a)(left)k_p=1.554 (b)(right)k_p=1.555. In figure (a) the system is converging very slowly to the zero equilibrium, while in (b) it circulates with constant amplitude (LCO).

4.6.2 LCO Frequency Modulation

Even in the presence of LCO, we are able to maintain the system performance through the change of the LCO frequency (period). If we send the LCO frequency to a higher band, the LCO amplitude can be reduced to an acceptable level because the linear system will attenuate the input signals in the high frequency domain just as a low-pass filter does. To this end, we design a lead compensator near a PN. How to design a linear compensator for the exact determination of the LCO frequency is presented in a companion paper [36]. To apply the design method to the rate saturated loop, we need to manipulate Equation 4.12 once again. For a typical linear compensator, the main parameters are τ and α. As in the following equation, however, one among α or τ_l is virtually the only parameter that we need to design [36].

$$\begin{aligned} L(s) &= \frac{\alpha\tau_l s + 1}{\tau_l s + 1}, \qquad \alpha > 1 \\ f_0 &= \frac{1}{2\pi\tau_l\sqrt{\alpha}}, \qquad T_d = 2\pi\tau_l\sqrt{\alpha} \end{aligned} \tag{4.21}$$

where $L(s)$ is the transfer function of a lead compensator, f_0 is the frequency at which the maximum amount of phase angle compensation takes place, and T_d is the desired period of LCO. The main drawback of a lead compensator is that it magnifies signals in the high

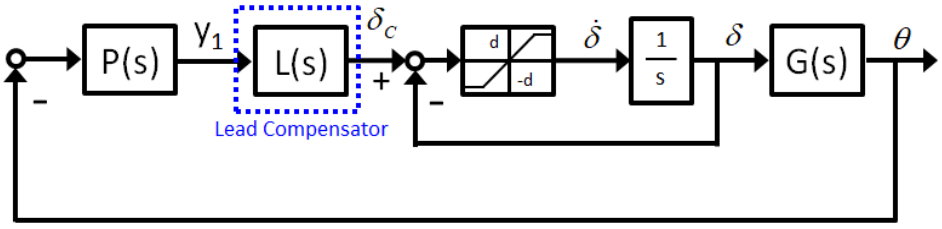

Figure 4.14: Rate saturation feedback system with a lead compensator.

frequency so that the system could become vulnerable to noise. However, we can take advantage of the fact that the saturation tends to cut the excessive amplitude magnification. Since a lead compensator is inserted in the loop shown in Fig.4.14, we need to construct a new state space representation accordingly. For the lead compensator, let

$$\begin{aligned} \dot{y_1} &= -\frac{k_p}{\tau_p}\mathbf{C}\mathbf{x} - \frac{1}{\tau_p}y_1 \\ \dot{\delta_c} &= -\alpha\frac{k_p}{\tau_p}\mathbf{C}\mathbf{x} + \Big(\frac{1}{\tau_l} - \frac{\alpha}{\tau_p}\Big)y_1 - \frac{\delta_c}{\tau_l} \end{aligned} \tag{4.22}$$

where y_1 is the output from the pilot model $P(s)$ and τ_l is a time constant for the lead compensator. Now we define a new state variable $\mathbf{x}_3 = [\mathbf{x}^T\, y_1\, \delta_c\, \delta]^T \in \mathbb{R}^6$. Then equation 4.22 along with equations 4.1 through 4.3 lead to

$$\dot{\mathbf{x}}_3 = \mathbf{f}_3(\mathbf{x}_3) = \begin{bmatrix} \mathbf{A}_3\mathbf{x}_2 + \mathbf{B}_3\delta \\ g(\delta_c - \delta) \end{bmatrix} \tag{4.23}$$

where

$$\mathbf{A}_3 = \begin{bmatrix} \mathbf{A} & \mathbf{O}_{3\times1} & \mathbf{O}_{3\times1} \\ -\frac{k_p}{\tau_p}\mathbf{C} & -\frac{1}{\tau_p} & 0 \\ -\frac{\alpha k_p}{\tau_p}\mathbf{C} & \frac{1}{\tau_l} - \frac{\alpha}{\tau_p} & -\frac{1}{\tau_l} \end{bmatrix}, \qquad \mathbf{B}_3 = \begin{bmatrix} \mathbf{B} \\ \mathbf{O}_{2\times1} \end{bmatrix}, \qquad \mathbf{x}_2 = \begin{bmatrix} \mathbf{x} \\ y_1 \\ \delta_c \end{bmatrix} \in \mathbb{R}^5 \tag{4.24}$$

in addition, the Jacobian matrix for equation 4.23 is

$$\mathbf{D}_3(t) = \begin{bmatrix} 0 & 1 & 0 & 0 & 0 & 0 \\ 0 & 0 & 1 & 0 & 0 & 0 \\ 0 & -5 & -2 & 0 & 0 & 1 \\ -5\frac{k_p}{\tau_p} & -6\frac{k_p}{\tau_p} & 0 & -\frac{1}{\tau_p} & 0 & 0 \\ -5\frac{\alpha k_p}{\tau_p} & -6\frac{\alpha k_p}{\tau_p} & 0 & \frac{1}{\tau_l} - \frac{\alpha}{\tau_p} & -\frac{1}{\tau_l} & 0 \\ 0 & 0 & 0 & 0 & h(t) & -h(t) \end{bmatrix} \tag{4.25}$$

where

$$h(t) = \frac{\partial g(\delta_c - \delta)}{\partial \delta_c} = \frac{1}{2}\Big(1 - \frac{\gamma(|\delta_c(t) - \delta(t)| - d)}{\sqrt{1 + (\gamma(|\delta_c(t) - \delta(t)| - d))^2}}\Big)$$

Now we apply the Floquet analysis and piecewise linear analysis to establish two necessary conditions to determine τ_l (or α) and A_{LCO}. With the new Jacobian matrix $\mathbf{D}_2$ we calculate PCM using an equation that is similar to Equation 4.11.

$$\mathbf{\Phi}(T, 0) = \Pi_{i=1}^{N} e^{\Delta \mathbf{D}_{3,i}}, \qquad \mathbf{D}_{3,i} = \frac{1}{\Delta} \int_{t_{i-1}}^{t_i} \mathbf{D}_3(\tau)\, d\tau$$

Since $\mathbf{\Phi}(T, 0)$ is a function of α and A, this leads to

$$F_\omega(\alpha, A) - 1 = 0 \tag{4.26}$$

In addition, switching equation is the same as Equation 4.15, but this time the coefficient matrices and affine terms are reconstructed as follows.

$$\begin{aligned} \dot{\mathbf{x}_3}(t) &= \mathbf{A}_{31}\mathbf{x}_3(t) + \mathbf{D}_{35}, && g(\delta_c - \delta) = d \\ \dot{\mathbf{x}_3}(t) &= \mathbf{A}_{32}\mathbf{x}_3(t), && g(\delta_c - \delta) = \delta_c - \delta \\ \dot{\mathbf{x}_3}(t) &= \mathbf{A}_{31}\mathbf{x}_3(t) - \mathbf{D}_{35}, && g(\delta_c - \delta) = -d \end{aligned} \tag{4.27}$$

where

$$\mathbf{A}_{31} = \begin{bmatrix} 0 & 1 & 0 & 0 & 0 & 0 \\ 0 & 0 & 1 & 0 & 0 & 0 \\ 0 & -5 & -2 & 0 & 0 & 1 \\ -5\frac{k_p}{\tau_p} & -6\frac{k_p}{\tau_p} & 0 & -\frac{1}{\tau_p} & 0 & 0 \\ -5\frac{\alpha k_p}{\tau_p} & -6\frac{\alpha k_p}{\tau_p} & 0 & \frac{1}{\tau_l} - \frac{1}{\tau_p} & -\frac{1}{\tau_l} & 0 \\ 0 & 0 & 0 & 0 & 0 & 0 \end{bmatrix}$$

$$\mathbf{A}_{32} = \begin{bmatrix} 0 & 1 & 0 & 0 & 0 & 0 \\ 0 & 0 & 1 & 0 & 0 & 0 \\ 0 & -5 & -2 & 0 & 0 & 1 \\ -5\frac{k_p}{\tau_p} & -6\frac{k_p}{\tau_p} & 0 & -\frac{1}{\tau_p} & 0 & 0 \\ -5\frac{\alpha k_p}{\tau_p} & -6\frac{\alpha k_p}{\tau_p} & 0 & \frac{1}{\tau_l} - \frac{1}{\tau_p} & -\frac{1}{\tau_l} & 0 \\ 0 & 0 & 0 & 0 & 1 & -1 \end{bmatrix}, \qquad \mathbf{D}_{35} = \begin{bmatrix} 0 \\ 0 \\ 0 \\ 0 \\ 0 \\ d \end{bmatrix} \tag{4.28}$$

Stepping on the same procedure as in the previous section we obtain another necessary condition from the switching equation.

$$S_\omega(\alpha, A) - 0 = 0 \tag{4.29}$$

Now, combining Equation 4.26 and 4.29 we obtain $\alpha = 20.80$ and $A_{LCO} = 16.16$ from the intersection of the two curves in Figure 4.15.

As a result we obtain $\tau_l = 0.0.0731$ and the integrated simulation of the lead compensated system shows that the LCO has changed so that its frequency $T = 2.094(sec)(\omega = 3.00(rad/s)$ (sec) and its amplitude of $A = 16.16$ (Fig.4.16). Characteristic multipliers at the new LCO are (1.000, 0.3069+0.3245i, 0.3069-0.3245i, 0.1987, -3.680e-12+1.198e-11i, -6.209e-12-1.198e-11i), implying that the new LCO is also a stable one. The LCO amplitude in terms of the physical output is the pitching angle of the aircraft (θ). By comparing

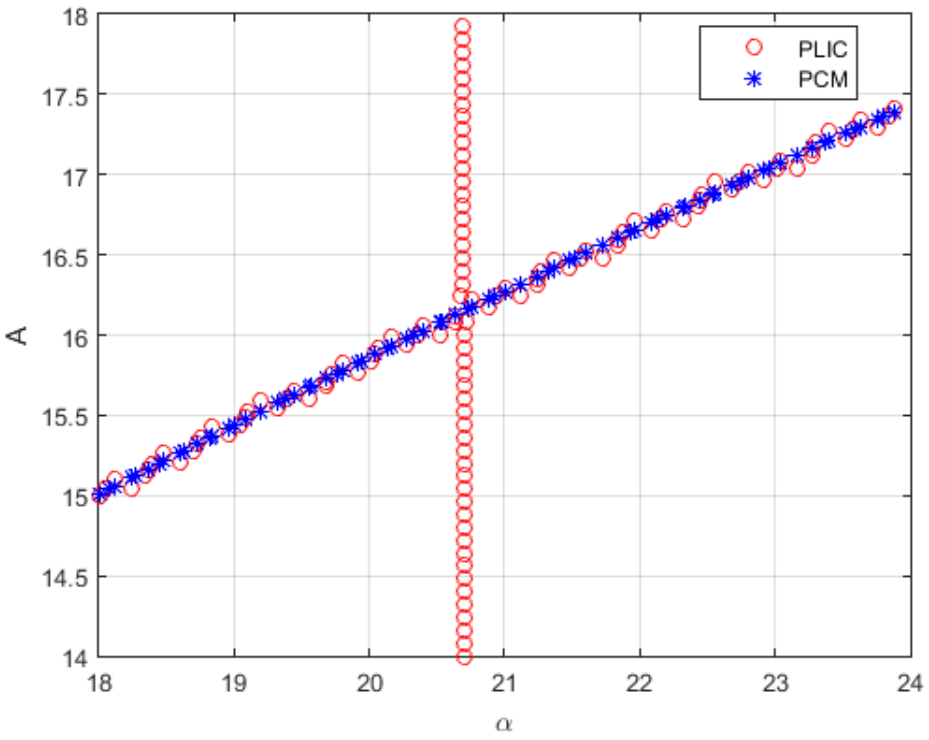

Figure 4.15: Equation (4.26) (blue stars) and Equation (4.29) (red circles) in α-A plane. The coordinates of the intersection between the two trajectories are α and A_{LCO}, respectively.

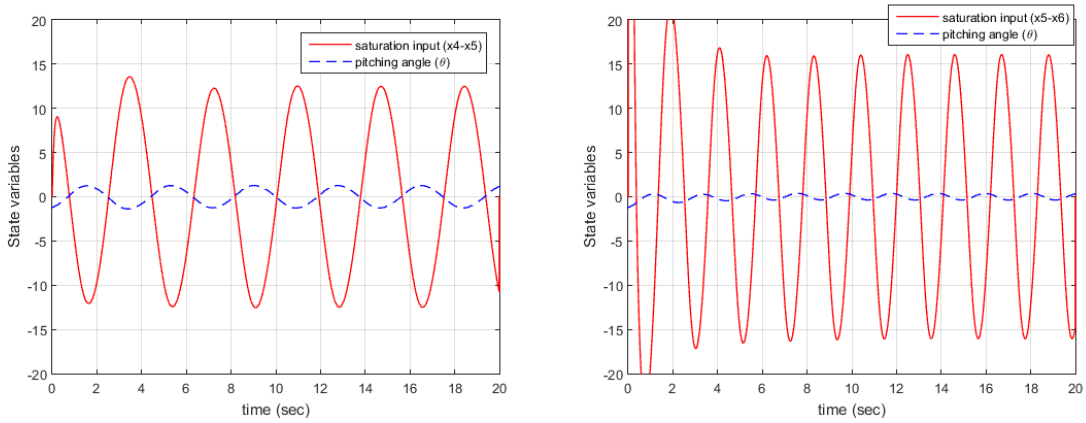

Figure 4.16: The integrated simulation of the rate saturated systems. (a) (left) the original system (b) (right) added lead compensation with $\alpha = 20.80$. Note that the LCO amplitude defined as the input amplitude to the saturation(solid red line in the figure below for each one) has increased, but the output of the airframe dynamics (pitching angle, θ, dashed blue line) has decreased.

the pitching angle in blue dashed line in Fig.4.16 along with table 4.4, it is clear that the lead compensation has effectively reduced the amplitude of LCO in pitching angle.

Table 4.4: LCO specifications before and after a lead compensation

	LCO frequency (rad/s)	LCO amplitude (rad)
Before compensation	1.685	1.271
After compensation	3.000	0.3799
+/-	78.04% increase	70.11% decrease

CHAPTER 5

ANALYSIS OF LCO IN THE PRESENCE OF MULTIPLE PNS

Analysis of LCO of a system that has more than one PN requires additional analytic considerations other than just the number of PNs and the degree of complexity of the system. Firstly, the assumption that the input signal to a PN is of unimodal sinusoidal shape may no longer be applied. This is exactly the case where there are more than two feedback loops in the system with each PN located in each loop, because the bandwidth of each loop may significantly differ. This difference leads to the different harmonics of frequency of the output sinusoidal of linear parts and therefore from the summing junction where those different harmonics are assimilated into one, the signal becomes multi-harmonic. Secondly, we need to take into account the difference of both amplitude and phase of the input signals to corresponding PNs. Since each input signal has gone through different linear parts before going into each PN, it is highly likely that each input signal would differ in amplitude and phase. Finally, there is the switching order. unlike the switching order for the system with a single PN, one with multiple PNs involves a number of possible cases depending on the expected LCO period and LCO amplitude. Therefore, we need to establish a switching order that is feasible for every possible combination of expected LCO period and LCO amplitude.

In this chapter we analyze a realistic example which requires one to resolve the special issues for the systems with multiple PNs mentioned above–the YF-12 flight control system. The basic procedure was introduced at the head of the previous chapter, but this time the procedure includes more, due to the multiple PNs. The detailed procedure is listed in Table 5.1.

Table 5.1: LCO Prediction Procedure

Steps	Detailed procedure
STEP1 Identify the system dynamics	a) Obtain the state space representation. b) Obtain the cascaded transfer function representation. c) Transform PNs into corresponding EAFs. d) Clarify the relative amplitude and phase between inputs to PNs. e) List all the linear affine systems that constitute the whole system.
STEP2 Approximate LCO parameters	f) Numerical integration with a) and c) g) DF analysis - Find or derive the DF for each PN. - Incorporate b) and d). h) Obtain the approximate range of T and A from f) and g).
STEP3 (part 1) Floquet theory	i) Assume an input signal model to a specific PN. j) For the LCO parameter range obtained in h), calculate PCM and obtain the PCM surface over T-A plane. k) Obtain the $\mathcal{F}$ equation from the intersection of the PCM surface and the horizontal plane of height one.
STEP3 (part 2) Switching Equation	l) Identify the feasible switch configuration by trying to prove the absolute stability of the Lur'e type system corresponding to each configuration. m) For feasible switching configurations, arrange the switching time in the phase-driven index system . n) Incorporate the phase-driven switching time index with d) and e) to build the switching equation. o) Obtain the initial phase condition from i) and incorporate in the switching equation to calculate the initial phase condition value (typically zero). p) Repeat from m) to o) for the range of the LCO parameters obtained in h) to yield the initial phase condition surface over T-A plane. q) Obtain the $\mathcal{S}$ equation from the intersection of the initial phase condition surface and the horizontal plane of height zero (typically).
Solve for T_{LCO} and A_{LCO}	r) Solve for T_{LCO} and A_{LCO} with the $\mathcal{F}$ equation from k) and the $\mathcal{S}$ equation from q). s) If the solution does not exist in r), go back to h), choose a more conservative range of T and A, and repeat i) through r).

Figure 5.1: Lockheed YF-12A [37].

5.1 YF-12 Flight Control System

YF-12 is a former model of the reconnaissance plane SR-71 back in 1970s and the flight test program was run by NASA [12]. The pilot of the program reported a pilot induced oscillation (PIO) depending on the fuel storage condition allegedly resulting from the aeroelasticity of airframe. The system diagram is in Figure 5.2 and the detailed specification of the system is in Equation 5.1 [12].

$$
\begin{aligned}
P(s) &= \frac{k_p}{\tau_p s + 1} \\
G_p(s) &= \frac{1}{s}\frac{6(s+0.8)}{s^2+1.5s+4} + \frac{5.17}{s^2+1.57s+246} \\
A(s) &= \frac{34}{s+34} \\
H(s) &= \frac{0.375s+3}{s+4} \\
G_h(s) &= \frac{6(s+0.8)}{s^2+1.5s+4}
\end{aligned}
\tag{5.1}
$$

where $P(s)$ is a pilot model, $A(s)$ an elevator actuator model, $G_p(s)$ and $G_h(s)$ transfer functions of the airframe, and $H(s)$ a lead-lag compensator of pitch rate feedback. Based

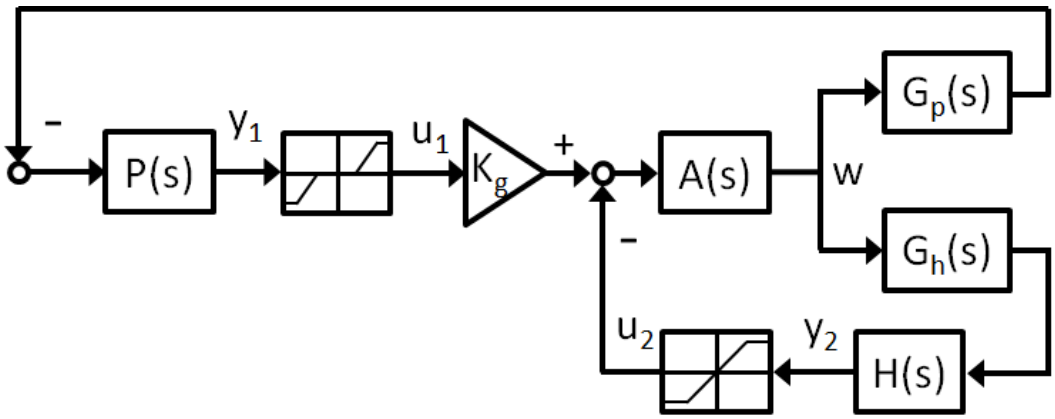

Figure 5.2: An analytic diagram of YF-12 flight control system of pitching axis. $H(s)$ in the feedback loop stands for a lead/lag filter of the stability augmentation system (SAS).

on the transfer functions, the state space model is established as follows.

$$\dot{\mathbf{x}}(t) = \mathbf{F}\mathbf{x}(t) + \mathbf{G}\boldsymbol{\phi}(\mathbf{H}\mathbf{x}(t)) \tag{5.2}$$

where

$$\mathbf{F} = \begin{bmatrix} -0.9 & 1.0 & 0 & 0 & 0 & 0.2 & 0 & 0 \\ -3.46 & -0.6 & 0 & 0 & 0 & k_6 & 0 & 0 \\ 0 & 1.0 & 0 & 0 & 0 & 0 & 0 & 0 \\ 0 & 0 & 0 & 0 & 1.0 & 0 & 0 & 0 \\ 0 & 0 & 0 & -246 & -1.57 & 5.17 & 0 & 0 \\ 0 & 0 & 0 & 0 & 0 & -34 & 0 & 0 \\ 0 & 0 & 1/\tau_p & 1/\tau_p & 0 & 0 & -1/\tau_p & 0 \\ 0 & 0.375 & 0 & 0 & 0 & 0 & 0 & -4.0 \end{bmatrix} \tag{5.3}$$

$$\mathbf{G} = \begin{bmatrix} 0 & 0 \\ 0 & 0 \\ 0 & 0 \\ 0 & 0 \\ 0 & 0 \\ 25.16 & 34 \\ 0 & 0 \\ 0 & 0 \end{bmatrix}, \qquad \mathbf{H} = \begin{bmatrix} 0 & 0 & 0 & 0 & 0 & 0 & -k_p & 0 \\ 0 & 3/8 & 0 & 0 & 0 & 0 & 0 & 4 \end{bmatrix}$$

where $k_6 = 5.99722$, $k_p = 20$, and $\tau_p = 0.1$. Pilot model parameters, k_p and τ_p, vary anytime during the operation but in this work we assume they are fixed ones. In addition, PNs are specified as below.

$$\boldsymbol{\phi}(\mathbf{Hx}(t)) = \boldsymbol{\phi}\Big(\begin{bmatrix} y_1 \\ y_2 \end{bmatrix} \Big) = \begin{bmatrix} g_1(y_1) \\ g_2(y_2) \end{bmatrix} \tag{5.4}$$

where $y_i = \mathbf{H}_i\mathbf{x}$, $i = 1, 2$ and PNs g_1 and g_2 are depicted in Figure 5.3.

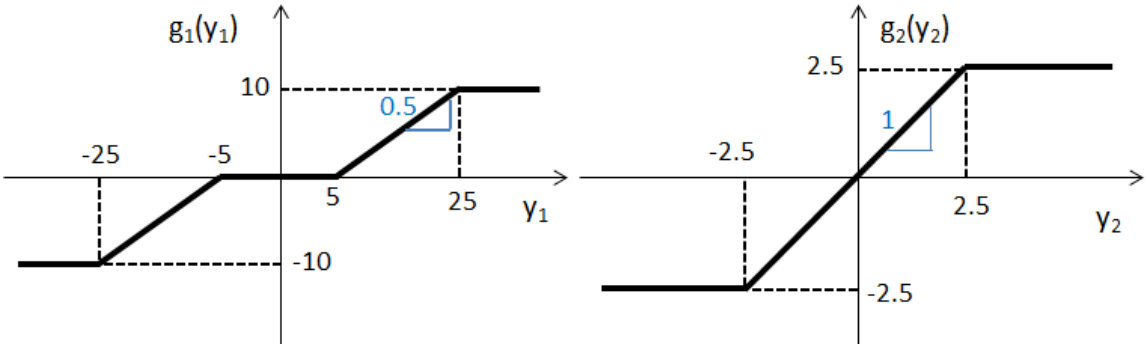

Figure 5.3: (a)(left)The first PN g_1 versus the input y_1. (b)(right)The second PN g_2 versus the input y_2.

And corresponding EAFs and their input-derivatives are as follows.

$$
\begin{aligned}
g_1(y_1) &= \frac{\text{sign}(y_1)}{4\gamma}\big[\big(\sqrt{1+(\gamma(|y_1|-d_5))^2}-\sqrt{1+(\gamma d_5)^2}\big) \\
&\quad -\big(\sqrt{1+(\gamma(|y_1|-d_{25}))^2}-\sqrt{1+(\gamma d_{25})^2}\big)\big] \\
h_1(y_1) &= \frac{dg_1}{dy_1} = \frac{1}{4}\big[\frac{\gamma(|y_1|-d_5)}{\sqrt{1+(\gamma(|y_1|-d_5))^2}}-\frac{\gamma(|y_1|-d_{25})}{\sqrt{1+(\gamma(|y_1|-d_{25}))^2}}\big] \\
g_2(y_2) &= \frac{1}{2}\big[y_2-\frac{\text{sign}(y_2)}{\gamma}\big(\sqrt{1+(\gamma(|y_2|-d_{2.5}))^2}-\sqrt{1+(\gamma d_{2.5})^2}\big)\big] \\
h_2(y_2) &= \frac{dg_2}{dy_2} = \frac{1}{2}\big[1-\frac{\gamma(|y_2|-d_{2.5})}{\sqrt{1+(\gamma(|y_2|-d_{2.5}))^2}}\big]
\end{aligned}
\tag{5.5}
$$

where $d_5 = 5$, $d_{25} = 25$, and $d_{2.5} = 2.5$. As shown in Figure 5.2, inputs of both the PNs are all coming after passing through a sufficient number of linear systems. Therefore we assume those inputs to be unimodal sinusoidal signals.

$$
\begin{aligned}
y_1(t) &= A_1\sin(\frac{2\pi}{T}t) = -k_p\mathbf{x}_7(t) \\
y_2(t) &= A_2\sin(\frac{2\pi}{T}t+\phi_{21}) = \frac{3}{8}\mathbf{x}_2(t)+4\mathbf{x}_8(t)
\end{aligned}
\tag{5.6}
$$

where A_1 and A_2 are the amplitudes of y_1 and y_2, respectively, and ϕ_{21} is the phase difference between y_2 and y_1. The relationship between the parameters of y_1 and y_2 is clarified

by the transfer function reasoning as below.

$$\frac{Y_2(i\omega)}{Y_1(i\omega)} = \frac{Y_2(i\omega)}{W(i\omega)}\frac{W(i\omega)}{Y_1(i\omega)} = \frac{H(i\omega)G_h(i\omega)}{P(i\omega)G_p(i\omega)}$$

where $Y_1(i\omega)$, $Y_2(i\omega)$, and $W(i\omega)$ are the frequency responses of y_1, y_2, and w in Figure 5.2, respectively, and $\omega = 2\pi/T$. Therefore we have

$$M_{12}(T) = \frac{A_2}{A_1} = \left|\frac{H(i\omega)G_h(i\omega)}{P(i\omega)G_p(i\omega)}\right| \qquad \text{and} \qquad \phi_{21}(T) = \angle\arg\left(\frac{H(i\omega)G_h(i\omega)}{P(i\omega)G_p(i\omega)}\right) \quad (5.7)$$

5.2 Approximate Range of the LCO Parameters

Before conducting an exact analysis we need to obtain close approximations of the LCO parameters–LCO period T_{LCO} and LCO amplitude A_{LCO}, because the exact analyses require an approximate range of the candidates for T_{LCO} and A_{LCO}. Approximation includes numerical integration and DF analysis.

5.2.1 DF Analysis

With the basic approach in Chapter 3.6 of [5], we get approximate values for T_{LCO} and A_{LCO}. This necessary condition is based on the observation that every signal in the loop, i.e. y_1, u_1, y_2, and u_2 are all non-zero in the presence of an LCO (Figure 5.2).

$$\begin{aligned} u_1 &= N_1 y_1, \\ u_2 &= N_2 y_2, \\ y_1 &= -P(i\omega)G_p(i\omega)A(i\omega)(u_1 - u_2), \\ y_2 &= H(i\omega)G_h(i\omega)A(i\omega)(u_1 - u_2) \end{aligned}$$

where N_1 and N_2 are the DFs of g_1 and g_2, respectively.

$$N_1 = \begin{cases} \frac{1}{\pi}[\sin^{-1}(\frac{d_{25}}{A_1}) + (\frac{d_{25}}{A_1})\sqrt{1-(\frac{d_{25}}{A_1})^2} - \sin^{-1}(\frac{d_5}{A_1}) - (\frac{d_5}{A_1})\sqrt{1-(\frac{d_5}{A_1})^2}], & A_1 > d_{25} \\ \frac{1}{2} - \frac{1}{\pi}[\sin^{-1}(\frac{d_5}{A_1}) + (\frac{d_5}{A_1})\sqrt{1-(\frac{d_5}{A_1})^2}], & d_5 < A_1 \leq d_{25} \\ 0, & A_1 \leq d_5 \end{cases} \tag{5.8}$$

$$N_2 = \begin{cases} \frac{2}{\pi}[\sin^{-1}(\frac{d_{2.5}}{A_2}) + (\frac{d_{2.5}}{A_2})\sqrt{1-(\frac{d_{2.5}}{A_2})^2}], & A_2 > d_{2.5} \\ 1, & A_2 \leq d_{2.5} \end{cases}$$

where d_{25}, d_d, and $d_{2.5}$ are the saturation value for N_1, dead-band range of N_1, and the saturation value forN_2 respectively, and A_1 and A_2 are the amplitudes of y_1 and y_2 as sinusoidal signals, respectively. Thus,

$$Nz = 0, \qquad \text{where} \qquad N = \begin{bmatrix} 1 & -N_1 & 0 & 0 \\ 0 & 0 & 1 & -N_2 \\ HG_hA & 0 & -HG_hA & -1 \\ PG_pA & 1 & -PG_pA & 0 \end{bmatrix}, \qquad z = \begin{bmatrix} u_1 \\ y_1 \\ u_2 \\ y_2 \end{bmatrix} \tag{5.9}$$

Since z in the equation above is a non-trivial solution in the presence of an LCO, $det(N) = 0$. This leads to

$$N_2(A_2)H(i\omega)G_h(i\omega)A(i\omega) + N_1(A_1)P(i\omega)G_p(i\omega)A(i\omega) = -1 \tag{5.10}$$

Another assumption is that state variables are approximated as unimodal sinusoidal forms, therefore the Laplace variable s in all the linear transfer functions are all replaced by $i\omega$. Given the unimodal sinusoidal assumption, we can also clarify the relationship between A_1 and A_2 in Equation 5.7. From Equations 5.10 and 5.7, we see that there are three equations (amplitude and phase condition from Equation 5.10 and amplitude condition

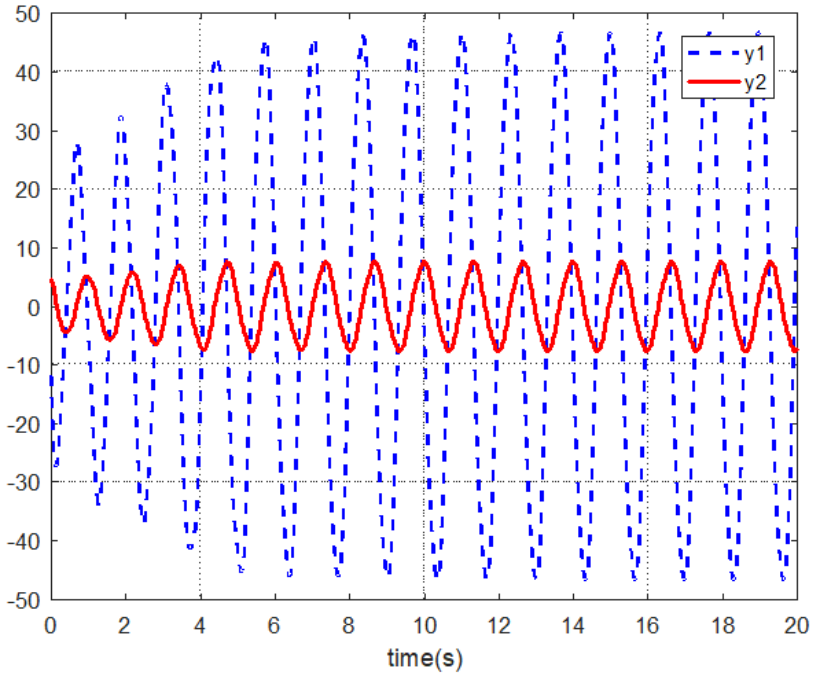

Figure 5.4: LCO of YF12 demonstrated with numerical integration. The dashed blue line is y_1 and the solid red one is y_2. The initial condition is x_0 = $[0\ 0\ 1.8\ 0\ 0\ 0\ 0.6\ 1.2]^T$.

from Equation 5.7) with three unknowns—A_1, A_2, and ω. A closed form solution for A_1, A_2, and ω is not available. A numerical solution found indicates that they are approximately $A_1 \approx 49.386$ (deg), $A_2 \approx 7.695$ (deg), and $\omega \approx 4.6480$ (deg/s), respectively. Therefore, $T_{LCO} \approx 1.352$ (sec) and $A_{LCO} \approx 49.386$ (deg). The details on how to solve Equation 5.10 are described in the Appendix C.

5.2.2 Numerical Integration

Even though we cannot fully trust the numerical integration as pointed out in Chapter 2, numerical integration is the easiest way of finding out how the system states are approximately behaving. For convenience and without loss of generality, we choose A_1 for A_{LCO}. With the appropriate initial condition, the YF-12 system shows a stable circulating behavior as shown in Figure 5.4 and we observe that $T_{LCO} \approx 1.318$ and $A_{LCO} \approx 45.426$.

5.3 Floquet Analysis

Assuming there is a periodic solution to this system, $\boldsymbol{\eta}(t)$, we linearize the equation of motion in Equation 5.2.

$$\dot{\delta\mathbf{x}}(t) = \mathbf{D}(t)\delta\mathbf{x}(t) = \frac{\partial \mathbf{f}}{\partial \mathbf{x}}\Big|_{\mathbf{x}=\boldsymbol{\eta}(t)} \delta\mathbf{x}(t) \tag{5.11}$$

where

$$\mathbf{D}(t) = \begin{bmatrix} -0.9 & 1.0 & 0 & 0 & 0 & 0.2 & 0 & 0 \\ -3.46 & -0.6 & 0 & 0 & 0 & k_6 & 0 & 0 \\ 0 & 1 & 0 & 0 & 0 & 0 & 0 & 0 \\ 0 & 0 & 0 & 0 & 1.0 & 0 & 0 & 0 \\ 0 & 0 & 0 & -246 & -1.57 & 5.17 & 0 & 0 \\ 0 & -\frac{51}{4}h_2(t) & 0 & 0 & 0 & -34 & -25.16k_p h_1(t) & -136h_2(t) \\ 0 & 0 & \frac{1}{\tau_p} & \frac{1}{\tau_p} & 0 & 0 & -\frac{1}{\tau_p} & 0 \\ 0 & 0.375 & 0 & 0 & 0 & 0 & 0 & -4.0 \end{bmatrix} \tag{5.12}$$

where $\delta\mathbf{x}$ is a linearized state variable vector around the LCO solution $\boldsymbol{\eta}(t)$ and $\mathbf{D}$ is a Jacobian matrix of the linearized system. Then we calculate the monodromy matrix $\boldsymbol{\Phi}(T, 0)$ for this LTP system.

$$\boldsymbol{\Phi}(T, 0) = \Pi_{i=1}^{N} e^{\Delta \mathbf{D}_i}, \qquad \mathbf{D}_i = \frac{1}{\Delta}\int_{t_{i-1}}^{t_i} \mathbf{D}(\tau)\, d\tau \tag{5.13}$$

Then we obtain the first equation based on the argument that PCM of the monodromy matrix is equal to a unity, because the magnitudes of other characteristic multipliers should be within a unit circle (sphere) to guarantee the stability of the LCO. Since the input derivatives h_1 and h_2 contain the sinusoidal form in the equation below, $\boldsymbol{\Phi}(T, 0)$ is a function of

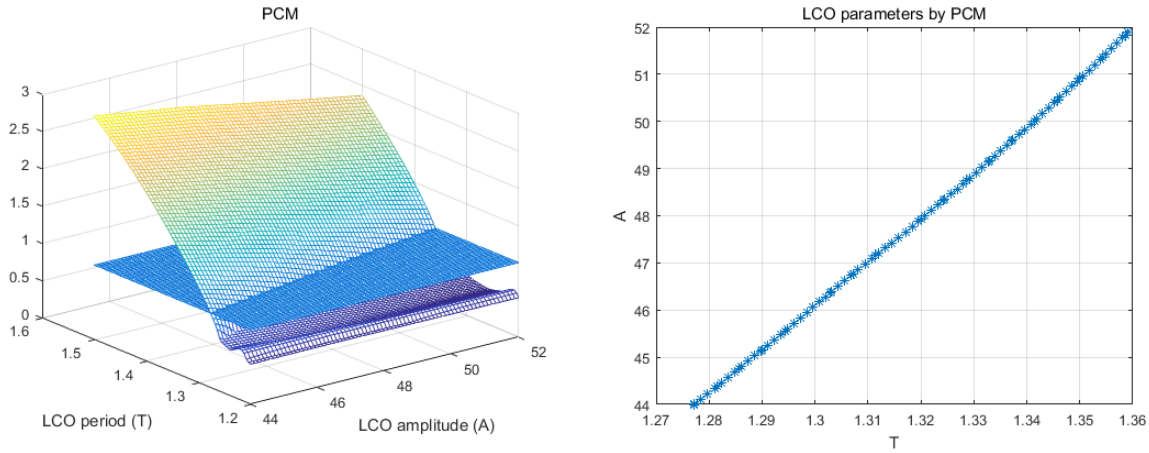

Figure 5.5: (a)(left)The PCM curve of YF-12 flight control system. Z-value represents PCM with respect to corresponding A and T. (b)(right)Intersection with PCM curve and the A-T plane. This represents the $\mathcal{F}$ equation 5.15

A and T. Equation 5.7, 5.6, and 5.5 lead to

$$h_1(A,T,t) = \frac{1}{4}\Big[\frac{\gamma(|A\sin(\frac{2\pi}{T}t)| - d_5)}{\sqrt{1+(\gamma(|A\sin(\frac{2\pi}{T}t)| - d_5))^2}} - \frac{\gamma(|A\sin(\frac{2\pi}{T}t)| - d_25)}{\sqrt{1+(\gamma(|A\sin(\frac{2\pi}{T}t)| - d_25))^2}}\Big]$$
$$h_2(A,T,t) = \frac{1}{2}\Big[1 - \frac{\gamma(|M_{12}(T)A\sin(\frac{2\pi}{T}t + \phi_{12}(T))| - d_{2.5})}{\sqrt{1+(\gamma(|M_{12}(T)A\sin(\frac{2\pi}{T}t + \phi_{12}(T))| - d_{2.5}))^2}}\Big] \tag{5.14}$$

Therefore, the relationship $PCM(\mathbf{\Phi}(T,0)) = 1$ leads to the $\mathcal{F}$ equation

$$\mathcal{F}(T,A) - 1 = 0 \tag{5.15}$$

The next step is to calculate the $\mathcal{F}$ equation through all the possible range of T_{LCO} and A_{LCO}. Fortunately, based on the approximation of LCO parameters in the previous section we have narrowed down their feasible range. If we fix the range as from 1.2 to 1.5 for T_{LCO} and 44 through to 52 for A_{LCO} then we obtain the $\mathcal{F}$ equation as depicted in Figure 5.5. Since the $\mathcal{F}$ equation is essentially a relationship between T_{LCO} and A_{LCO}, it is only one necessary condition. Therefore we need another one, a switching equation, through the piecewise linear analysis.

5.4 Switching Equation

The establishment of a switching equation involves multiple steps. Firstly, we need to identify the combination of partially bounded sectors associated with each PN. For example, if we assume the amplitude of y_1 is less than $d_5 = 5$ and the amplitude of y_2 is less than $d_{2.5} = 2.5$, we may assume g_1 as just a flat, zero valued PN and g_2 as a unity scalar gain. The next step is to verify what combinations of partial PNs are feasible as a switching order in the presence of an LCO. The verification will be based on the analysis of the relationship between y_1 and y_2 and the proof of absolute stability of the system with each combination of partial PNs. Once the feasible combinations are confirmed we identify the switching order. Unlike the system with a single PN, one with multiple PNs involves a number of possibilities depending on the expected T_{LCO} and A_{LCO}, because the relative amplitude and phase between y_1 and y_2 depend on T_{LCO} and A_{LCO}, as in Equation 5.7. The final stage is to build up a switching equation for each range of T_{LCO} and A_{LCO} of interest, in which for a single combination of them a single switching equation is assigned. The group of switching equations, along with corresponding rules on initial conditions, are the $\mathcal{S}$ equation for the identification of LCO.

5.4.1 Switching Feasiblity

Depending on A_1 and A_2, switching in a certain region or direction may or may not happen in the presence of LCO. The possible switchings in a single PN, in combination with the possible switchings in other PNs form a finite number of switching combinations shown in Table 5.2 for the YF-12 example. Each combination has its own state space representation.

Table 5.2: Switching combinations for g_1 and g_2 in YF-12 flight control system and corresponding state space representations.

g_1 / g_2	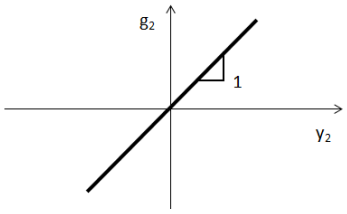	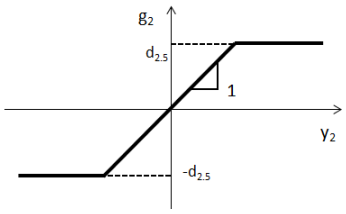
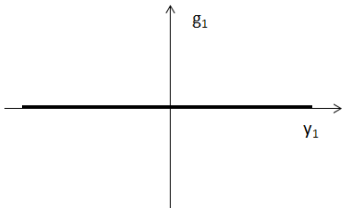	(NO LCO, Pure linear system)	$\dot{\mathbf{x}}(t) = \mathbf{F}_2\mathbf{x}(t) + \mathbf{G}_2\boldsymbol{\phi}(\mathbf{H}_2\mathbf{x}(t))$
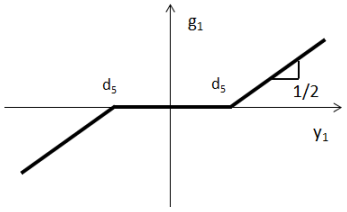	$\dot{\mathbf{x}}(t) = \mathbf{F}_3\mathbf{x}(t) + \mathbf{G}_3\boldsymbol{\phi}(\mathbf{H}_3\mathbf{x}(t))$	$\dot{\mathbf{x}}(t) = \mathbf{F}_4\mathbf{x}(t) + \mathbf{G}_4\boldsymbol{\phi}(\mathbf{H}_4\mathbf{x}(t))$
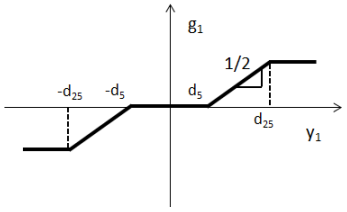	$\dot{\mathbf{x}}(t) = \mathbf{F}_5\mathbf{x}(t) + \mathbf{G}_5\boldsymbol{\phi}(\mathbf{H}_5\mathbf{x}(t))$	$\dot{\mathbf{x}}(t) = \mathbf{F}_6\mathbf{x}(t) + \mathbf{G}_6\boldsymbol{\phi}(\mathbf{H}_6\mathbf{x}(t))$

Starting from system two in Table 5.2, we have

$$\begin{aligned} &\mathbf{F}_2 = \mathbf{F} \\ &\mathbf{G}_2 = \begin{bmatrix} 0 & 0 & 0 & 0 & 0 & -34 & 0 & 0 \end{bmatrix}^T \quad \mathbf{H}_2 = \begin{bmatrix} 0 & \frac{3}{8} & 0 & 0 & 0 & 0 & 0 & 4 \end{bmatrix} \end{aligned} \tag{5.16}$$

where $\mathbf{F}$ is from Equation 5.2. If we succeed in proving that the system 5.16 is absolutely stable, we may say that there is no LCO in this system. This is because, according to the definition of the absolute stability of Lur'e type system in Definition 2.4, the absolute stability implies the global asymptotic stability towards the zero equilibrium. To this end, we need to

1. find its equilibriums and prove its stability

2. show the transfer function $M(i\omega)$ (Equation 2.21) is positive real (PR), or find a solution to Equation 2.26 (positive definite matrix **P**) in conjunction with Equation 2.27

Claim: The following Lur'e type system corresponding to the switching configuration two in Table 5.2 is absolutely stable.

$$\dot{\mathbf{x}}(t) = \mathbf{F}_2\mathbf{x}(t) + \mathbf{G}_2\boldsymbol{\phi}(\mathbf{H}_2\mathbf{x}(t))$$

where $\mathbf{F}_2$, $\mathbf{G}_2$, and $\mathbf{H}_2$ are in Equation 5.16, and $\boldsymbol{\phi}(\mathbf{H}_2\mathbf{x}(t)) = g_2(\frac{3}{8}\mathbf{x}_2(t) + 4\mathbf{x}_8(t))$.

Proof. To find the equilibrium, we solve the following algebraic equation

$$\mathbf{F}_2\mathbf{x}_e + \mathbf{G}_2\boldsymbol{\phi}_2(\mathbf{H}_2\mathbf{x}_e) = 0$$

Firstly we assume that $\mathbf{x}_e \in \mathbb{N}(\mathbf{F}_2)$. Then, $\mathbf{x}_e = k[0\ 0\ 1\ 0\ 0\ 0\ 1\ 0]$ with some real scalar k and $\mathbf{G}_2\boldsymbol{\phi}_2(\mathbf{H}_2\mathbf{x}_e) = 0$. Since $\mathbf{G}_2\boldsymbol{\phi}(\mathbf{H}_2\mathbf{x}_e) = g_2(\frac{3}{8}\mathbf{x}_{e2} + 4\mathbf{x}_{e8}) = 0$, the entire null space of $\mathbf{F}_2$ is an equilibrium set. Now assume $\mathbf{x}_e \notin \mathbb{N}(\mathbf{F}_2)$. Then

$$\begin{aligned}
-0.9\mathbf{x}_{e1} + \mathbf{x}_{e2} + 0.2\mathbf{x}_{e6} &= 0 \\
-3.46\mathbf{x}_{e1} - 0.6\mathbf{x}_{e2} + k_6\mathbf{x}_{e6} &= 0 \\
\mathbf{x}_{e2} = 0,\ \mathbf{x}_{e5} &= 0 \\
\mathbf{x}_{e6} - 34g_2(\frac{3}{8}\mathbf{x}_{e2} + 4\mathbf{x}_{e8}) &= 0 \\
-246\mathbf{x}_{e4} - 1.57\mathbf{x}_{e5} + 5.17\mathbf{x}_{e6} &= 0 \\
\mathbf{x}_{e3} + \mathbf{x}_{e4} - \mathbf{x}_{e7} &= 0 \\
\frac{3}{8}\mathbf{x}_{e2} - 4\mathbf{x}_{e8} &= 0
\end{aligned}$$

Then it directly follows that $\mathbf{x}_{e1} = \mathbf{x}_{e6} = \mathbf{x}_{e8} = 0$, and then $\mathbf{x}_{e4} = 0$. Therefore, the

equilibrium set is

$$\mathbf{x}_e = k[0\ 0\ 1\ 0\ 0\ 0\ 1\ 0] \text{ with } k \in \mathbb{R} \tag{5.17}$$

We now check the stability of this equilibrium. The Jacobian matrix around this equilibrium is

$$\mathbf{J}(\mathbf{x}_e) = \begin{bmatrix} -0.9 & 1.0 & 0 & 0 & 0 & 0.2 & 0 & 0 \\ -3.46 & -0.6 & 0 & 0 & 0 & k_6 & 0 & 0 \\ 0 & 1.0 & 0 & 0 & 0 & 0 & 0 & 0 \\ 0 & 0 & 0 & 0 & 1.0 & 0 & 0 & 0 \\ 0 & 0 & 0 & -246 & -1.57 & 5.17 & 0 & 0 \\ 0 & -\frac{51}{4}h_2(y_2(\mathbf{x}_e)) & 0 & 0 & 0 & -34 & 0 & -136h_2(y_2(\mathbf{x}_e)) \\ 0 & 0 & 1/\tau_p & 1/\tau_p & 0 & 0 & -1/\tau_p & 0 \\ 0 & 0.375 & 0 & 0 & 0 & 0 & 0 & -4.0 \end{bmatrix}$$

Since $y_2(\mathbf{x}_e) = 0$, $\mathbf{J}(\mathbf{x}_e) = \mathbf{F}$ and its eigenvalues are -4, -10, 0, -0.785$\pm$15.665i, -0.750$\pm$1.854i, -34. Therefore, the equilibrium is stable with only one mode marginally stable. Since we have nonzero equilibrium $\mathbf{x}_e$, we need to check the absolute stability of the following system with zero equilibrium, because proving the absolute stability based on PR and KYP lemma implies the absolute stability towards the zero equilibrium.

$$\frac{d}{dt}(\mathbf{x} - \mathbf{x}_e) = \mathbf{F}_2(\mathbf{x} - \mathbf{x}_e) + \mathbf{G}_2(\boldsymbol{\phi}_2(\mathbf{H}_2(\mathbf{x} - \mathbf{x}_e)))$$

or, equivalently

$$\dot{\mathbf{x}} = \mathbf{F}_2\mathbf{x} + \mathbf{G}_2(\boldsymbol{\phi}_2(\mathbf{H}_2\mathbf{x} - \mathbf{H}_2\mathbf{x}_e) + \boldsymbol{\phi}_2(\mathbf{H}_2\mathbf{x}_e))$$

Define $\boldsymbol{\psi}_2(\mathbf{H}_2\mathbf{x}) \equiv \boldsymbol{\phi}_2(\mathbf{H}_2\mathbf{x} - \mathbf{H}_2\mathbf{x}_e) + \boldsymbol{\phi}_2(\mathbf{H}_2\mathbf{x}_e)$ then $\boldsymbol{\psi}_2(\mathbf{H}_2\mathbf{x}) = \boldsymbol{\phi}_2(\mathbf{H}_2\mathbf{x})$ because $\mathbf{H}_2\mathbf{x}_e = 0$. Therefore, the equivalent zero equilibrium system is identical to the original system of configuration two, and $\boldsymbol{\psi}_2(\mathbf{H}_2\mathbf{x})$ should look like the one in Figure 5.6.

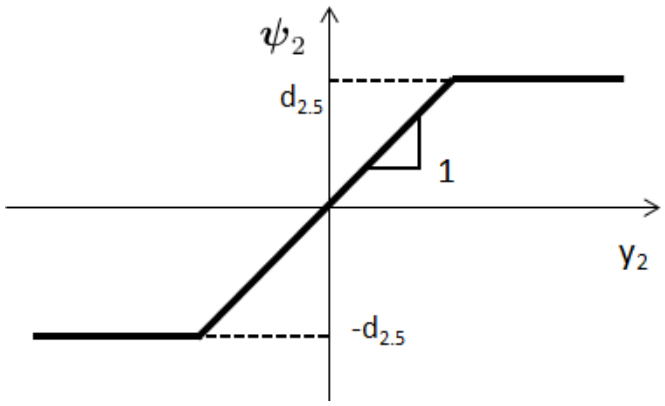

Figure 5.6: Input nonlinearity ψ_2 of the system of configuration two. Note that the output of this PN is bounded within a line of slope one and x (horizontal) axis.

Now we need to check if the piecewise linear system of this configuration is absolutely stable towards the stable equilibrium set obtained in Equation 5.17. If we succeed in proving that this system of the configuration above is absolutely stable, we are assured that there exists no LCO for this configuration, because the whole state space will be attracted to the the equilibrium set in Equation 5.17. The proof is done using either of the two methods, which are equivalent statements to each other: prove that the transfer function $M(i\omega)$ in Equation 2.21 that corresponds to the system 5.4.1 is positive real, or find a positive definite matrix $\mathbf{P}$ that satisfies Equation 2.26. Here, we try to find the matrix $\mathbf{P}$ in Equation 2.26, which is equivalent to the following LMI problem [38].

$$\mathbf{P} = \mathbf{P}^T > 0$$
$$\begin{bmatrix} \mathbf{F}_2^T\mathbf{P} + \mathbf{P}\mathbf{F}_2 & \mathbf{P}\mathbf{B}_2 - \mathbf{C}_2^T \\ \mathbf{B}_2^T\mathbf{P} - \mathbf{C}_2 & -\mathbf{D}_2\mathbf{D}_2^T \end{bmatrix} < 0$$

where $\mathbf{B}_2 = -\mathbf{G}_2$, $\mathbf{C}_2 = \mathbf{H}_2 + \mathbf{N}_2\mathbf{H}_2\mathbf{F}_2$, and $\mathbf{D}_2 = \mathbf{K}_2^{-1} + \mathbf{N}_2\mathbf{H}_2\mathbf{G}_2$ with $\mathbf{N}_2 = \alpha_{20} > 0$. $\mathbf{K}_2 = 1$ because the input nonlinearity ψ_2 is bounded by a line of slope one, as shown in

Figure 5.6. The solution to the LMI above exists when $\alpha_{20} = 0.3$ as follows.

$$\mathbf{P} = \begin{bmatrix} 3.7627 & 0.1166 & 20.7476 & 4.4360 & -0.5492 & -0.0248 & -20.7480 & -40.8084 \\ 0.1166 & 1.7172 & -22.5994 & -9.1178 & 0.5630 & -0.1367 & 22.5994 & 7.8081 \\ 20.7476 & -22.5994 & 761.5679 & 234.4392 & -19.5276 & 2.6095 & -761.5681 & -717.1517 \\ 4.4360 & -9.1178 & 234.4392 & 149.7104 & -5.8802 & 0.8263 & -234.4393 & -189.9813 \\ -0.5492 & 0.5630 & -19.5276 & -5.8802 & 0.8042 & -0.0856 & 19.5276 & 18.7723 \\ -0.0248 & -0.1367 & 2.6095 & 0.8263 & -0.0856 & 0.1416 & -2.6095 & -1.2440 \\ -20.7480 & 22.5994 & -761.5681 & -234.4393 & 19.5276 & -2.6095 & 761.5686 & 717.1530 \\ -40.8084 & 7.8081 & -717.1517 & -189.9813 & 18.7723 & -1.2440 & 717.1530 & 959.7637 \end{bmatrix}$$

Therefore by KYP lemma, the system with following transfer function $\mathbf{M}(i\omega)$ is PR.

$$\mathbf{M}(i\omega) = (\mathbf{I} + i\omega\mathbf{N}_2)\mathbf{J}_2(i\omega) + \mathbf{K}_2^{-1}$$

where

$$\mathbf{J}_2 \sim \left[\begin{array}{c|c} \mathbf{F}_2 & \mathbf{G}_2 \\ \hline \mathbf{H}_2 & \mathbf{0} \end{array}\right]$$

Hence, by the Popov criterion, the system of the switching configuration two is absolutely stable to its equilibrium of Equation 5.17. □

Therefore, we may say that the linear affine system of combination index 2 is globally absolutely stable towards its stable equilibrium in Equation 5.17, implying that no LCO can exist in this switching combination.

Likewise, we can check the switching feasibility for each of index from 3 to 6 in Table 5.2. Details on the feasibility check of all the combinations are described in Appendix B, but it is worth mentioning that the last index is the only one that cannot be proven to be PR. One of the necessary conditions to check the PR of a system is to check if the Nyquist plot of the transfer function $M(i\omega)$ (Equation 2.21) of the system is entirely in the right half

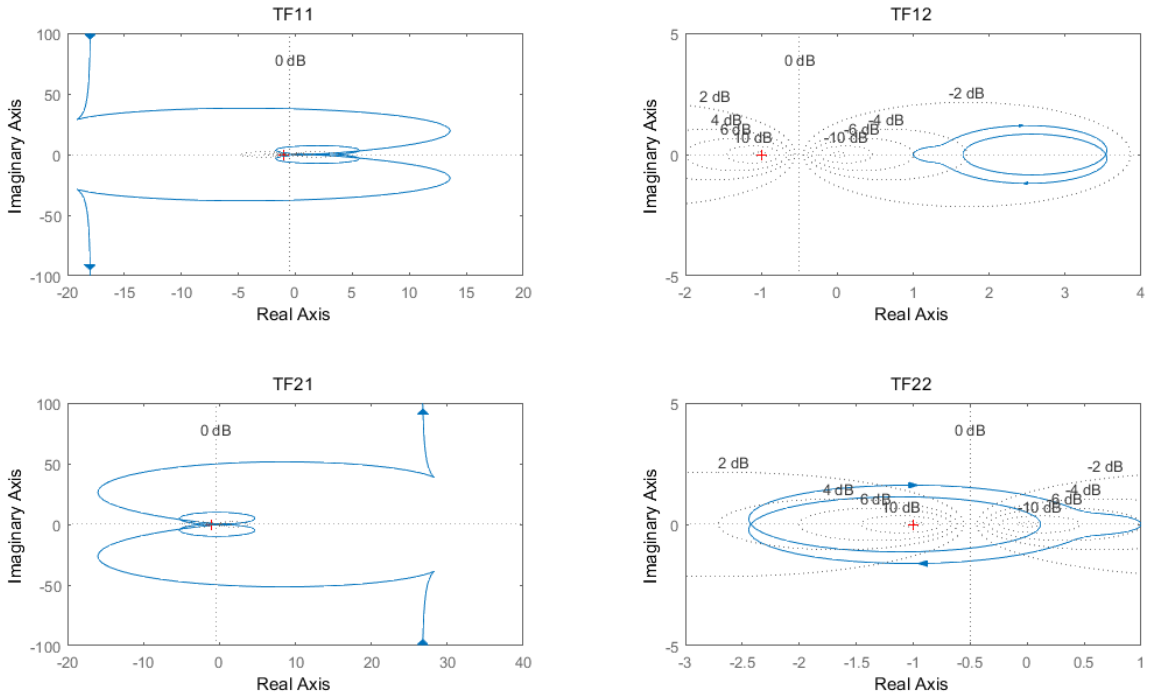

Figure 5.7: The Nyquist plot of the transfer function of **M** in Equation 5.18 with $\alpha_{20} = 0.3$ and $\mathbf{K}^{-1} = 1$.

complex plane [21]. In the case of the MIMO system, $M(i\omega)$ becomes

$$\mathbf{M}(s) = \left[(1 + \mathbf{N}s)\mathbf{H}(s\mathbf{I} - \mathbf{F})^{-1}\mathbf{G}\right] + \mathbf{K}^{-1} \tag{5.18}$$

where $\mathbf{N} = \begin{bmatrix} \alpha_1 & 0 \\ 0 & \alpha_2 \end{bmatrix}$, $\alpha_1 > 0,\ \alpha_2 > 0$, $\mathbf{K} = \begin{bmatrix} k_1 & 0 \\ 0 & k_2 \end{bmatrix}$, $k_1 = 0.5,\ k_2 = 1$, and with **F**, **G**, and **H** all in Equation 5.2. It is not difficult to show that for all $\alpha_1, \alpha_2 > 0$ and **K** we always find a part of the trajectory of **M** belonging to the left half complex plane in Figure 5.7. This implies that the matrix **P** that satisfies Equation 2.21 does not exist and therefore the combination six, or the original YF-12 flight control system is not globally absolutely stable towards its stable equilibrium. Hence the sixth combination in Table 5.2 is the only feasible switching configuration in which LCO can exist.

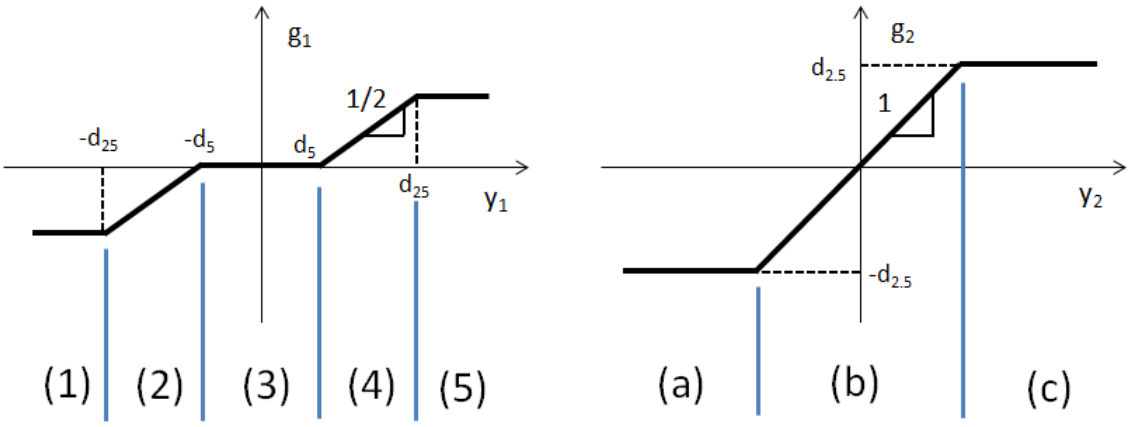

Figure 5.8: Linear or affine sections for g_1(left) and g_2(right).

5.4.2 Switching Order

In this subsection we find each of the switching orders depending on the pair of expected LCO parameters–T_{LCO} and A_{LCO}. This procedure is based on the results of the previous subsection that the YF-12 system needs the configuration with full PN segments (configuration six in Table 5.2) for any LCO to exist. We start from defining switching times for each PN. Define the linear or affine section each PN–ranging from (1) to (5) for g_1 and from (a) to (c) for g_2, as shown in Figure 5.8. In addition, since we proved that $A_1 > d_{25}$ and $A_2 > d_{2.5}$, the output signal versus the input sinusoidal to g_1 and g_2 should look like the Figure 5.9, where t_{ij} stands for the switching time that transits from linear affine section i to j. i and j could be 1,2,3,4, or 5 for g_1 and a,b, or c for g_2, respectively. The switching order in a single PN is straightforward– for g_1, it is (3)-(4)-(5)-(4)-(3)-(2)-(1)-(2)-(3) and for g_2 (b)-(c)-(b)-(a)-(b), assuming that the input signals start from the zero phase.

However, the initial phase is different for each PN, as we discussed about the phase difference between y_1 and y_2 in Equation 5.7. For the approximate range of T_{LCO} discussed in section 5.2, the frequency response looks like the one in the Figure 5.10. Therefore, the phase difference between y_1 and y_2 should also be taken into consideration when we sort the overall switching time in order. For example, if we want to calculate the switching

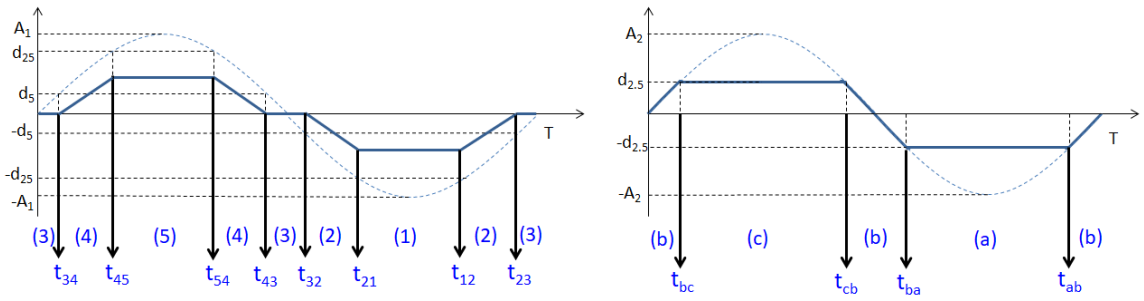

Figure 5.9: Switching time for g_1(left) and g_2(right).

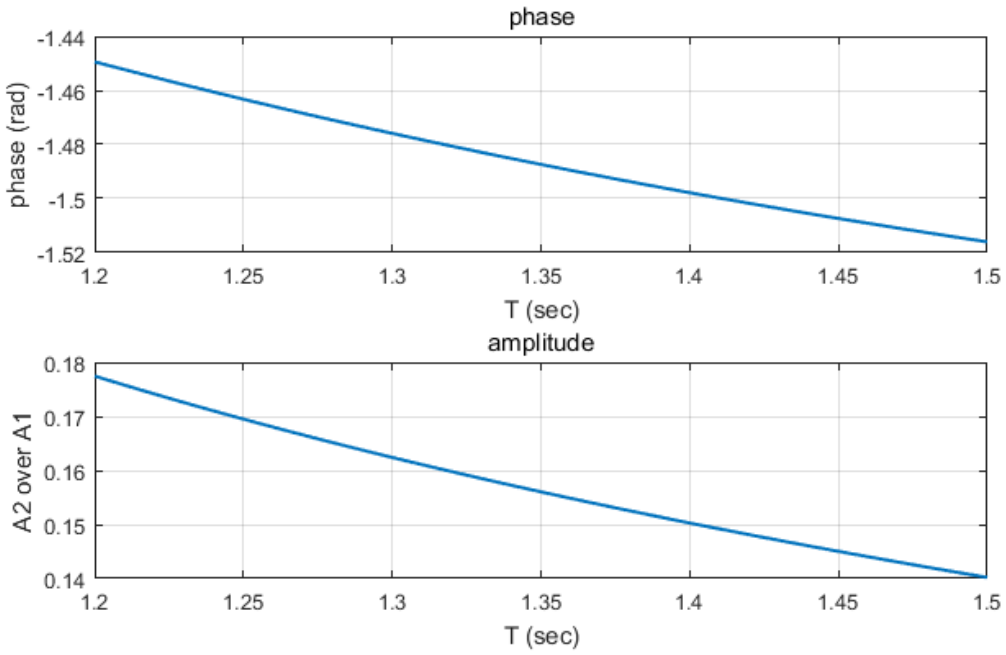

Figure 5.10: The frequency response of y_2 over y_1 over the expected LCO period range.

order at $T = 1.24$(sec) with which $\phi_{21} = -1.46$(rad), the absolute switching time of t_{bc} is $1.46\frac{1.24}{2\pi} + \sin^{-1}(\frac{d_{2.5}}{A_2})$. Likewise, all of the twelve switching times–t_{34}, t_{45}, t_{54}, t_{43}, t_{32}, t_{21}, t_{12}, t_{23}, t_{bc}, t_{cb}, t_{ba}, t_{ab} are calculated as below.

$$
\begin{aligned}
&t_{34} = \frac{T}{2\pi}\sin^{-1}(\frac{d_5}{A_1}),\ t_{45} = \frac{T}{2\pi}\sin^{-1}(\frac{d_{25}}{A_1}),\ t_{54} = \frac{T}{2} - t_{45} \\
&t_{43} = \frac{T}{2} - t_{34},\ t_{32} = \frac{T}{2} + t_{34},\ t_{21} = \frac{T}{2} + t_{45} \\
&t_{12} = T - t_{45},\ t_{23} = T - t_{34} \\
&t_{bc} = -\phi_{21}(T)\frac{T}{2\pi} + \frac{T}{2\pi}\sin^{-1}(\frac{d_{2.5}}{A_2}),\ t_{cb} = -\phi_{21}(T)\frac{T}{2\pi} + \frac{T}{2} - \frac{T}{2\pi}\sin^{-1}(\frac{d_{2.5}}{A_2}) \\
&t_{ba} = -\phi_{21}(T)\frac{T}{2\pi} + \frac{T}{2} + \frac{T}{2\pi}\sin^{-1}(\frac{d_{2.5}}{A_2}),\ t_{ab} = -\phi_{21}(T)\frac{T}{2\pi} + T - \frac{T}{2\pi}\sin^{-1}(\frac{d_{2.5}}{A_2})
\end{aligned}
\tag{5.19}
$$

5.4.3 Switching Equation

After calculating all the switching times we can sort the twelve switching times in an increasing order over the range of T and assign indexes from 1 to 12 in ascending order–τ_1, τ_2,. . . ,τ_{12}. Also, we define each linear affine system based on the combination of indexes. For example, if g_1 belongs to the section '1' and g_2 in section 'a' in Figure 5.8, respectively, the system index is '1a' as specified below.

$$
\dot{\mathbf{x}} = \mathbf{A}_{1a}\mathbf{x} + \mathbf{D}_{1a},\ \text{where}
$$

$$
\mathbf{A}_{1a} = \mathbf{F}, \qquad \mathbf{D}_{1a} = [0\ 0\ 0\ 0\ 0\ \ -166.6\ 0\ 0]^T
$$

Likewise, all linear affine systems are defined in Table 5.3. Once a switching order is established for a specific T and A pair extracted from the feasible ranges determined through the subsection 5.2, we now can construct the switching equation.

To help improve understanding of how the switching function is generated, a phase-driven index system needs to be introduced, as opposed to the linear system specific index system. The phase-driven index system is an index system that starts from one and in-

Table 5.3: Piecewise linear affine systems in YF-12 flight control system

Index($i-j$)	Specifications ($\dot{\mathbf{x}} = \mathbf{A}_{ij}\mathbf{x} + \mathbf{D}_{ij}$)
$1-a$	$\mathbf{A}_{1a} = \mathbf{F}$, $\mathbf{D}_{1a} = [0\ 0\ 0\ 0\ 0\ -166.6\ 0\ 0]^T$
$2-a$	$\mathbf{A}_{2a} = \mathbf{F}$ with $\mathbf{A}_{2a}(6,7) = -12.58k_p$, $\mathbf{D}_{2a} = [0\ 0\ 0\ 0\ 0\ 147.9\ 0\ 0]^T$
$3-a$	$\mathbf{A}_{3a} = \mathbf{F}$, $\mathbf{D}_{3a} = [0\ 0\ 0\ 0\ 0\ 85\ 0\ 0]^T$
$4-a$	$\mathbf{A}_{4a} = \mathbf{A}_{2a}$, $\mathbf{D}_{4a} = [0\ 0\ 0\ 0\ 0\ 22.1\ 0\ 0]^T$
$5-a$	$\mathbf{A}_{5a} = \mathbf{F}$, $\mathbf{D}_{5a} = [0\ 0\ 0\ 0\ 0\ 336.6\ 0\ 0]^T$
$1-b$	$\mathbf{A}_{1b} = \mathbf{F}$ with $\mathbf{A}_{1b}(6,2) = -\frac{51}{4}$, $\mathbf{A}_{1b}(6,8) = -136$, $\mathbf{D}_{1b} = [0\ 0\ 0\ 0\ 0\ -251.6\ 0\ 0]^T$
$2-b$	$\mathbf{A}_{2b} = \mathbf{F}$ with $\mathbf{A}_{2b}(6,2) = -\frac{51}{4}$, $\mathbf{A}_{2b}(6,7) = -12.58k_p$, $\mathbf{A}_{2b}(6,8) = -136$, $\mathbf{D}_{2b} = [0\ 0\ 0\ 0\ 0\ 62.9\ 0\ 0]^T$
$3-b$	$\mathbf{A}_{3b} = \mathbf{A}_{1b}$, $\mathbf{D}_{3b} = [0\ 0\ 0\ 0\ 0\ 0\ 0\ 0]^T$
$4-b$	$\mathbf{A}_{4b} = \mathbf{A}_{2b}$, $\mathbf{D}_{4b} = [0\ 0\ 0\ 0\ 0\ -62.9\ 0\ 0]^T$
$5-b$	$\mathbf{A}_{5b} = \mathbf{A}_{1b}$, $\mathbf{D}_{5b} = [0\ 0\ 0\ 0\ 0\ 251.6\ 0\ 0]^T$
$1-c$	$\mathbf{A}_{1c} = \mathbf{F}$, $\mathbf{D}_{1c} = [0\ 0\ 0\ 0\ 0\ -336.6\ 0\ 0]^T$
$2-c$	$\mathbf{A}_{2c} = \mathbf{A}_{2a}$, $\mathbf{D}_{2c} = [0\ 0\ 0\ 0\ 0\ -22.1\ 0\ 0]^T$
$3-c$	$\mathbf{A}_{3c} = \mathbf{F}$, $\mathbf{D}_{3c} = [0\ 0\ 0\ 0\ 0\ -85\ 0\ 0]^T$
$4-c$	$\mathbf{A}_{4c} = \mathbf{A}_{2a}$, $\mathbf{D}_{4c} = [0\ 0\ 0\ 0\ 0\ -147.9\ 0\ 0]^T$
$5-c$	$\mathbf{A}_{5c} = \mathbf{F}$, $\mathbf{D}_{5c} = [0\ 0\ 0\ 0\ 0\ 166.6\ 0\ 0]^T$

creases by one all the way up to twelve, representing the ascending order of phase across time during one period (T). Once the switching order of each linear system is fixed, the phase-driven index system takes over the existing linear system specific index order. For example, assume the switching time is as follows in increasing order.

$$t_{ab},\ t_{34},\ t_{45},\ t_{bc},\ t_{54},\ t_{43},\ t_{cb},\ t_{32},\ t_{21},\ t_{ba},\ t_{12},\ t_{23}$$

Then for each τ_i, the switching time of the phase-driven index is assigned from one to twelve from the sequence of switching times above.

$$\begin{aligned}&\tau_1 = t_{ab},\ \tau_2 = t_{34},\ \tau_3 = t_{45},\ \tau_4 = t_{bc},\ \tau_5 = t_{54},\ \tau_6 = t_{43},\ \tau_7 = t_{cb},\ \tau_8 = t_{32},\\ &\tau_9 = t_{21},\ \tau_{10} = t_{ba},\ \tau_{11} = t_{12},\ \tau_{12} = t_{23}\end{aligned} \tag{5.20}$$

Furthermore, we define a few more terms based on the phase-driven index. For all $i =$

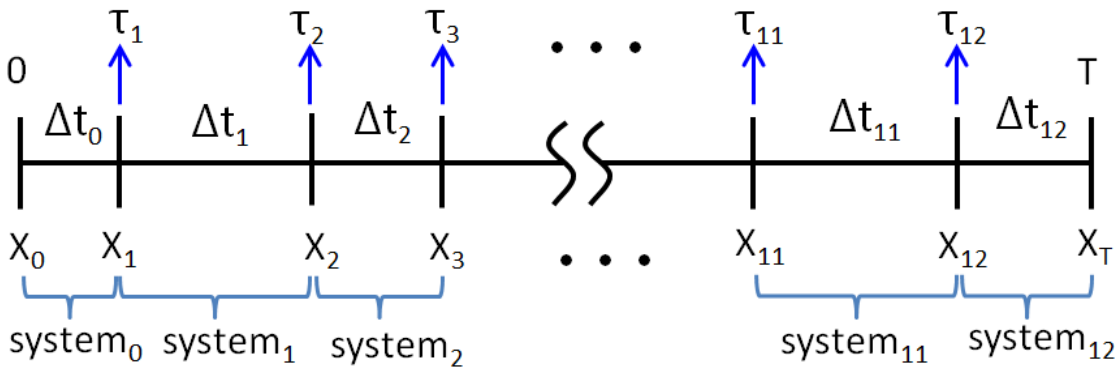

Figure 5.11: Definitions of switching time, system, and state variables based on the phase-driven index system. Times emphasized with blue arrow is the actual switching time. Time at zero and T represents just the start and end of a period. By definition, $\mathbf{x}_0 = \mathbf{x}_T$ and system$_0$=system$_{12}$.

$1, 2, \ldots, 12$,

$$\begin{aligned} \Delta t_i &\equiv \tau_{i+1} - \tau_i, \qquad i = 1, 2, \ldots, 11 (\Delta t_0 = \tau_1,\ \Delta t_{12} = T - \tau_{12}) \\ \mathbf{x}_i &\equiv \mathbf{x}(\tau_i), \qquad i = 1, 2, \ldots, 12,\ (\mathbf{x}_0 = \mathbf{x}(0),\ \mathbf{x}_T = \mathbf{x}(T)) \\ \text{system}_i &\equiv \text{a linear affine system representing each system during } \Delta t_i \end{aligned} \tag{5.21}$$

An illustration intuitively depicts all the definitions above in Figure 5.11.

Now we are ready to derive the switching equation. State transition from system$_i$ to system$_{i+1}$ is formulated by the standard solution of linear time invariant systems.

$$\mathbf{x}_{i+1} = e^{\mathbf{A}_i(\tau_{i+1}-\tau_i)}\mathbf{x}_i + \int_{\tau_i}^{\tau_{i+1}} e^{\mathbf{A}_i(\tau_{i+1}-\sigma)}\mathbf{D}_i d\sigma$$

in other words,

$$\mathbf{x}_{i+1} = e^{\mathbf{A}_i\Delta t_i}\mathbf{x}_i + \int_0^{\Delta t_i} e^{\mathbf{A}_i\tau} d\tau \mathbf{D}_i \tag{5.22}$$

Given this, the following claim will lead to the switching equation.

Claim: Recurrence equation:

$$
\begin{aligned}
\mathbf{x}_{i+n} &= \Big(\prod_{j=i+n-1}^{i} e^{\mathbf{A}_j \Delta t_j} \Big) \mathbf{x}_i + \int_0^{\Delta t_{i+n-1}} e^{\mathbf{A}_{i+n-1}\tau} d\tau \mathbf{D}_{i+n-1} \\
&\quad + \sum_{k=0}^{n-2} \Big[\Big(\prod_{l=n-1}^{k+1} e^{\mathbf{A}_{i+l}\Delta t_{i+l}} \Big) \int_0^{\Delta t_{i+k}} e^{\mathbf{A}_{i+k}\tau} d\tau \mathbf{D}_{i+k} \Big], && n > 2 \\
\mathbf{x}_{i+1} &= e^{\mathbf{A}_i \Delta t_i} \mathbf{x}_i + \int_0^{\Delta t_i} e^{\mathbf{A}_i \tau} d\tau \mathbf{D}_i, && n = 1 \\
\mathbf{x}_{i+2} &= e^{\mathbf{A}_{i+1}\Delta t_{i+1}} e^{\mathbf{A}_i \Delta t_i} \mathbf{x}_i + e^{\mathbf{A}_{i+1}\Delta t_{i+1}} \int_0^{\Delta t_i} e^{\mathbf{A}_i \tau} d\tau \mathbf{D}_i \\
&\quad + \int_0^{\Delta t_{i+1}} e^{\mathbf{A}_{i+1}\tau} d\tau \mathbf{D}_{i+1}, && n = 2
\end{aligned}
\tag{5.23}
$$

Proof. This claim is proven by a mathematical induction. The cases of $n = 1$ and $n = 2$ are straightforward. Then try to propagate from i to $i + 1$ in the equation above, then we obtain

$$
\begin{aligned}
\mathbf{x}_{i+n+1} &= e^{\mathbf{A}_{i+n}\Delta t_{i+n}} \mathbf{x}_{i+n} + \int_0^{\Delta t_{i+n}} e^{\mathbf{A}_{i+n}\tau} d\tau \mathbf{D}_{i+n} \\
&= \Big(e^{\mathbf{A}_{i+n}\Delta t_{i+n}} \prod_{j=1+n-1}^{i} e^{\mathbf{A}_j \Delta t_j} \Big) \mathbf{x}_i + \sum_{k=0}^{n-2} \Big[e^{\mathbf{A}_{i+n}\Delta t_{i+n}} \Big(\prod_{l=n-1}^{k+1} e^{\mathbf{A}_{i+l}\Delta t_{i+l}} \Big) \int_0^{\Delta t_{i+k}} e^{\mathbf{A}_{i+k}\tau} d\tau \mathbf{D}_{i+k} \Big] \\
&\quad + e^{\mathbf{A}_{i+n}\Delta t_{i+n}} \int_0^{\Delta t_{i+n-1}} e^{\mathbf{A}_{i+n-1}\tau} d\tau \mathbf{D}_{i+n-1} + \int_0^{\Delta t_{i+n}} e^{\mathbf{A}_{i+n}\tau} d\tau \mathbf{D}_{i+n} \\
&= \Big(\prod_{j=1+n}^{i} e^{\mathbf{A}_j \Delta t_j} \Big) \mathbf{x}_i + \int_0^{\Delta t_{i+n}} e^{\mathbf{A}_{i+n}\tau} d\tau \mathbf{D}_{i+n} + \sum_{k=0}^{n-1} \Big[\Big(\prod_{l=n}^{k+1} e^{\mathbf{A}_{i+l}\Delta t_{i+l}} \Big) \int_0^{\Delta t_{i+k}} e^{\mathbf{A}_{i+k}\tau} d\tau \mathbf{D}_{i+k} \Big]
\end{aligned}
$$

Therefore, Equation 5.23 holds also for $i + 1$. □

Now let $i = 0$ and $n = 12$ in Equation 5.23, then

$$
\mathbf{x}_{12} = \Big(\prod_{j=11}^{i} e^{\mathbf{A}_j \Delta t_j} \Big) \mathbf{x}_0 + \int_0^{\Delta t_{11}} e^{\mathbf{A}_{11}\tau} d\tau \mathbf{D}_{11} + \sum_{k=0}^{10} \Big[\Big(\prod_{l=11}^{k+1} e^{\mathbf{A}_l \Delta t_l} \Big) \int_0^{\Delta t_k} e^{\mathbf{A}_k \tau} d\tau \mathbf{D}_k \Big]
$$

Since $\mathbf{A}_0 = \mathbf{A}_{12}$ and $\mathbf{x}_0 = \mathbf{x}_T$, the switching equation for the LCO of YF-12 flight control

system is finally derived.

$$\mathbf{x}_0 = \Big[\mathbf{I} - \Big(\prod_{j=12}^{0} e^{\mathbf{A}_j \Delta t_j}\Big)\Big]^{-1} \Big[\int_0^{\Delta t_{12}} e^{\mathbf{A}_{12}\tau} d\tau \mathbf{D}_{12} + \sum_{k=0}^{11} \Big(\prod_{l=12}^{k+1} e^{\mathbf{A}_l \Delta t_l} \int_0^{\Delta t_k} e^{\mathbf{A}_k \tau} d\tau \mathbf{D}_k\Big)\Big] \tag{5.24}$$

Since the phase from zero to T is for y_1, $\mathbf{x}_0$ in the switching equation above has its phase identical to y_1. Therefore, according to the assumption of y_1 signal in Equation 5.6, $\mathbf{x}_0(7) = 0$ at phase zero. This initial phase condition plays for another necessary condition, the $\mathcal{S}$ equation, along with Equation 5.15.

$$\mathcal{S}(T, A) - 0 = 0 \tag{5.25}$$

The $\mathcal{S}$ equation can be visualized over the appropriate range of T and A and is depicted in the T-A plane in Figure 5.12. A blurred line on the right side of the solid line in the right part of Figure 5.12 comes from a part of the initial phase condition surface of $\mathbf{x}_0(7)$ in the left part of Figure 5.24. Unlike the smooth part, this blurred part is due to the singularity of the surface, i.e., the evaluation of $\mathbf{x}_0(7)$ oscillates so radically that we cannot guarantee the continuity of the surface around this part. Therefore, only the solid line is convincing and reliable for the $\mathcal{S}$ equation.

5.5 Determination of the LCO Parameters

Now that we have two necessary conditions (Equation 5.15 and 5.25) regarding two unknowns (T_{LCO} and A_{LCO}), we may determine them uniquely. Figure 5.13 depicts the two necessary conditions in the T-A plane so the intersection of the two solid curves should make the solution–T_{LCO}=1.327 (sec) and A_{LCO}=48.61 (deg). In Table 5.4 the results are summarized as to the LCO parameters for the YF-12 flight control system with different approaches. The characteristic multipliers at T_{LCO}=1.327 and A_{LCO}=48.61 are 1.000 (PCM), -0.1805$\pm$0.395i, 0.4806, 0.4469, 7.277e-3, 1.798e-7, and 9.873e-18, respectively,

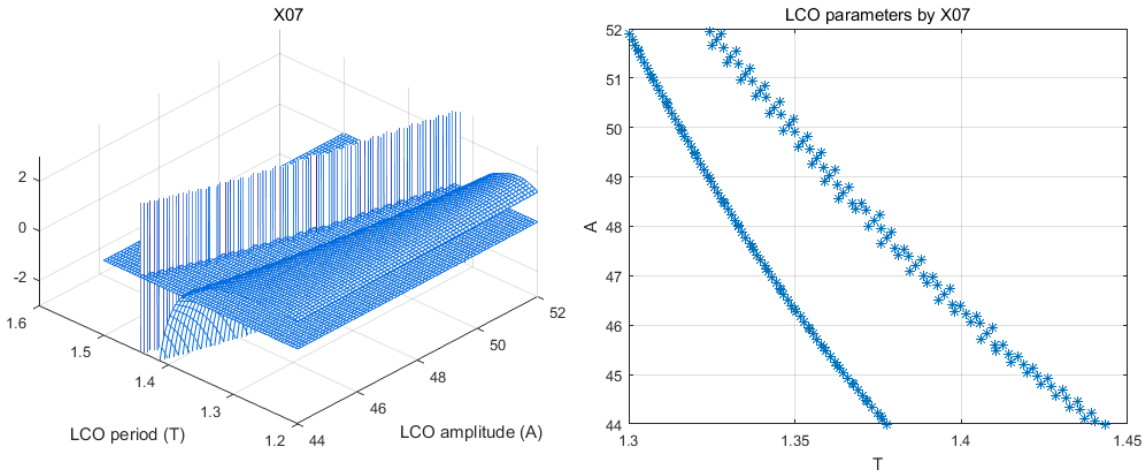

Figure 5.12: (a)(left)The initial phase condition surface of $\mathbf{x}_0(7)$ in T-A plane. (b)(right)Intersection of $\mathbf{x}_0(7)$ surface and the zero T-A plane.

hence we confirm this LCO is a stable one.

Table 5.4: LCO parameters estimation based on different methods.

	LCO period (sec)	LCO amplitude
Numerical Integration	1.312	44.31
DF analysis	1.352	49.39
Floquet theory with PL analysis	1.327	48.61

5.6 Dual Modal Sinusoidal as an Input to PN

All of the formulation for the identification of LCO parameters was based on the assumption that the LCO of input to each PN was of unimodal sinusoids in Equation 5.6. In reality, however, this assumption can fail, especially in a system where there are more than one summing junction within the loop or a transfer function through which the input signal passes before it gets into a PN, and the YF-12 flight control system example is no exception in this regard. When we perform the FFT over the numerically integrated y_1 signal in Figure 5.4, we can easily confirm that there is a prominent component in the frequency of about three times the LCO frequency, along with the main LCO harmonic component, as shown in Figure 5.14.

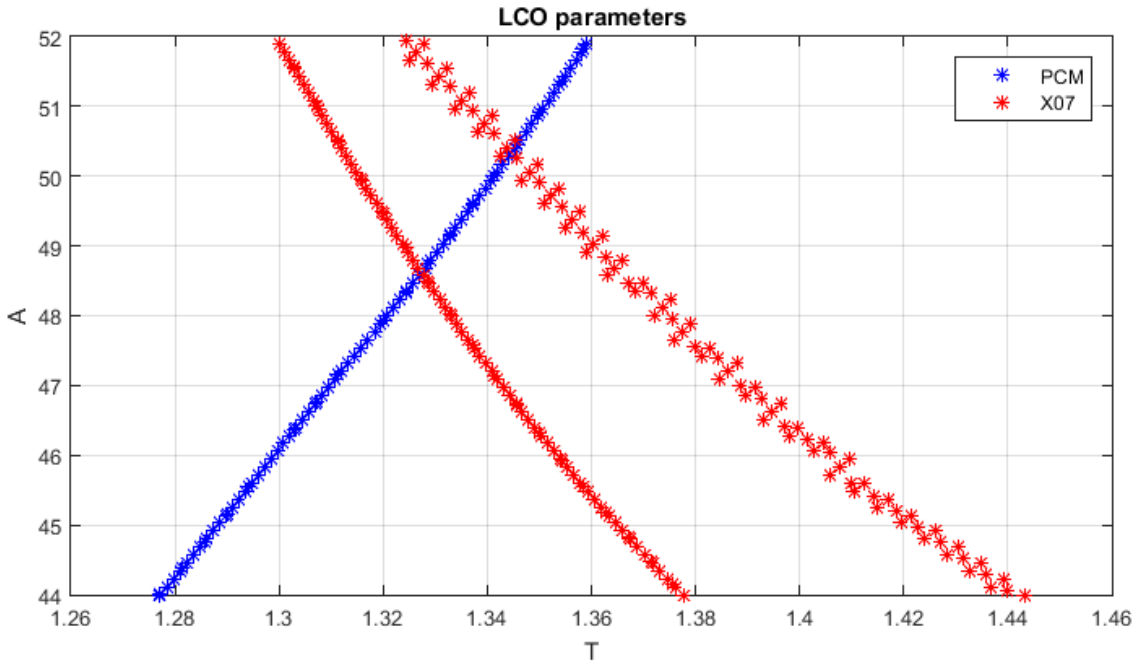

Figure 5.13: Determination of LCO parameters for YF-12 flight control system. Expected period and amplitude(A_1) are 1.327(sec) and 48.61, respectively.

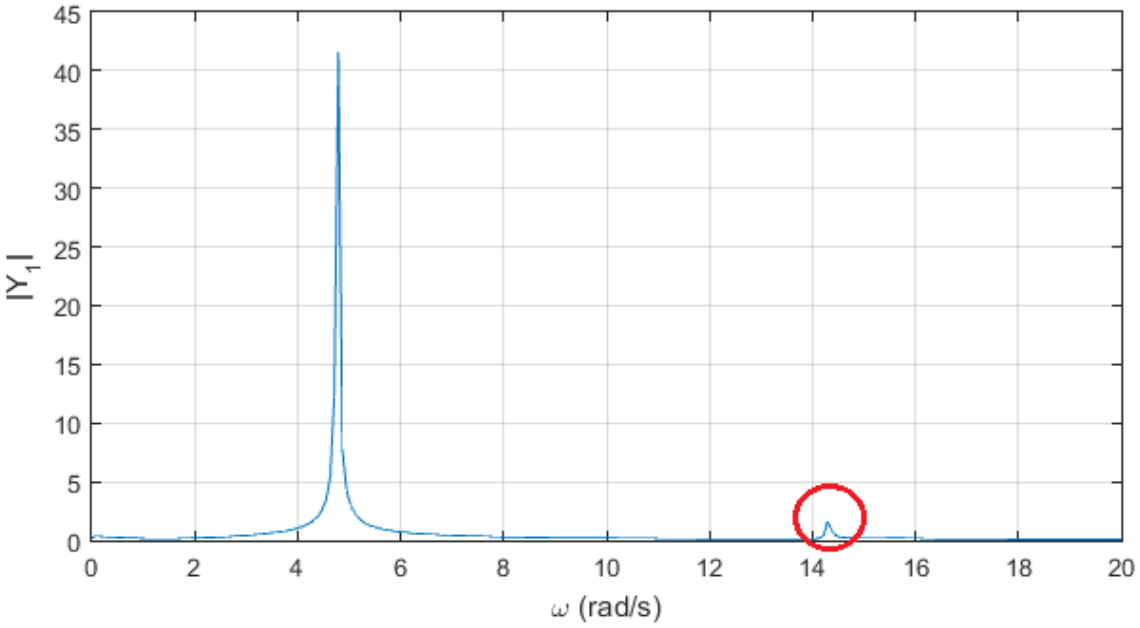

Figure 5.14: FFT of y_1 in Figure 5.4. The second harmonic component is at 14.29 (rad/s) which is about three times the first harmonic frequency 4.79 (rad/s).

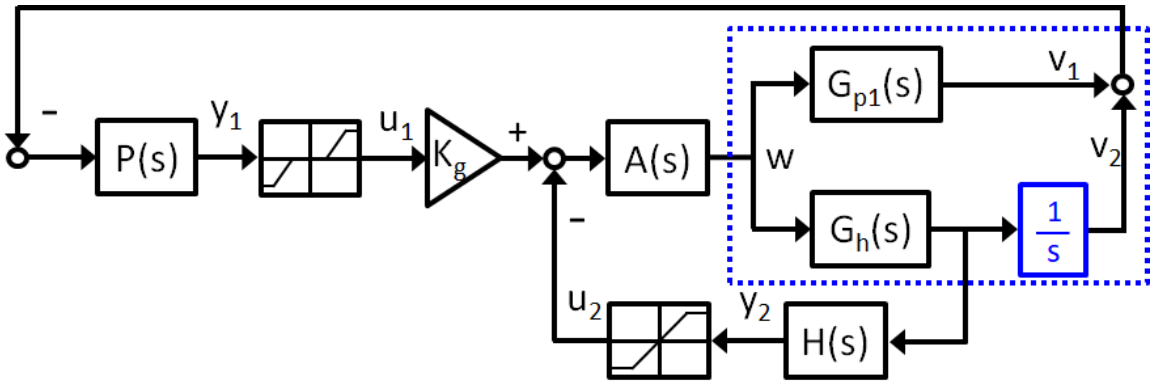

Figure 5.15: Another representation of YF-12 flight control loop equivalent to Figure 5.2. Transfer function $G_p(s)$ is expressed in a cascaded form as in the blue dotted rectangular.

The existence of this second harmonics is due to the significant difference of bandwidth between linear transfer functions of the loop that is organized by the summing junction depicted as the dotted rectangular in Figure 5.15, where

$$G_{p1}(s) = \frac{5.17}{s^2 + 1.57s + 246}$$

The frequency response of the two transfer functions in the loop ($G_{p1}(s)$ and $G_h(s)\frac{1}{s}$) illustrates the difference in bandwidth in Figure 5.16. Although the resonant frequency of $G_{p1}(s)$ is slightly greater than exactly three times the expected LCO frequency, the magnitude around the resonance frequency is high enough to produce the harmonic with its frequency three times the fundamental one, as in Figure 5.14. Therefore, the assumption on y_1, the input signal to the first PN g_1, should be modified from Equation 5.6 to

$$y_1(t) = A_1 \sin(\omega t) + A_3 \sin(3\omega t + \phi_3) \tag{5.26}$$

where $\omega = \frac{2\pi}{T}$ and ϕ_3 is the phase angle of the second harmonic term with respect to the first harmonic signal at the entrance of g_1. Note that we do not need to change the assumption of the unimodal sinusoidal for y_2 because the series of linear transfer functions from signal w to y_1 (Figure 5.15) rejects the second harmonic frequency components just as a low-

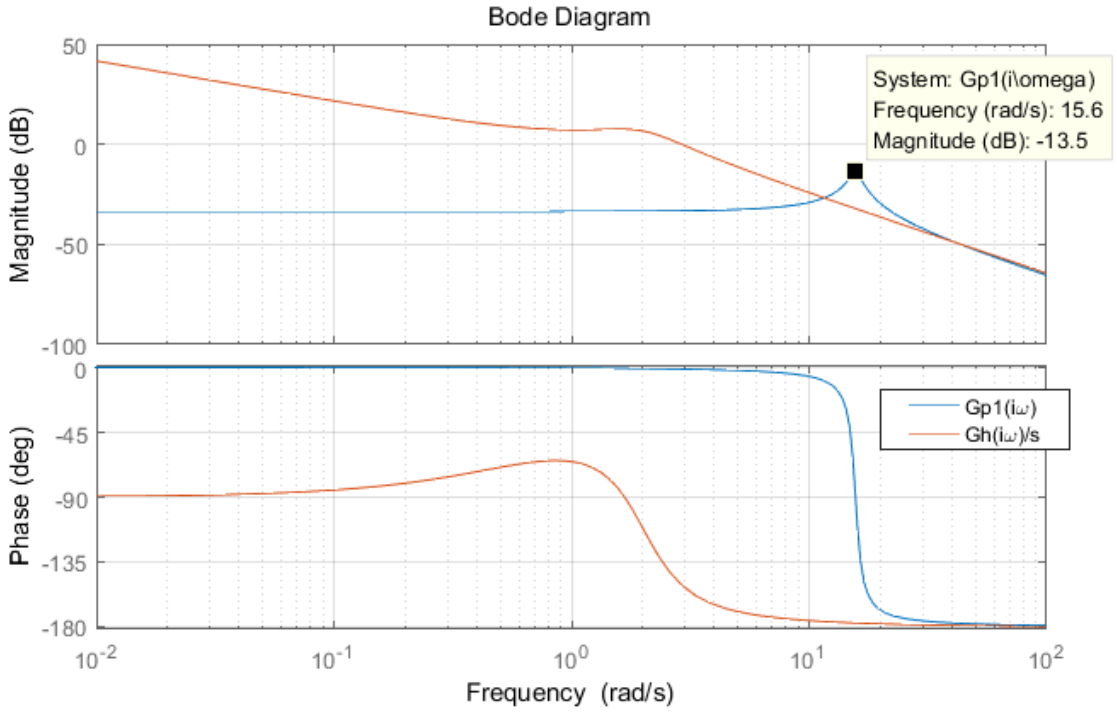

Figure 5.16: Bode plot of transfer function $G_{p1}(s)$ in blue solid line and $G_h(s)$ in red solid line. Note that for $G_{p1}(s)$, the resonant frequency is at about 15.6 (rad/s) which is a bit over three times the LCO frequency (4.79 (rad/s)).

pass filter does. The assumption of Equation 5.26 is justified because only if the second harmonic frequency is an integer multiple of the first harmonic can this LCO be classified as a stable one. Otherwise, the LCO is not a stable one because the second harmonic signal of the frequency of other real multiples of the first harmonic frequency results in a different phase angle at the moment when time has been elapsed by T.

Now the interest lies in how to handle the new unknown parameters–A_3 and ϕ_3. This remains an open problem in this work, but instead we assume that the ratio of the amplitude and the relative phase between the first and the second harmonic term is constant when the signal passed at w. When $T = T_{LCO}$ and $A = A_{LCO}$ they are approximately $\frac{A_3}{A_1}\Big|_w =$ 0.1889 and $\phi_3|_w$ =-1.3301 (rad). Therefore, for example when $T = T_{LCO}$ and $A = A_{LCO}$, w passes through $G_p(s)$ and $P(s)$ to yield $\frac{A_3}{A_1}\Big|_{y_1}$ =0.0389 and $\phi_3|_{y_1}$ =0.3830 (rad). Based on this argument we can renew parameters A_3 and ϕ_3 in Equation 5.26 to reproduce the first and the $\mathcal{S}$ equation as in Equation 5.15 and Equation 5.25, respectively. As a

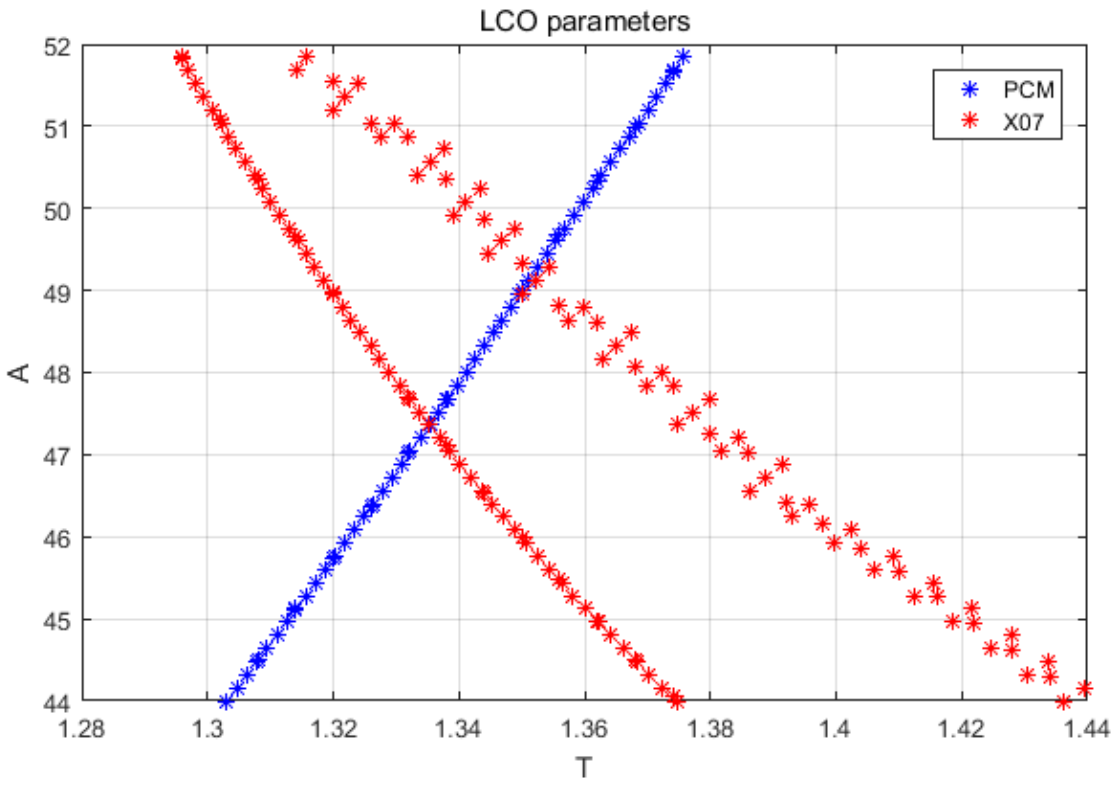

Figure 5.17: The $\mathcal{F}$ and the $\mathcal{S}$ equations depicted in T-A plane. The intersection($T_LCO = 1.335$ (sec) and $A_{LCO} = 47.36$ (deg)) stands for the identified LCO parameters on the assumption of dual modal sinusoidal input signal to y_1.

result, we graphically obtain the LCO parameters in Figure 5.17–T_{LCO} =1.335 (sec) and A_{LCO} =47.36 (deg). Although the results of LCO parameter identification in Table 5.5 imply that the dual modal assumption does not necessarily narrow down the difference between each result, it does suggest that we may introduce any type of periodic function as a template for a basic LCO solution and incorporate it in the Floquet analysis and switching function.

Table 5.5: LCO parameters estimation based on different methods.

	LCO period (sec)	LCO amplitude (deg)
Numerical Integration	1.312	44.31
DF analysis	1.352	49.39
Floquet theory with PL analysis	1.327	48.61
Floquet theory with PL analysis (Dual modal sinusoidal assumption)	1.335	47.36

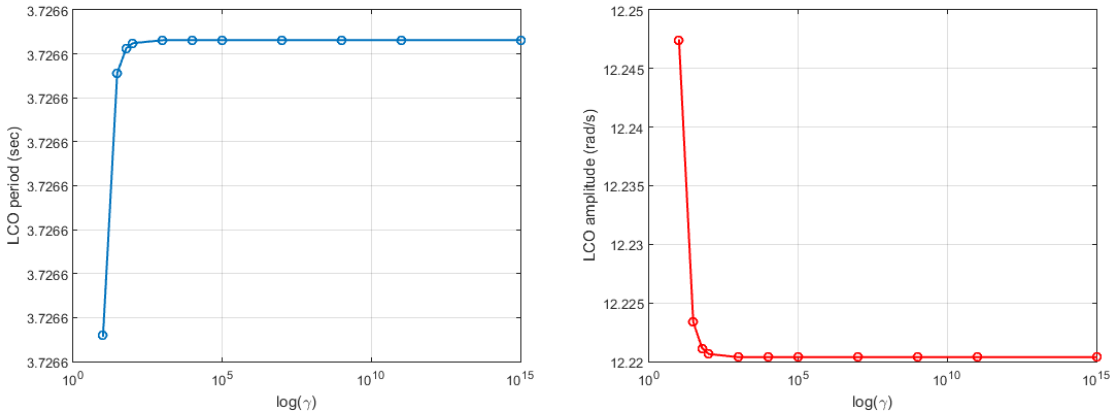

Figure 5.18: (a)(left)The LCO period of the simple rate saturated loop. Note that the predicted period is stabilized from when γ is around 10^5. (b)(right)The LCO amplitude of the simple rate saturated loop. Note that the predicted value is stabilized from when γ is around 10^5.

5.7 Parametric Analysis

Since the LCO parameters depend on the system characteristics, they will vary with system parameters such as pilot (system) gain and lead/lag parameters. Although we expect the varying system parameters would yield a corresponding smooth change of LCO parameters, it is worth analyzing the influence of the system parameters on the LCO parameters so as to provide qualitative description on what those system parameters play for the LCO characteristic.

5.7.1 EAF Parameter (γ)

As discussed in Section 3.3, the accuracy of EAF depends on the γ value. As γ increases, the closer the EAF becomes to the original PN, but a study is needed on how much we should raise γ to obtain sufficient accuracy. In addition, the LCO parameters and its stability might bifurcate with varying γ. We may analyze the LCO of the systems in this work with various γ following all the necessary steps discussed already and the result is illustrated from Figure 5.18 through Figure 5.20.

As in the figures, with γ greater than 10^5, the LCO parameters predicted begins to be

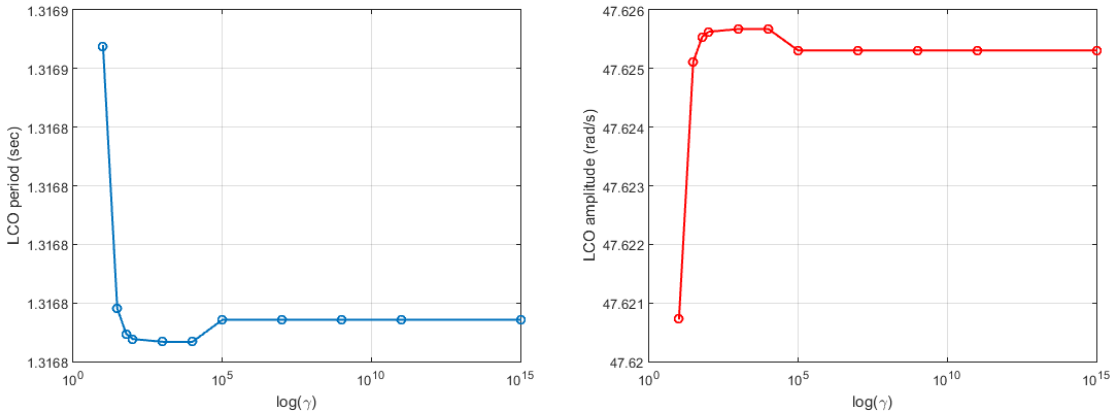

Figure 5.19: (a)(left)The LCO period of YF-12 pitch loop. Note that the predicted period is stabilized from when γ is around 10^5. (b)(right)The LCO amplitude of YF-12 pitch loop. Note that the predicted value is stabilized from when γ is around 10^5.

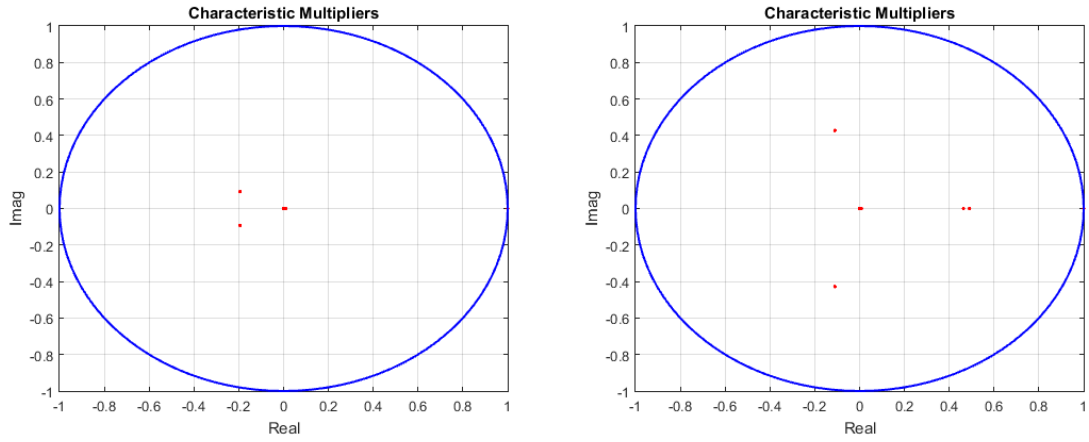

Figure 5.20: (a)(left)The characteristic multipliers corresponding to the LCO of the simple rate saturated loop, depicted as red dots. (b)(right)The characteristic multipliers corresponding to the LCO of YF-12 pitch loop, depicted as red dots. Note that all the rest of the characteristic multipliers other than PCM stay within a unit circle and do not change much with various γ values.

stabilized, implying that 10^5 is a proper lower bound for γ to obtain sufficient accuracy. Additionally, we can observe that the stability of LCO is not affected much from varying γ as in Figure 5.20.

5.7.2 Pilot Gain (k_p)

Pilot gain or system gain is one of the most dominant parameters that influences LCO parameters as well as the existence of the LCO as discussed in subsection 4.6.1. The same argument applies to YF-12 flight control system but this time with a little more issues to discuss. One of them is the prediction accuracy of the DF method. As shown in Table 5.6, the LCO parameters predicted by DF analysis is relatively apart from the ones obtained by others. This does not always mean that the DF method is not accurate, but DF methods can be said to be inconsistent. This inconsistency stems from the fact that a unimodal sinusoidal assumption leads to the violation of one of the assumptions on which DF analysis stands on–input to each PN is a unimodal sinusoidal signal, and the linear transfer functions play as a low pass filter. Considering that the unimodal sinusoidal assumption also applies to the Floquet theory and the switching equation, we may conclude that the violation of the second assumption is more serious. It is true that each series of linear transfer functions in each of feedback loop rejects the high frequency components. However, the difference of the rejecting frequency band can cause the advent of another harmonics in the input signal to a certain PN, as shown in Figure 5.16. Therefore, we may encounter inconsistency with DF method depending on the relative amplitude of higher order harmonic terms.

More importantly, the prediction of the LCO parameters accompany a bifurcation phenomena that makes the prediction difficult near the critical system gain. As shown in Figure 5.21, the critical level of the pilot gain k_p that generates an LCO of the system is between 15 and 16, where the prediction of LCO based on the proposed framework is not easy due to the ambiguity of the intersections between $\mathcal{F}$ and the $\mathcal{S}$ equations. Therefore, determination of the exact critical gain needs to involve the switching configuration analysis. In

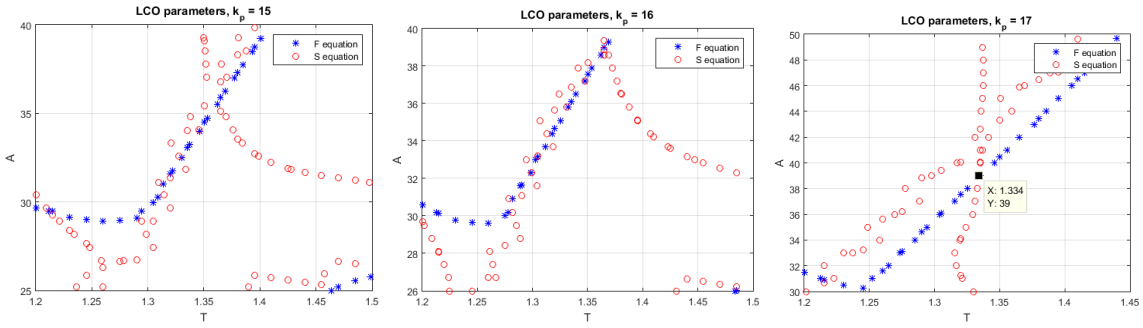

Figure 5.21: The $\mathcal{F}$ and the $\mathcal{S}$ equations with varying pilot gain k_p. Solutions are not definite when k_p is near the critical value ($k_p \in (15, 16)$). (a)(left) $k_p = 15$ (b)(center) $k_p = 16$ (c)(right) $k_p = 17$

addition, we observe that the LCO period is relatively invariant with respect to the system gain k_p, because a gain typically changes the amplitude rather than the phase of the states.

Table 5.6: LCO parameter obtained with varying pilot gain k_p ('-' implies no solution or unable to obtain).

k_p	DF T_{LCO}/A_{LCO} (sec,deg)	Numerical Integration T_{LCO}/A_{LCO} (sec,deg)	$\mathcal{F}$ and $\mathcal{S}$ equations T_{LCO}/A_{LCO} (sec,deg)
30	1.371 / 79.57	1.307 / 67.73	1.323 / 72.00
20	1.352 / 49.39	1.312 / 44.31	1.327 / 48.61
17	1.331 / 38.74	1.314 / 36.18	1.334 / 39.03
16	1.311 / 33.87	1.306 / 32.61	- / -
15	- / -	- / -	- / -

CHAPTER 6
CONCLUSION

In this thesis a new framework is established to analyze the Limit-Cycle Oscillation (LCO) of piecewise linear systems. While the piecewise nonlinearities (PN) in the piecewise linear system prevented the application of analytic methods such as Floquet theory to the analysis of LCO, the equivalent analytic functions of corresponding PNs are developed to practically incorporate the PNs into the Floquet analysis of the piecewise linear system. In addition, the switching function based on the exact switching order of pure linear affine systems that organize the piecewise linear system plays another necessary condition along with one obtained from the Floquet analysis. The stability of LCO is also analyzed with Floquet theory, by inspecting the location of characteristic multipliers of the perturbed linearized system evaluated at the expected periodic solution. The example of a simple rate saturated system along with the flight control system of YF-12 demonstrates the effectiveness of this framework.

Profound knowledge on LCO of a piecewise system enables the design of high performance controller. Since the switching configuration that can host an LCO always has a critical level of input amplitude to a specific PN, control engineers can determine the upper bound of the system gain, or design an appropriate adaptive gain law that adjusts the gain whenever the PN input is near the level that can generate an LCO. If we want to minimize the amplitude of LCO, we design a proper lead/lag filter to shift the LCO frequency to a higher band so that the new LCO frequency component is rejected sufficiently by the linear transfer functions following PNs. Furthermore, this analytic framework entails insights into the main cause of LCO in piecewise linear systems. The arguments on determining the switching configuration that leads to an LCO reveal that the critical switching between specific piecewise linear systems creates an LCO.

6.1 Important Findings

A few notable discoveries are obtained through this work and presented as follows. While some of them are expected, the others are not, leading to a source of future studies.

- Floquet theory provides only a necessary condition because it is about the dynamics of the linear time varying system perturbed or evaluated at the periodic solution of the original system. This entails another necessary condition that describes the behavior of the periodic solution itself.

- Despite the fact that PNs are discontinuous with respect to both space and time, by transforming the PNs into corresponding equivalent analytic functions (EAF) we are able to apply Floquet theory. The precision of the LCO parameter prediction is saturated with a sufficiently large finite value (γ) for each EAF.

- We observe that if the primary characteristic multiplier (PCM) is equal to one, then the rest of the characteristic multipliers are within a unit circle in the complex plane. Therefore, if PCM is a unity in the presence of corresponding LCO then this LCO is stable.

- Even though a piecewise linear system has a stable LCO, not every initial condition is eventually attracted to the LCO. Only some of them are converging to an LCO and others are attracted to a set of stable equilibrium points of the system.

- Preliminary prediction of LCO parameters helps to significantly enhance the efficiency of the LCO parameter determination. This preliminary work includes the describing function (DF) analysis and numerical integration.

- If an LCO exists in a piecewise linear system, this system should not be absolutely stable in terms of the stability of Lur'e type system. If it is absolutely stable, no LCO exists in the system.

- With multiple feedback loops in a system, LCO may take a multi-modal sinusoidal form. This is true especially when there is at least one PN in each closed loop.

6.2 Future Work

Although this thesis takes an example of relatively simple systems of up to eight dimensional state space with two PNs, it can be expanded to the application to more complicated and realistic systems of possibly all kinds of piecewise linear systems including, but not limited to, flight control systems of high performance flying objects, hybrid mechanical/electrical systems with exact nonlinearity models, and other physical/chemical dynamic systems. Wing-rock phenomena is also interpretable in the framework of LCO and worth investigating the essence of the inherent LCO [39, 40]. In addition, an enhanced method is needed to solve the LMI problem for the proof of the absolute stability of a Lur'e type system, since there is a chance that it is difficult to prove the absolute stability of a certain switching configuration depending on the system.

To add the generic procedure for arbitrarily complex models to the analysis of real systems, consideration of a variety of model uncertainties such as time delay, dynamic parameters, and disturbances is desirable. In addition, to upgrade the performance of this framework in terms of the LCO identification accuracy, we need to complete the argument on the dual modal sinusoidal assumption. In this thesis we assumed that the difference of phase and the ratio of amplitude of the second harmonic term of a certain state is constant, but for reliability this difference should be incorporated into the $\mathcal{F}$ or the $\mathcal{S}$ equation, or be justified properly as an assumption. In addition, we need to investigate the possibility of the existence of multiple LCOs. Even though multiple intersections between the $\mathcal{F}$ and the $\mathcal{S}$ equation does not necessarily mean the presence of multiple LCOs, we need to pay a special attention if the system has multiple closed loops.

Another potential topic is how to model multiple PNs in the case where they are just one linear transfer function away. If PNs are in series they are treated as just a single,

synthesized PN, and if they have more than two linear transfer functions between them the sinusoidal input assumption to each PN is valid. However, if PNs and linear transfer functions are uniformly mixed in serial order neither of the methods just mentioned can be applied.

Finally, finding the region of attraction to LCO will be a substantial contribution to the effort to prevent adverse LCO in the system. We treat the region of attraction as the subset of initial points that we need to avoid if we do not want an LCO in our system. Therefore, combined with the research on the finite horizon control to avoid a specific subset, the region of attraction will play as a rule of thumb in avoiding adverse LCO along with the critical system parameters.

Appendices

APPENDIX A

EAFS OF COMMON PNS

In this appendix section, details on Table 3.1 are described. Every EAF is obtained following steps below.

- Obtain the profile of the spatial derivative ($h(u)$) of corresponding PN ($g(u)$) except at singular points.
- From the EAF of a simple relay, find the EAF of $h(u)$.
- Obtain $g(u)$ from $h(u)$ by a proper integration with respect to space.

From Equation 3.3,

$$EAF(r(u)) = g(u) = \lim_{\gamma \to \infty} \frac{\gamma u}{\sqrt{1 + (\gamma u)^2}}$$

A.1 Saturation

We observe that $h(u)$ of a saturation is obtained from translational shift of $EAF(r(u))$ by $(-d, \frac{a}{2})$ followed by symmetric replication of the part in the left half plane to right, as

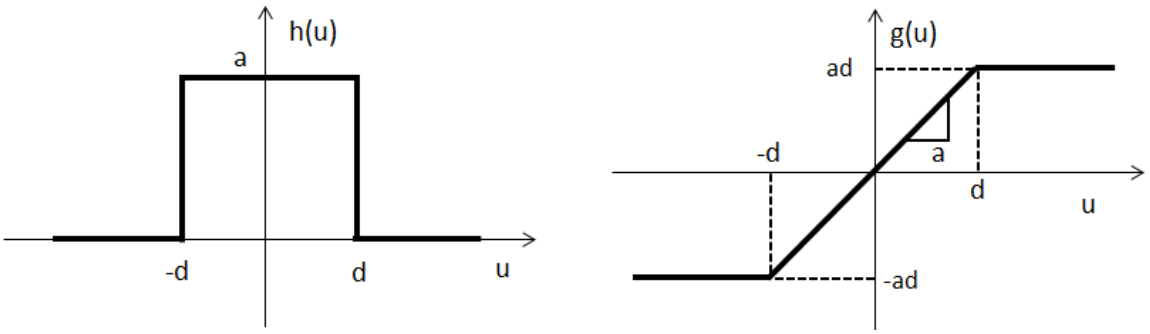

Figure A.1: (a) (left) The input derivative ($h(u)$) of a saturation. (b) (right) A saturation ($g(u)$).

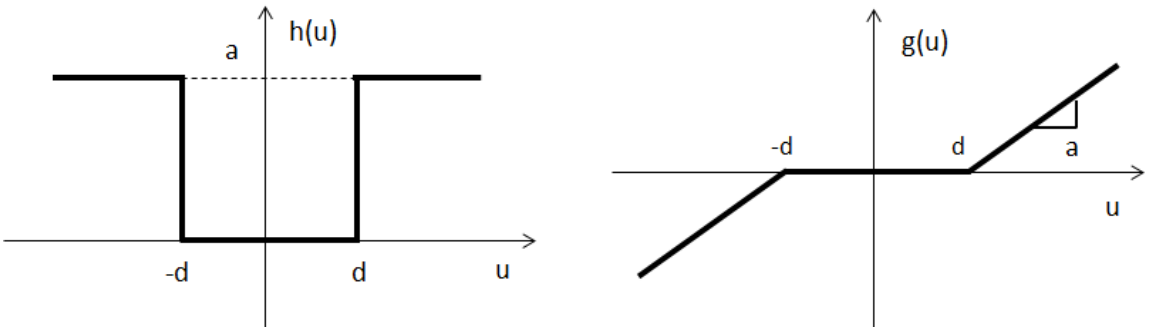

Figure A.2: (a) (left) The input derivative ($h(u)$) of a dead-zone. (b) (right) A dead-zone ($g(u)$).

shown in Figure A.1. Therefore,

$$h(u) = \frac{a}{2}\Big(1 - \frac{\gamma(|u| - d)}{\sqrt{1 + (\gamma(|u| - d))^2}}\Big)$$

integration of $h(u)$ with respect to u yields

$$g(u) = \frac{a}{2}\Big(u - \text{sign}(u)\frac{\sqrt{1 + (\gamma(|u| - d))^2} - \sqrt{1 + (\gamma d)^2}}{\gamma}\Big)$$

A.2 Dead-zone

We observe that $h(u)$ of a dead-zone is obtained from translational shift of $EAF(r(u))$ by $(d, \frac{a}{2})$ followed by symmetric replication of the part in the right half plane to left, as shown in Figure A.2. Therefore,

$$h(u) = \frac{a}{2}\Big(1 + \frac{\gamma(|u| - d)}{\sqrt{1 + (\gamma(|u| - d))^2}}\Big)$$

integration of $h(u)$ with respect to u yields

$$g(u) = \frac{a}{2}\Big(u + \text{sign}(u)\frac{\sqrt{1 + (\gamma(|u| - d))^2} - \sqrt{1 + (\gamma d)^2}}{\gamma}\Big)$$

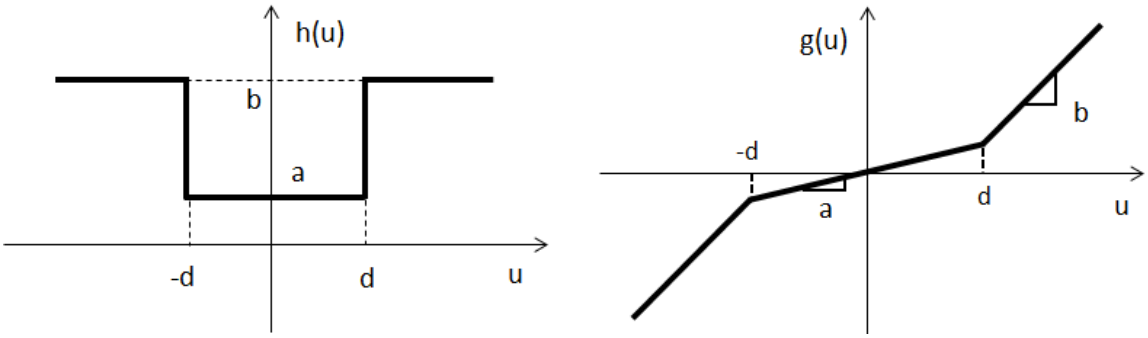

Figure A.3: (a) (left) The input derivative ($h(u)$) of a nonlinear shaping. (b) (right) A nonlinear shaping ($g(u)$).

A.3 Nonlinear Shaping

We observe that $h(u)$ of a nonlinear shaping is obtained from translational shift of $EAF(r(u))$ by $(d, \frac{a+b}{2})$ followed by symmetric replication of the part in the right half plane to left, as shown in Figure A.3. Therefore,

$$h(u) = \frac{a+b}{2} + \frac{b-a}{2} \frac{\gamma(|u|-d)}{\sqrt{1+(\gamma(|u|-d))^2}}$$

integration of $h(u)$ with respect to u yields

$$g(u) = \frac{1}{2}\Big((b+a)u + (b-a)\text{sign}(u)\frac{\sqrt{1+(\gamma(|u|-d))^2} - \sqrt{1+(\gamma d)^2}}{\gamma}\Big)$$

A.4 Relay with Hysteresis

A relay with hysteresis has two-fold profile depending on the previous event. Depending on the sign of $\dot{u}_c = \frac{du}{dt}\Big|_{u=u_c}$, the output takes either of the two paths shown in Figure A.4, where u_c is the input of the latest critical input ($u = e$ or $-e$). For example, the latest critical input is $u_c = e$ or $-e$ and $\dot{u}_c > 0$, the output path will track the solid line in Figure

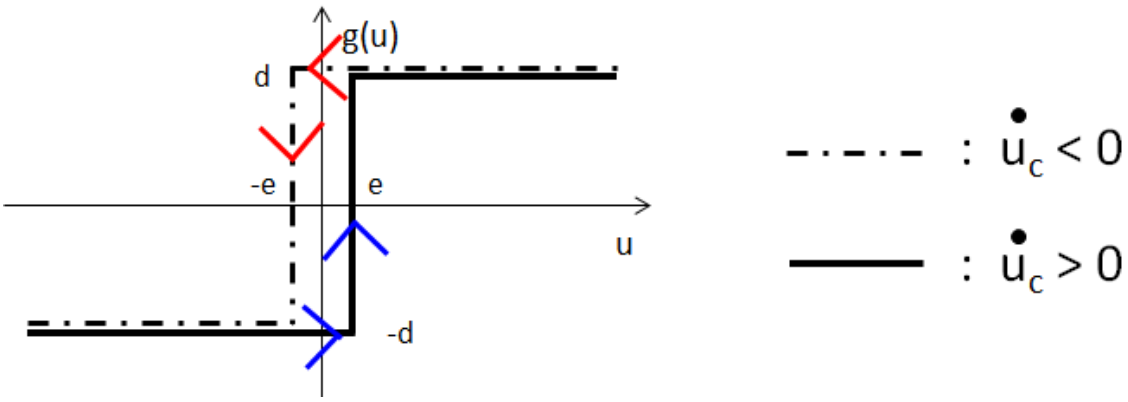

Figure A.4: A relay with hysteresis e. Depending on the previous direction of input, the output trajectory takes either solid line or dotted line.

A.4. Since the solid line is equivalent to a simple relay with translational shift by $(e, 0)$,

$$g(u) = \frac{d\gamma(u-e)}{\sqrt{1+(\gamma(u-e))^2}}$$

On the other hand, when $\dot{u}_c < 0$ the dotted line is equivalent to

$$g(u) = \frac{d\gamma(u+e)}{\sqrt{1+(\gamma(u+e))^2}}$$

Therefore, the EAF for the relay with hysteresis is

$$g(u) = \frac{d\gamma(u-\text{sign}(\dot{u}_c)e)}{\sqrt{1+(\gamma(u-\text{sign}(\dot{u}_c)e))^2}}$$

A.5 Backlash

In a backlash the output signal trajectory lies in either of the two operation zones (Figure A.5). When input is increasing output will be in operation zone two, and vice versa. If the input direction is changed at one moment, the trajectory is on the horizontal, no incremental line called as a dead-zone, until the trajectory meets operation zone one or operation zone two. Therefore, the basic shape of backlash is identical to a deadzone that is shifted as much as the center point of the dead-zone section shown in Figure A.5 as red dashed horizontal

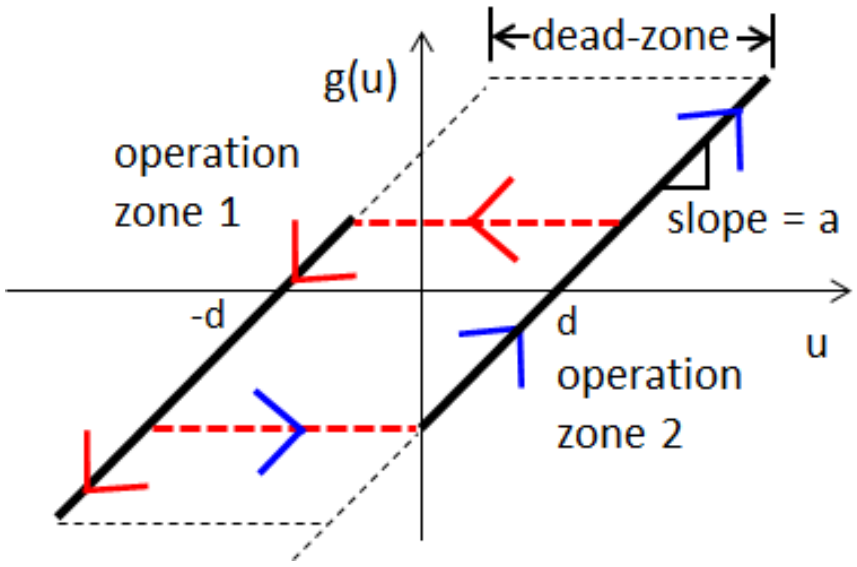

Figure A.5: A relay with hysteresis e. Depending on the previous direction of input, the output trajectory takes either solid line or dotted line.

lines. Let's define u_c as the latest input value which has left a certain operation zone, then the shifting quantity is determined based on which operation zone u_c stays on. For example, u_c is on the operation zone one and the input u has begun to increase. In this case the backlash profile is determined as a dead-band PN shifted by $(u_c + d, a(u_c + d))$, as depicted in the profile with blue arrow heads in Figure A.5. Therefore,

$$g(u) = a(u_c + d) + \frac{a}{2}\left((u - u_c - d) + \text{sign}(u - u_c - d)\frac{\sqrt{1+(\gamma(|u-u_c-d|-d))^2}-\sqrt{1+(\gamma d)^2}}{\gamma}\right)$$

Likewise, if u_c is on the operation zone two,

$$g(u) = a(u_c - d) + \frac{a}{2}\left((u - u_c + d) + \text{sign}(u - u_c + d)\frac{\sqrt{1+(\gamma(|u-u_c+d|-d))^2}-\sqrt{1+(\gamma d)^2}}{\gamma}\right)$$

Finally,

$$g(u) = av + \frac{a}{2}\Big((u-v) + \text{sign}(u-v)\frac{\sqrt{1+(\gamma(|u-v|-d))^2} - \sqrt{1+(\gamma d)^2}}{\gamma}\Big)$$

$$v = \begin{cases} u_c + d, & u_c \in \text{ operation zone one}, \\ u_c - d, & u_c \in \text{ operation zone two} \end{cases}$$

APPENDIX B

SWITCHING FEASIBILITY FOR YF-12 FLIGHT CONTROL SYSTEM

The YF-12 flight control system has two PNs, therefore we need to check the switching feasibility per every combined configuration from the two PNs. Several constants are common in use– $k_p = 20$, $\tau_p = 0.1$, and $k_6 = 5.99722$.

B.1 Configuration One

There is no LCO because the system is a pure linear system.

$$\dot{\mathbf{x}} = \mathbf{F}_1\mathbf{x}$$

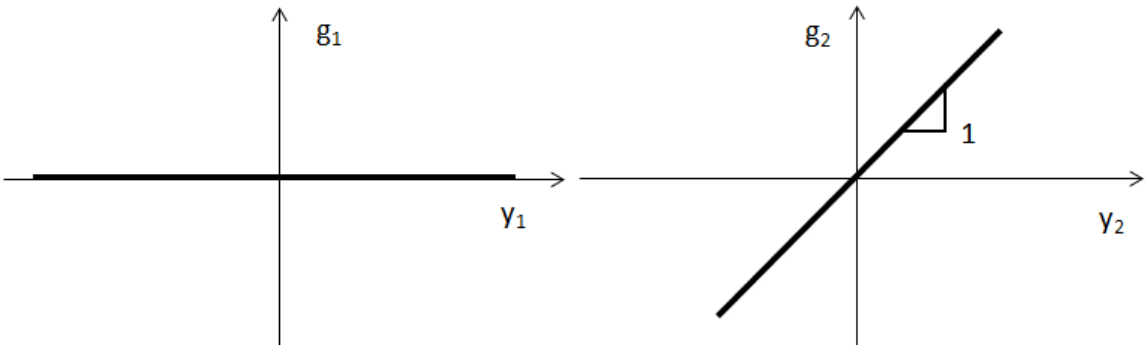

Figure B.1: Combined configuration one: (a)(left)The first PN g_1 versus the input y_1. (b)(right)The second PN g_2 versus the input y_2.

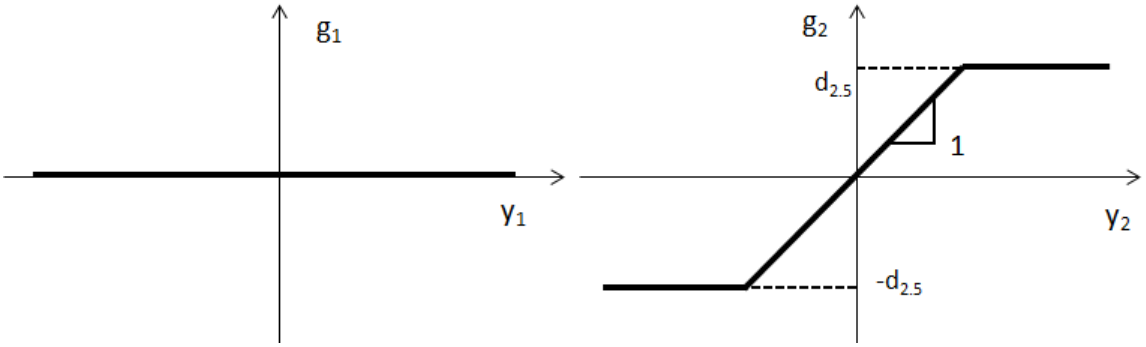

Figure B.2: Switching configuration two: (a)(left)The first PN g_1 versus the input y_1. (b)(right)The second PN g_2 versus the input y_2.

where

$$\mathbf{F}_1 = \begin{bmatrix} -0.9 & 1.0 & 0 & 0 & 0 & 0.2 & 0 & 0 \\ -3.46 & -0.6 & 0 & 0 & 0 & k_6 & 0 & 0 \\ 0 & 1.0 & 0 & 0 & 0 & 0 & 0 & 0 \\ 0 & 0 & 0 & 0 & 1.0 & 0 & 0 & 0 \\ 0 & 0 & 0 & -246 & -1.57 & 5.17 & 0 & 0 \\ 0 & -\frac{51}{4} & 0 & 0 & 0 & -34 & 0 & -136 \\ 0 & 0 & \frac{1}{\tau_p} & \frac{1}{\tau_p} & 0 & 0 & -\frac{1}{\tau_p} & 0 \\ 0 & 0.375 & 0 & 0 & 0 & 0 & 0 & -4.0 \end{bmatrix}$$

B.2 Configuration Two

Equation of motion for this linear affine system is

$$\dot{\mathbf{x}}(t) = \mathbf{F}_2\mathbf{x}(t) + \mathbf{G}_2\boldsymbol{\phi}_2(\mathbf{H}_2\mathbf{x}(t))$$

where

$$\mathbf{F}_2 = \mathbf{F} = \begin{bmatrix} -0.9 & 1.0 & 0 & 0 & 0 & 0.2 & 0 & 0 \\ -3.46 & -0.6 & 0 & 0 & 0 & k_6 & 0 & 0 \\ 0 & 1.0 & 0 & 0 & 0 & 0 & 0 & 0 \\ 0 & 0 & 0 & 0 & 1.0 & 0 & 0 & 0 \\ 0 & 0 & 0 & -246 & -1.57 & 5.17 & 0 & 0 \\ 0 & 0 & 0 & 0 & 0 & -34 & 0 & 0 \\ 0 & 0 & \frac{1}{\tau_p} & \frac{1}{\tau_p} & 0 & 0 & -\frac{1}{\tau_p} & 0 \\ 0 & 0.375 & 0 & 0 & 0 & 0 & 0 & -4.0 \end{bmatrix},$$

$$\mathbf{G}_2 = \begin{bmatrix} 0 & 0 & 0 & 0 & 0 & -34 & 0 & 0 \end{bmatrix}^T, \qquad \mathbf{H}_2 = \begin{bmatrix} 0 & \frac{3}{8} & 0 & 0 & 0 & 0 & 0 & 4 \end{bmatrix}$$

To find the equilibrium, we solve the following algebraic equation

$$\mathbf{F}_2\mathbf{x}_e + \mathbf{G}_2\boldsymbol{\phi}_2(\mathbf{H}_2\mathbf{x}_e) = 0$$

Firstly we assume that $\mathbf{x}_e \in \mathbb{N}(\mathbf{F}_2)$. Then, $\mathbf{x}_e = k[0\ 0\ 1\ 0\ 0\ 0\ 1\ 0]$ with some real scalar k and $\mathbf{G}_2\boldsymbol{\phi}_2(\mathbf{H}_2\mathbf{x}_e) = 0$. Since $\mathbf{G}_2\boldsymbol{\phi}(\mathbf{H}_2\mathbf{x}_e) = g_2(\frac{3}{8}\mathbf{x}_{e2} + 4\mathbf{x}_{e8})) = 0$, the entire null space of $\mathbf{F}_2$ is an equilibrium set. Now assume $\mathbf{x}_e \notin \mathbb{N}(\mathbf{F}_2)$. Then

$$\begin{aligned} -0.9\mathbf{x}_{e1} + \mathbf{x}_{e2} + 0.2\mathbf{x}_{e6} &= 0 \\ -3.46\mathbf{x}_{e1} - 0.6\mathbf{x}_{e2} + k_6\mathbf{x}_{e6} &= 0 \\ \mathbf{x}_{e2} = 0,\ \mathbf{x}_{e5} &= 0 \\ \mathbf{x}_{e6} - 34g_2(\frac{3}{8}\mathbf{x}_{e2} + 4\mathbf{x}_{e8}) &= 0 \\ -246\mathbf{x}_{e4} - 1.57\mathbf{x}_{e5} + 5.17\mathbf{x}_{e6} &= 0 \\ \mathbf{x}_{e3} + \mathbf{x}_{e4} - \mathbf{x}_{e7} &= 0 \\ \frac{3}{8}\mathbf{x}_{e3} - 4\mathbf{x}_{e8} &= 0 \end{aligned}$$

Then it directly follows that $\mathbf{x}_e(1) = \mathbf{x}_e(6) = \mathbf{x}_e(4) = 0$, and then $\mathbf{x}_e(8) = \mathbf{x}_e(3) = \mathbf{x}_e(7) = 0$, therefore, $\mathbf{x}_e = \mathbf{0}$. Therefore, the equilibrium set is

$$\mathbf{x}_e = k[0\ 0\ 1\ 0\ 0\ 0\ 1\ 0] \text{ with } k \in \mathbb{R}$$

We now check the stability of this equilibrium. The Jacobian matrix around this equilibrium is

$$\mathbf{J}(\mathbf{x}_e) = \begin{bmatrix} -0.9 & 1.0 & 0 & 0 & 0 & 0.2 & 0 & 0 \\ -3.46 & -0.6 & 0 & 0 & 0 & k_6 & 0 & 0 \\ 0 & 1.0 & 0 & 0 & 0 & 0 & 0 & 0 \\ 0 & 0 & 0 & 0 & 1.0 & 0 & 0 & 0 \\ 0 & 0 & 0 & -246 & -1.57 & 5.17 & 0 & 0 \\ 0 & -\frac{51}{4}h_2(y_2(\mathbf{x}_e)) & 0 & 0 & 0 & -34 & 0 & -136h_2(y_2(\mathbf{x}_e)) \\ 0 & 0 & 1/\tau_p & 1/\tau_p & 0 & 0 & -1/\tau_p & 0 \\ 0 & 0.375 & 0 & 0 & 0 & 0 & 0 & -4.0 \end{bmatrix}$$

Since $y_2(\mathbf{x}_e) = 0$, $\mathbf{J}(\mathbf{x}_e) = \mathbf{F}$ and its eigenvalues are -4, -10, 0, -0.785$\pm$15.665i, -0.750$\pm$1.854i, -34. Therefore, the equilibrium is stable with only one mode marginally stable. Since we have nonzero equilibrium $\mathbf{x}_e$, we need to check the absolute stability of the following system with zero equilibrium, because proving the absolute stability based on PR and KYP lemma implies the absolute stability towards the zero equilibrium.

$$\frac{d}{dt}(\mathbf{x} - \mathbf{x}_e) = \mathbf{F}_2(\mathbf{x} - \mathbf{x}_e) + \mathbf{G}_2(\boldsymbol{\phi}_2(\mathbf{H}_2(\mathbf{x} - \mathbf{x}_e)))$$

or, equivalently

$$\dot{\mathbf{x}} = \mathbf{F}_2\mathbf{x} + \mathbf{G}_2(\boldsymbol{\phi}_2(\mathbf{H}_2\mathbf{x} - \mathbf{H}_2\mathbf{x}_e) + \boldsymbol{\phi}_2(\mathbf{H}_2\mathbf{x}_e))$$

Define $\boldsymbol{\psi}_2(\mathbf{H}_2\mathbf{x}) \equiv \boldsymbol{\phi}_2(\mathbf{H}_2\mathbf{x} - \mathbf{H}_2\mathbf{x}_e) + \boldsymbol{\phi}_2(\mathbf{H}_2\mathbf{x}_e)$ then $\boldsymbol{\psi}_2(\mathbf{H}_2\mathbf{x}) = \boldsymbol{\phi}_2(\mathbf{H}_2\mathbf{x})$ because

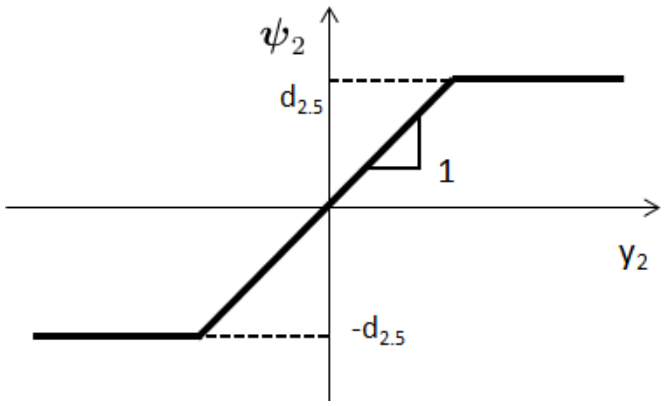

Figure B.3: Input nonlinearity ψ_2 of the system of configuration two. Note that the output of this PN is bounded within a line of slope one and x (horizontal) axis

$\mathbf{H}_2\mathbf{x}_e = 0$. Therefore, the equivalent zero equilibrium system is identical to the original system of configuration two, and $\psi_2(\mathbf{H}_2\mathbf{x})$ should look like the one in Figure B.3.

Now we try to find the matrix $\mathbf{P}$ in the following LMI problem.

$$\mathbf{P} = \mathbf{P}^T > 0$$

$$\begin{bmatrix} \mathbf{F}_2^T\mathbf{P} + \mathbf{P}\mathbf{F}_2 & \mathbf{P}\mathbf{B}_2 - \mathbf{C}_2^T \\ \mathbf{B}_2^T\mathbf{P} - \mathbf{C}_2 & -\mathbf{D}_2\mathbf{D}_2^T \end{bmatrix} < 0$$

where $\mathbf{B}_2 = -\mathbf{G}_2$, $\mathbf{C}_2 = \mathbf{H}_2 + \mathbf{N}_2\mathbf{H}_2\mathbf{F}_2$, and $\mathbf{D}_2 = \mathbf{K}_2^{-1} + \mathbf{N}_2\mathbf{H}_2\mathbf{G}_2$ with $\mathbf{N}_2 = \alpha_{20} > 0$. and $\mathbf{K}_2 = 1$ because the input nonlinearity ψ_2 is bounded by a line of slope one, as shown in Figure B.3. The solution to the LMI above exists as follows: $\alpha_{20} = 0.3$ and

$$\mathbf{P} = \begin{bmatrix} 3.7627 & 0.1166 & 20.7476 & 4.4360 & -0.5492 & -0.0248 & -20.7480 & -40.8084 \\ 0.1166 & 1.7172 & -22.5994 & -9.1178 & 0.5630 & -0.1367 & 22.5994 & 7.8081 \\ 20.7476 & -22.5994 & 761.5679 & 234.4392 & -19.5276 & 2.6095 & -761.5681 & -717.1517 \\ 4.4360 & -9.1178 & 234.4392 & 149.7104 & -5.8802 & 0.8263 & -234.4393 & -189.9813 \\ -0.5492 & 0.5630 & -19.5276 & -5.8802 & 0.8042 & -0.0856 & 19.5276 & 18.7723 \\ -0.0248 & -0.1367 & 2.6095 & 0.8263 & -0.0856 & 0.1416 & -2.6095 & -1.2440 \\ -20.7480 & 22.5994 & -761.5681 & -234.4393 & 19.5276 & -2.6095 & 761.5686 & 717.1530 \\ -40.8084 & 7.8081 & -717.1517 & -189.9813 & 18.7723 & -1.2440 & 717.1530 & 959.7637 \end{bmatrix}$$

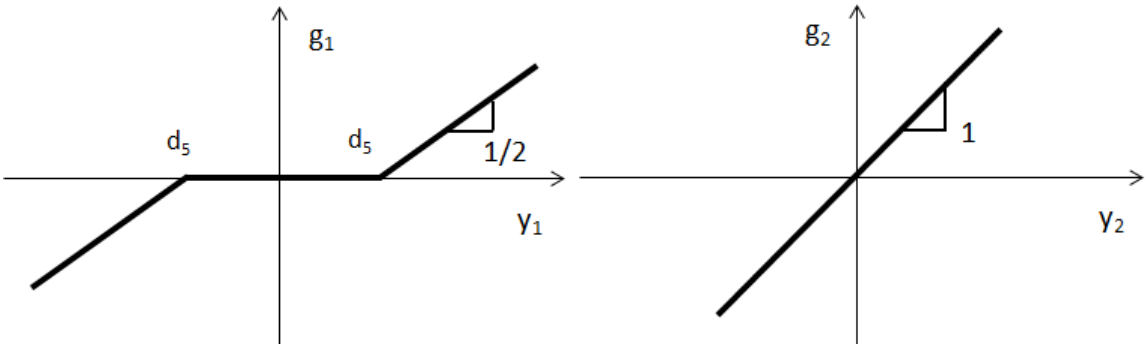

Figure B.4: Switching configuration three: (a)(left)The first PN g_1 versus the input y_1. (b)(right)The second PN g_2 versus the input y_2.

Therefore, we may say that the linear affine system of combination index 2 is globally absolutely stable towards its stable equilibrium, implying that no LCO can exist in this switching combination.

B.3 Configuration Three

Equation of motion for this linear affine system is

$$\dot{\mathbf{x}}(t) = \mathbf{F}_3\mathbf{x}(t) + \mathbf{G}_3\boldsymbol{\phi}_3(\mathbf{H}_3\mathbf{x}(t))$$

where

$$\mathbf{F}_3 = \begin{bmatrix} -0.9 & 1.0 & 0 & 0 & 0 & 0.2 & 0 & 0 \\ -3.46 & -0.6 & 0 & 0 & 0 & k_6 & 0 & 0 \\ 0 & 1.0 & 0 & 0 & 0 & 0 & 0 & 0 \\ 0 & 0 & 0 & 0 & 1.0 & 0 & 0 & 0 \\ 0 & 0 & 0 & -246 & -1.57 & 5.17 & 0 & 0 \\ 0 & -\frac{51}{4} & 0 & 0 & 0 & -34 & 0 & -136 \\ 0 & 0 & \frac{1}{\tau_p} & \frac{1}{\tau_p} & 0 & 0 & -\frac{1}{\tau_p} & 0 \\ 0 & 0.375 & 0 & 0 & 0 & 0 & 0 & -4.0 \end{bmatrix},$$

$$\mathbf{G}_3 = \begin{bmatrix} 0 & 0 & 0 & 0 & 0 & 25.16 & 0 & 0 \end{bmatrix}^T, \qquad \mathbf{H}_3 = \begin{bmatrix} 0 & 0 & 0 & 0 & 0 & 0 & -k_p & 0 \end{bmatrix}$$

$$\boldsymbol{\phi}(\mathbf{H}_3\mathbf{x}) = g_3(-k_p\mathbf{x}(7))$$

where g_3 and its derivative h_3 are

$$g_3(y_1) = \frac{1}{4}\Big(y_1 + \text{sign}(y_1)\frac{\sqrt{1+(\gamma(|y_1|-d_5))^2} - \sqrt{1+(d_5\gamma)^2}}{\gamma}\Big)$$
$$h_3(y_1) = \frac{dg_3}{dy_1} = \frac{1}{4} + \frac{\gamma(|y_1|-d_5))}{\sqrt{1+(\gamma(|y_1|-d_5))^2}}$$

To find the equilibrium, we solve the following algebraic equation

$$\mathbf{F}_3\mathbf{x}_e + \mathbf{G}_3\boldsymbol{\phi}(\mathbf{H}_3\mathbf{x}_e) = 0$$

Firstly we assume that $\mathbf{x}_e \in \mathbb{N}(\mathbf{F}_3)$. Then, $\mathbf{x}_e = k[0\ 0\ 1\ 0\ 0\ 0\ 1\ 0]$ with $k \in \mathbb{R}$ and $\mathbf{G}_3\boldsymbol{\phi}(\mathbf{H}_3\mathbf{x}_e) = 0$. Since $\mathbf{G}_3\boldsymbol{\phi}(\mathbf{H}_3\mathbf{x}_e) = g_3(-k_p\mathbf{x}_{e7}) = 0$ when $-k_p\mathbf{x}_{e7} \in [-d_5, d_5]$, the k

should be $k \in [-\frac{d_5}{k_p}, \frac{d_5}{k_p}] = [-0.25, 0.25]$. Now assume $\mathbf{x}_e \notin \mathbb{N}(\mathbf{F}_3)$. Then

$$\begin{aligned}
-0.9\mathbf{x}_{e1} + \mathbf{x}_{e2} + 0.2\mathbf{x}_{e6} &= 0 \\
-3.46\mathbf{x}_{e1} - 0.6\mathbf{x}_{e2} + k_6\mathbf{x}_{e6} &= 0 \\
\mathbf{x}_{e2} = 0,\ \mathbf{x}_{e5} &= 0 \\
-246\mathbf{x}_e(4) - 1.57\mathbf{x}_{e5} + 5.17\mathbf{x}_{e6} &= 0 \\
-\frac{51}{4}\mathbf{x}_{e2} - 34\mathbf{x}_{e6} - 136\mathbf{x}_{e8} + 25.16g_3(-k_p\mathbf{x}_{e7}) &= 0 \\
\mathbf{x}_{e3} + \mathbf{x}_{e4} - \mathbf{x}_{e7} &= 0 \\
\frac{3}{8}\mathbf{x}_{e2} - 4\mathbf{x}_{e8} &= 0
\end{aligned}$$

Then it follows that $\mathbf{x}_e = k[0\ 0\ 1\ 0\ 0\ 0\ 1\ 0]$ with $k \in [-0.25, 0.25]$, which is a contradiction. Therefore, the equilibrium set is

$$\mathbf{x}_e = k[0\ 0\ 1\ 0\ 0\ 0\ 1\ 0] \text{ with } k \in [-0.25, 0.25]$$

We now check the stability of this equilibrium. The Jacobian matrix around this equilibrium is

$$\mathbf{J}(\mathbf{x}_e) = \begin{bmatrix}
-0.9 & 1.0 & 0 & 0 & 0 & 0.2 & 0 & 0 \\
-3.46 & -0.6 & 0 & 0 & 0 & k_6 & 0 & 0 \\
0 & 1.0 & 0 & 0 & 0 & 0 & 0 & 0 \\
0 & 0 & 0 & 0 & 1.0 & 0 & 0 & 0 \\
0 & 0 & 0 & -246 & -1.57 & 5.17 & 0 & 0 \\
0 & -\frac{51}{4} & 0 & 0 & 0 & -34 & -25.16k_p h_3(y_1(\mathbf{x}_e)) & -136 \\
0 & 0 & 1/\tau_p & 1/\tau_p & 0 & 0 & -1/\tau_p & 0 \\
0 & 0.375 & 0 & 0 & 0 & 0 & 0 & -4.0
\end{bmatrix}$$

Since $y_1(\mathbf{x}_e) = -k_p\mathbf{x}_e(7) = 0$, $\mathbf{J}(\mathbf{x}_e) = \mathbf{F}_3$ and its eigenvalues are -10, 0, -31.907

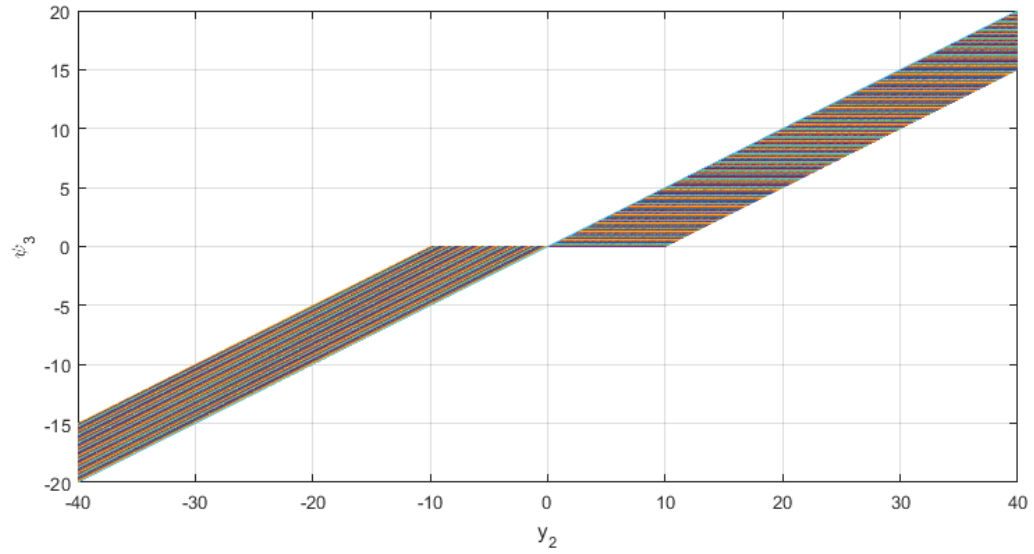

Figure B.5: Input nonlinearity $\boldsymbol{\psi}_3$ of the system of configuration three. Shaded area stands for the possible occupancy of $\boldsymbol{\psi}_3$. Note that the whole area is bounded within a line of slope $\frac{1}{2}$ and x axis.

-0.785$\pm$15.665i, -3.079$\pm$3.590i, -1.434. Therefore, the equilibrium is stable with only one mode marginally stable. Since we have nonzero equilibrium $\mathbf{x}_e$, we need to check the absolute stability of the following system with zero equilibrium, because proving the absolute stability based on PR and KYP lemma implies the absolute stability towards zero equilibrium.

$$\frac{d}{dt}(\mathbf{x}-\mathbf{x}_e) = \mathbf{F}_3(\mathbf{x}-\mathbf{x}_e) + \mathbf{G}_3(\boldsymbol{\phi}_3(\mathbf{H}_3(\mathbf{x}-\mathbf{x}_e)))$$

or, equivalently

$$\dot{\mathbf{x}} = \mathbf{F}_3\mathbf{x} + \mathbf{G}_3(\boldsymbol{\phi}_3(\mathbf{H}_3\mathbf{x}-\mathbf{H}_3\mathbf{x}_e) + \boldsymbol{\phi}_3(\mathbf{H}_3\mathbf{x}_e))$$

Define $\boldsymbol{\psi}_3(\mathbf{H}_3\mathbf{x}) \equiv \boldsymbol{\phi}_3(\mathbf{H}_3\mathbf{x}-\mathbf{H}_3\mathbf{x}_e) + \boldsymbol{\phi}_3(\mathbf{H}_3\mathbf{x}_e)$ then $\boldsymbol{\psi}_3(\mathbf{H}_3\mathbf{x}) = \boldsymbol{\phi}_3(\mathbf{H}_3\mathbf{x}-\mathbf{H}_3\mathbf{x}_e)$ because $\boldsymbol{\phi}_3(\mathbf{H}_3\mathbf{x}_e) = 0$. Then, since $\mathbf{H}_3\mathbf{x}_e \in [-d_5, d_5]$, $\boldsymbol{\psi}_3$ should look like Figure B.5, where the shaded area is bounded by a line of slope $\frac{1}{2}$.

Now we try to find the matrix **P** in the following LMI problem.

$$\mathbf{P} = \mathbf{P}^T > 0$$

$$\begin{bmatrix} \mathbf{F}_3^T\mathbf{P} + \mathbf{P}\mathbf{F}_2 & \mathbf{P}\mathbf{B}_3 - \mathbf{C}_3^T \\ \mathbf{B}_3^T\mathbf{P} - \mathbf{C}_2 & -\mathbf{D}_3\mathbf{D}_3^T \end{bmatrix} < 0$$

where $\mathbf{B}_3 = -\mathbf{G}_3$, $\mathbf{C}_3 = \mathbf{H}_3 + \mathbf{N}_3\mathbf{H}_3\mathbf{F}_3$, and $\mathbf{D}_3 = \mathbf{K}_3^{-1} + \mathbf{N}_3\mathbf{H}_3\mathbf{G}_3$ with $\mathbf{N}_3 = \alpha_{30} > 0$. and $\mathbf{K}_3 = 0.5$ because the input nonlinearity ψ_3 is bounded by a line of slope 0.5, as shown in Figure B.5. The solution to the LMI above exists as follows: $\alpha_{30} = 0.1$ and

$$\mathbf{P} = \begin{bmatrix} 53.9421 & 1.5880 & -21.91680 & -5.04080 & -0.21710 & -0.1790 & 2.0435 & -137.0435 \\ 1.5880 & 2.3749 & -3.5427 & -5.8888 & 0.12270 & -0.0894 & 8.7120 & -21.09320 \\ -21.91680 & -3.5427 & 248.3186 & 63.12010 & -5.1710 & 2.11030 & -205.0734 & -198.5732 \\ -5.04080 & -5.8888 & 63.12010 & 140.0008 & -1.24967 & 1.09730 & -63.12010 & 11.5833 \\ -0.21710 & 0.12270 & -5.1710 & -1.2496 & 0.59310 & -0.08560 & 5.1710 & 6.4538 \\ -0.1790 & -0.0894 & 2.11030 & 1.09730 & -0.08560 & 0.4085 & -1.3154 & 2.4376 \\ 2.04357 & 8.7120 & -205.0734 & -63.12010 & 5.1710 & -1.3154 & 205.0734 & 171.5462 \\ -137.04357 & -21.09320 & -198.5732 & 11.5833 & 6.4538 & 2.4376 & 171.5462 & 1025.2847 \end{bmatrix}$$

Therefore, we may say that the linear affine system of combination index 3 is globally absolutely stable towards its stable equilibrium, implying that no LCO can exist in this switching combination.

B.4 Configuration Four

Switching configuration four is identical to configuration six, because the linear slope boundary for g_1 and g_2 is the same as in configuration six, i.e.,

$$\mathbf{K}_4 = \begin{bmatrix} k_{41} & 0 \\ 0 & k_{42} \end{bmatrix}$$

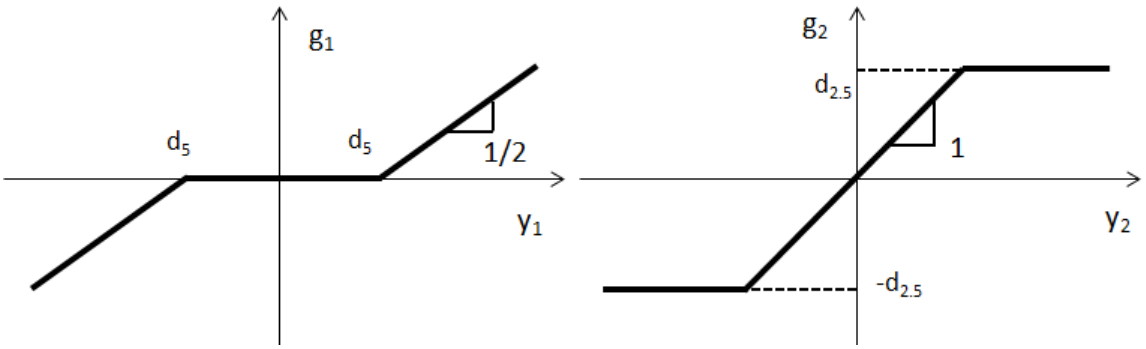

Figure B.6: Switching configuration four: (a)(left)The first PN g_1 versus the input y_1. (b)(right)The second PN g_2 versus the input y_2.

where $k_{41} = 0.5$ and $k_{41} = 1$ for both configuration four and six. Therefore, the LMI formulation of KYP lemma is all the same as

$$\mathbf{P} = \mathbf{P}^T > 0$$

$$\begin{bmatrix} \mathbf{F}^T\mathbf{P} + \mathbf{PF} & \mathbf{PB} - \mathbf{C}_4^T \\ \mathbf{B}_4^T\mathbf{P} - \mathbf{C}_4 & -\mathbf{D}_4\mathbf{D}_4^T \end{bmatrix} < 0$$

where $\mathbf{B}_4 = -\mathbf{G}$, $\mathbf{C}_4 = \mathbf{H} + \mathbf{NHF}$, and $\mathbf{D}_4 = \mathbf{K}_4^{-1} + \mathbf{NHG}$ with $\mathbf{N} = \begin{bmatrix} \alpha_{41} & 0 \\ 0 & \alpha_{42} \end{bmatrix}$, $\alpha_{41} > 0$, $\alpha_{42} > 0$, and with **F**, **G**, and **H** all in Equation 5.2. We are coming back to the absolute stability of this system in configuration six.

B.5 Configuration Five

Equation of motion for this linear affine system is

$$\dot{\mathbf{x}}(t) = \mathbf{F}_5\mathbf{x}(t) + \mathbf{G}_5\boldsymbol{\phi}_5(\mathbf{H}_5\mathbf{x}(t))$$

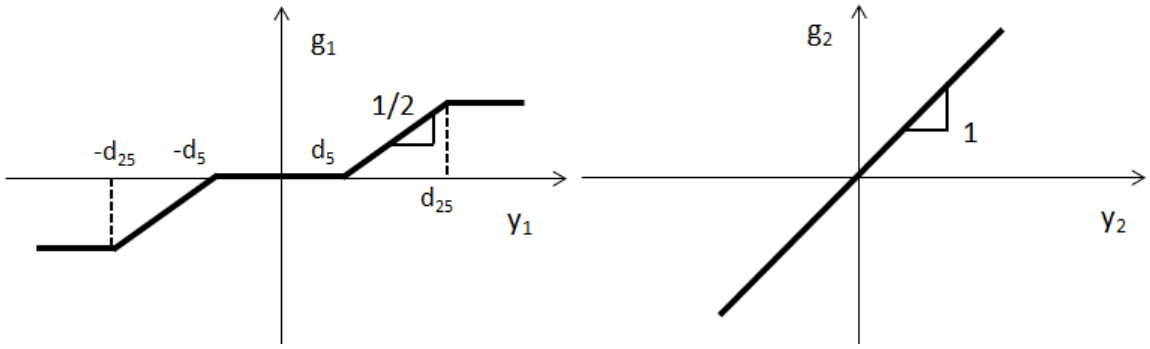

Figure B.7: Switching configuration five: (a)(left)The first PN g_1 versus the input y_1. (b)(right)The second PN g_2 versus the input y_2.

where

$$\mathbf{F}_5 = \begin{bmatrix} -0.9 & 1.0 & 0 & 0 & 0 & 0.2 & 0 & 0 \\ -3.46 & -0.6 & 0 & 0 & 0 & k_6 & 0 & 0 \\ 0 & 1.0 & 0 & 0 & 0 & 0 & 0 & 0 \\ 0 & 0 & 0 & 0 & 1.0 & 0 & 0 & 0 \\ 0 & 0 & 0 & -246 & -1.57 & 5.17 & 0 & 0 \\ 0 & -\frac{51}{4} & 0 & 0 & 0 & -34 & 0 & -136 \\ 0 & 0 & \frac{1}{\tau_p} & \frac{1}{\tau_p} & 0 & 0 & -\frac{1}{\tau_p} & 0 \\ 0 & 0.375 & 0 & 0 & 0 & 0 & 0 & -4.0 \end{bmatrix},$$

$$\mathbf{G}_5 = \begin{bmatrix} 0 & 0 & 0 & 0 & 0 & 25.16 & 0 & 0 \end{bmatrix}^T, \qquad \mathbf{H}_5 = \begin{bmatrix} 0 & 0 & 0 & 0 & 0 & 0 & -k_p & 0 \end{bmatrix}$$

$$\boldsymbol{\phi}(\mathbf{H}_5\mathbf{x}) = g_1(-k_p\mathbf{x}(7))$$

where g_1 and its derivative h_1 are in Equation 5.5. To find the equilibrium, we solve the following algebraic equation

$$\mathbf{F}_5\mathbf{x}_e + \mathbf{G}_5\boldsymbol{\phi}(\mathbf{H}_5\mathbf{x}_e) = 0$$

Firstly we assume that $\mathbf{x}_e \in \mathbb{N}(\mathbf{F}_5)$. Then, $\mathbf{x}_e = k[0\ 0\ 1\ 0\ 0\ 0\ 1\ 0]$ with $k \in \mathbb{R}$ and

$\mathbf{G}_5\boldsymbol{\phi}(\mathbf{H}_5\mathbf{x}_e) = 0$. Since $\mathbf{G}_5\boldsymbol{\phi}(\mathbf{H}_5\mathbf{x}_e) = g_1(-k_p\mathbf{x}_{e7}) = 0$ when $-k_p\mathbf{x}_{e7} \in [-d_5, d_5]$, the k should be $k \in [-\frac{d_5}{k_p}, \frac{d_5}{k_p}] = [-0.25, 0.25]$. Now assume $\mathbf{x}_e \notin \mathbb{N}(\mathbf{F}_5)$. Then

$$\begin{aligned}
-0.9\mathbf{x}_{e1} + \mathbf{x}_{e2} + 0.2\mathbf{x}_{e6} &= 0 \\
-3.46\mathbf{x}_{e1} - 0.6\mathbf{x}_{e2} + k_6\mathbf{x}_{e6} &= 0 \\
\mathbf{x}_{e2} = 0,\ \mathbf{x}_{e5} &= 0 \\
-246\mathbf{x}_{e4} - 1.57\mathbf{x}_{e5} + 5.17\mathbf{x}_{e6} &= 0 \\
-\frac{51}{4}\mathbf{x}_{e2} - 34\mathbf{x}_{e6} - 136\mathbf{x}_{e8} + 25.16g_1(-k_p\mathbf{x}_{e7}) &= 0 \\
\mathbf{x}_{e3} + \mathbf{x}_{e4} - \mathbf{x}_{e7} &= 0 \\
\frac{3}{8}\mathbf{x}_{e2} - 4\mathbf{x}_{e8} &= 0
\end{aligned}$$

Then it follows that $\mathbf{x}_e = k[0\ 0\ 1\ 0\ 0\ 0\ 1\ 0]$ with $k \in [-0.25, 0.25]$, which is a contradiction. Therefore, the equilibrium set is

$$\mathbf{x}_e = k[0\ 0\ 1\ 0\ 0\ 0\ 1\ 0] \text{ with } k \in [-0.25, 0.25]$$

We now check the stability of this equilibrium. The Jacobian matrix around this equilibrium is

$$\mathbf{J}(\mathbf{x}_e) = \begin{bmatrix}
-0.9 & 1.0 & 0 & 0 & 0 & 0.2 & 0 & 0 \\
-3.46 & -0.6 & 0 & 0 & 0 & k_6 & 0 & 0 \\
0 & 1.0 & 0 & 0 & 0 & 0 & 0 & 0 \\
0 & 0 & 0 & 0 & 1.0 & 0 & 0 & 0 \\
0 & 0 & 0 & -246 & -1.57 & 5.17 & 0 & 0 \\
0 & -\frac{51}{4} & 0 & 0 & 0 & -34 & -25.16k_p h_1(y_1(\mathbf{x}_e)) & -136 \\
0 & 0 & 1/\tau_p & 1/\tau_p & 0 & 0 & -1/\tau_p & 0 \\
0 & 0.375 & 0 & 0 & 0 & 0 & 0 & -4.0
\end{bmatrix}$$

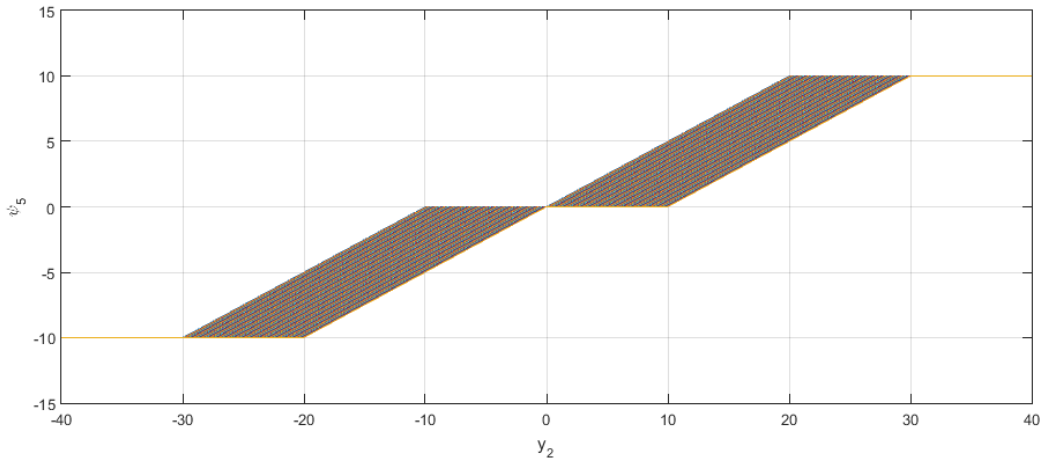

Figure B.8: Input nonlinearity $\boldsymbol{\psi}_5$ of the system of configuration five. Shaded area stands for the possible occupancy of $\boldsymbol{\psi}_5$. Note that the whole area is bounded within a line of slope $\frac{1}{2}$ and x axis.

Since $y_1(\mathbf{x}_e) = -k_p \mathbf{x}_e(7) = 0$, $\mathbf{J}(\mathbf{x}_e) = \mathbf{F}_5$ and its eigenvalues are -10, 0, -31.907 -0.785$\pm$15.665i, -3.079$\pm$3.590i, -1.434. Therefore, the equilibrium is stable with only one mode marginally stable. Since we have nonzero equilibrium $\mathbf{x}_e$, we need to check the absolute stability of the following system with zero equilibrium, because proving the absolute stability based on PR and KYP lemma implies the absolute stability towards zero equilibrium.

$$\frac{d}{dt}(\mathbf{x} - \mathbf{x}_e) = \mathbf{F}_5(\mathbf{x} - \mathbf{x}_e) + \mathbf{G}_5(\boldsymbol{\phi}_5(\mathbf{H}_5(\mathbf{x} - \mathbf{x}_e)))$$

or, equivalently

$$\dot{\mathbf{x}} = \mathbf{F}_5\mathbf{x} + \mathbf{G}_5(\boldsymbol{\phi}_5(\mathbf{H}_5\mathbf{x} - \mathbf{H}_5\mathbf{x}_e) + \boldsymbol{\phi}_5(\mathbf{H}_5\mathbf{x}_e))$$

Define $\boldsymbol{\psi}_5(\mathbf{H}_5\mathbf{x}) \equiv \boldsymbol{\phi}_5(\mathbf{H}_5\mathbf{x} - \mathbf{H}_5\mathbf{x}_e) + \boldsymbol{\phi}_5(\mathbf{H}_5\mathbf{x}_e)$ then $\boldsymbol{\psi}_5(\mathbf{H}_5\mathbf{x}) = \boldsymbol{\phi}_5(\mathbf{H}_5\mathbf{x} - \mathbf{H}_5\mathbf{x}_e)$ because $\boldsymbol{\phi}_5(\mathbf{H}_5\mathbf{x}_e) = 0$. Then, since $\mathbf{H}_5\mathbf{x}_e \in [-d_5, d_5]$, $\boldsymbol{\psi}_5$ should look like Figure B.8, where the shaded area is bounded by a line of slope $\frac{1}{2}$.

Now we try to find the matrix $\mathbf{P}$ in the following LMI problem. Since $\mathbf{F}_5 = \mathbf{F}_3$, $\mathbf{B}_5 = \mathbf{B}_3$, $\mathbf{C}_5 = \mathbf{C}_3$, and $\mathbf{D}_5 = \mathbf{D}_3$ the LMI problem is identical to one for configuration three. Furthermore, $\mathbf{K}_5 = \mathbf{K}_3$ because the input nonlinearity $\boldsymbol{\psi}_5$ is bounded by a line of slope 0.5 as shown in Figure B.8, just like $\boldsymbol{\psi}_3$. Therefore, we have the same solution $\mathbf{P}$ for the LMI

problem and again, no LCO can exist in this switching combination.

B.6 Configuration Six

This configuration is identical to the original YF-12 flight control system. It is difficult to find the feasible solution to the LMI problem

$$\begin{aligned} \mathbf{P} = \mathbf{P}^T > 0 \\ \begin{bmatrix} \mathbf{F}^T\mathbf{P} + \mathbf{PF} & \mathbf{PB} - \mathbf{C}^T \\ \mathbf{B}^T\mathbf{P} - \mathbf{C} & -\mathbf{D}_4\mathbf{D}^T \end{bmatrix} < 0 \end{aligned} \tag{B.1}$$

where $\mathbf{B} = -\mathbf{G}$, $\mathbf{C} = \mathbf{H} + \mathbf{NHF}$, and $\mathbf{D} = \mathbf{K}^{-1} + \mathbf{NHG}$ with $\mathbf{N} = \begin{bmatrix} \alpha_1 & 0 \\ 0 & \alpha_2 \end{bmatrix}$, $\alpha_1 > 0$, $\alpha_2 > 0$, $\mathbf{K} = \begin{bmatrix} k_1 & 0 \\ 0 & k_2 \end{bmatrix}$, $k_1 = 0.5$, $k_2 = 1$, and with **F**, **G**, and **H** all in Equation 5.2. Therefore we turn to check one of the necessary conditions for PR of the transfer function $\mathbf{M}(s)$.

$$\mathbf{M}(s) = \left[(1 + \mathbf{N}s)\mathbf{H}(s\mathbf{I} - \mathbf{F})^{-1}(-\mathbf{G})\right] + \mathbf{K}^{-1}$$

The necessary condition of the PR is checked if the Nyquist plot of the transfer function above is entirely in the right half complex plane. To this end we evaluate the $\mathbf{M}(s)$ in the frequency domain, i.e. $\mathbf{M}(i\omega)$ to see if for some $\alpha_1 > 0$ and $\alpha_2 > 0$ all the entries of the transfer function matrix $\mathbf{M}(i\omega)$ always stay in the right half complex plane. In other words, if we prove that for all $\alpha_1 > 0$ or $\alpha_2 > 0$ the transfer function $\mathbf{M}(i\omega)$ always has at least part of its Nyquist plot in the left half complex plane, then $\mathbf{M}(i\omega)$ is not PR. $\mathbf{M}(i\omega)$ in s-domain is as follows

$$\begin{aligned} \mathbf{M}(1,1)(s) &= \frac{N_{11}(s)}{D_{11}(s)}, & \mathbf{M}(1,2)(s) &= \frac{N_{12}(s)}{D_{12}(s)} \\ \mathbf{M}(2,1)(s) &= \frac{N_{21}(s)}{D_{21}(s)}, & \mathbf{M}(2,2)(s) &= \frac{N_{22}(s)}{D_{22}(s)} \end{aligned}$$

where $\mathbf{M}(i,j)(s)$ is the ith row and jth column entry of $\mathbf{M}(s)$ and $N_{ij}(s)$, $D_{ij}(s)$ are corresponding nominator and denominator, respectively. Then

$$
\begin{aligned}
N_{11}(s) &= 10^4\big(5.619\alpha_1 s^4 + (5.619 + 11.05\alpha_1)s^3 + (11.05 + 756.5\alpha_1)s^2 \\
&\quad + (756.5 + 582.5\alpha_1)s + 582.5\big) \\
D_{11}(s) &= s^7 + 47.07s^6 + 727.4s^5 + 1.252e4s^4 + 1.033e5s^3 + 1.709e5s^2 + 3.346e5s \\
N_{12}(s) &= 10^4\big(7.594\alpha_1 s^4 + (7.594 + 14.88\alpha_1)s^3 + (14.88 + 1022\alpha_1)s^2 \\
&\quad + (1022 + 787.1\alpha_1)s + 787.1\big) \\
D_{12}(s) &= D_{11}(s) \\
N_{21}(s) &= -\big(56.58\alpha_2 s^3 + (56.58 + 497.1\alpha_2)s^2 + (671.7 + 480\alpha_2)s + 480\big) \\
D_{21}(s) &= s^4 + 3905s^3 + 197s^2 + 356s + 544 \\
N_{22}(s) &= 76.42\alpha_2 s^3 + (76.42 + 671.7\alpha_2)s^2 + (671.7 + 480\alpha_2)s + 480 \\
D_{22}(s) &= D_{21}
\end{aligned}
$$

We want to confirm if the real part of at least one of $\mathbf{M}(i,j)(i\omega)$ always has negative real value for some ω. To this end we take $\mathbf{M}(2,1)(i\omega)$.

$$
\begin{aligned}
&\text{sign}\big[\text{Re}\big(\mathbf{M}(2,1)(i\omega)\big)\big] \\
&= \text{sign}\Big[\big((56.58 + 497.1\alpha_2)\omega^2 - 355.2\big)\big(\omega^4 - 197\omega^2 + 544\big) \\
&+ \big(56.58\alpha_2\omega^3 - (497.1 + 355.2\alpha_2)\omega\big)\big(-39.5\omega^3 + 356\omega\big)\Big] \\
&= 56.58\omega^6 + 8133.99\omega^4 - 76213.7\omega^2 - (1737.81\omega^6 + 63755.8\omega^4 - 143971\omega^2)\alpha_2 - 193229
\end{aligned}
$$

For $\text{sign}\big[\text{Re}\big(\mathbf{M}(2,1)(i\omega)\big)\big]$ to have negative real value for any positive real α_1 and α_2, ω needs to satisfy the following.

$$
\begin{aligned}
1737.81\omega^6 + 63755.8\omega^4 - 143971\omega^2 > 0, \\
56.58\omega^6 + 8133.99\omega^4 - 76213.7\omega^2 - 193229 < 0
\end{aligned}
$$

the solution to this problem is $\omega \in [1.4608, 3.2816]$. Therefore, the Lur'e type system corresponding to configuration six is not PR, and not absolutely stable.

APPENDIX C

DF ANALYSIS FOR YF-12 FLIGHT CONTROL SYSTEM

Identifying the LCO parameters with DF analysis is simple in concept but complicated in calculation. With three equations in Equation 5.7, 5.8, and 5.10, we can theoretically solve for the three unknowns A_1, A_2, and ω. However, solving those equations in closed form is difficult because each DF for $g_1(N_1)$ and $g_2(N_2)$ is a nonlinear function of A_1 and A_2, respectively. Therefore we turn to expressing N_1 and N_2 with ω along with A_1 and A_2 respectively and see if there is any intersection between the DF expressed in ω and the DF expressed in A_1 or A_2 for possible range of those three unknowns. Firstly we express DFs in ω. From the real part and the imaginary parts of Equation 5.10, respectively, we obtain

$$
\begin{aligned}
N_1 = (&0.0183607\omega^2(-4.94536e6 + 2.25722e6\omega^2 - 9.89072e6\tau_p^2\omega^2 + 42498.5\omega^4 \\
&- 4.06069e(-10)\tau_p\omega^4 + 4.51443e6\tau_p^2\omega^4 - 4.94536e6\tau_p^4\omega^4 - 452.897\omega^6 + 84997\tau_p^2\omega^6 \\
&- 4.06069e(-10)\tau_p^3\omega^6 + 2.25722e6\tau_p^4\omega^6 + \omega^8 - 905.793\tau_p^2\omega^8 + 42498.5\tau_p^4\omega^8 + 2\tau_p^2\omega^{10} \\
&- 452.897\tau_p^4\omega^{10} + \tau_p^4\omega^{12}))/(151210k_p + 241771kp\omega^2 + 21549.5k_p\tau_p\omega^2 + 151210k_p\tau_p^2\omega^2 \\
&+ 4606.78k_p\omega^4 + 30308.6k_p\tau_p\omega^4 + 241771k_p\tau_p^2\omega^4 + 21549.5k_p\tau_p^3\omega^4 - 78.7861k_p\omega^6 \\
&- 322.523k_p\tau_p\omega^6 + 4606.78k_p\tau_p^2\omega^6 + 30308.6k_p\tau_p^3\omega^6 + 0.227135k_p\omega^8 + k_p\tau_p\omega^8 \\
&- 78.7861k_p\tau_p^2\omega^8 - 322.523k_p\tau_p^3\omega^8 + 0.227135k_p\tau_p^2\omega^10 + k_p\tau_p^3\omega^10)
\end{aligned}
\tag{C.1}
$$

in addition, for N_2,

$$
\begin{aligned}
N_2 = (0.104223(&-3.38086e8k_p - 4.89489e8k_p\tau_p - 9.96524e7k_p\omega^2 - 3.55648e8k_p\tau_p\omega^2 \\
&- 4.22479e8k_p\tau_p^2\omega^2 - 4.89489e8k_p\tau_p^3\omega^2 - 678200k_p\omega^4 + 1.18245e8k_p\tau_p\omega^4 \\
&+ 2.07612e8k_p\tau_p^2\omega^4 - 6.38453e7k_p\tau_p^3\omega^4 - 8.43932e7k_p\tau_p^4\omega^4 + 205991k_p\omega^6 \\
&+ 5.79507e6k_p\tau_p\omega^6 - 1.49516e7k_p\tau_p^2\omega^6 + 2.2799e7k_p\tau_p^3\omega^6 + 3.07265e8k_p\tau_p^4\omega^6 \\
&+ 2.91803e8k_p\tau_p^5\omega^6 - 3360.42k_p\omega^8 - 156248k_p\tau_p\omega^8 - 1.43298e6k_p\tau_p.^2\omega^8 + 481340k_p\tau_p^3\omega^8 \\
&- 1.42734e7k_p\tau_p^4\omega^8 - 9.54464e7k_p\tau_p^5\omega^8 + 17.4402k_p\omega^{10} + 1349.72k_p\tau_p\omega^{10} + 24000.4k_p\tau_p^2\omega^{10} \\
&- 53623.3k_p\tau_p^3\omega^{10} - 1.63897e6k_p\tau_p^4\omega^{10} - 5.31373e6k_p\tau_p^5\omega^{10} - 0.0284879k_p\omega^{12} \\
&- 4.67396k_p\tau_p\omega^{12} - 120.452k_p\tau_p^2\omega^{12} + 781.672k_p\tau_p^3\omega^{12} + 27360.8k_p\tau_p^4\omega^{12} \\
&+ 102625k_p\tau_p^5\omega^{12} + 0.00549428k_p\tau_p\omega^{14} + 0.192864k_p\tau_p^2\omega^{14} - 3.67396k_p\tau_p^3\omega^{14} \\
&- 137.892k_p\tau_p^4\omega^{14} - 568.052k_p\tau_p^5\omega^{14} + 0.00549428k_p\tau_p^3\omega^{16} + 0.221352k_p\tau_p^4\omega^{16} \\
&+ k_p\tau_p^5\omega^{16}))/((209.725 + 303.645\tau_p - \omega^2 - 51.3435\tau_p\omega^2 - 209.725\tau_p^2\omega^2 + 0.192864\tau_p\omega^4 \\
&+ \tau_p^2\omega^4)(151210k_p + 241771k_p\omega^2 + 21549.5k_p\tau_p\omega^2 + 151210k_p\tau_p^2\omega^2 + 4606.78k_p\omega^4 \\
&+ 30308.6k_p\tau_p\omega^4 + 241771k_p\tau_p^2\omega^4 + 21549.5k_p\tau_p^3\omega^4 - 78.7861k_p\omega^6 - 322.523k_p\tau_p\omega^6 \\
&+ 4606.78k_p\tau_p^2\omega^6 + 30308.6k_p\tau_p^3\omega^6 + 0.227135k_p\omega^8 + k_p\tau_p\omega^8 - 78.7861k_p\tau_p^2\omega^8 \\
&- 322.523k_p\tau_p^3\omega^8 + 0.227135k_p\tau_p^2\omega^{10} + k_p\tau_p^3\omega^{10}))
\end{aligned}
\tag{C.2}
$$

N_1 and N_2 expressed in A_1 and A_2 appear in Equation 5.8 but we repeat it here for convenience.

$$N_1 = \begin{cases} \frac{1}{\pi}[\sin^{-1}(\frac{d_{25}}{A_1}) + (\frac{d_{25}}{A_1})\sqrt{1-(\frac{d_{25}}{A_1})^2} - \sin^{-1}(\frac{d_5}{A_1}) - (\frac{d_5}{A_1})\sqrt{1-(\frac{d_5}{A_1})^2}], & A_1 > d_{25} \\ \frac{1}{2} - \frac{1}{\pi}[\sin^{-1}(\frac{d_5}{A_1}) + (\frac{d_5}{A_1})\sqrt{1-(\frac{d_5}{A_1})^2}], & d_5 < A_1 \leq d_{25} \\ 0, & A_1 \leq d_5 \end{cases} \tag{C.3}$$

$$N_2 = \begin{cases} \frac{2}{\pi}[\sin^{-1}(\frac{d_{2.5}}{A_2}) + (\frac{d_{2.5}}{A_2})\sqrt{1-(\frac{d_{2.5}}{A_2})^2}], & A_2 > d_{2.5} \\ 1, & A_2 \leq d_{2.5} \end{cases}$$

To incorporate this with Equation C.1 and Equation C.2, we need to express the relationship between A_1 and A_2 in terms of ω, as in the equation below. This equation is embodied in detail from Equation 5.7.

$$\begin{aligned} \left|\frac{A_2}{A_1}\right| = \frac{1}{k_p}[\big((&1.28498e10\omega^2 + 1.55567e10\omega^4 + 1.28498e10\tau_p^2\omega^4 - 6.29725e9\omega^6 \\ &+ 1.55567e10\tau_p^2\omega^6 + 1.20484e9\omega^8 - 6.29725e9\tau_p^2\omega^8 + 1.01647e7\omega^10 + 1.20484e9\tau_p^2\omega^10 \\ &- 139529\omega^{12} + 1.01647e7\tau_p^2\omega^{12} + 324\omega^14 - 139529\tau_p^2\omega^14 + 324\tau_p^2\omega^16)/ \\ &(2.2844e10 + 2.94394e10\omega^2 - 1.03812e10\omega^4 + 1.70265e9\omega^6 + 1.19155e8\omega^8 \\ &- 2.03791e6\omega^{10} + 7985.21\omega^{12})\big)^{\frac{1}{2}}] \end{aligned} \tag{C.4}$$

We may now organize an algorithm to solve for A_1, A_2, and ω. Since A_2 is a function of both A_1 and ω through Equation C.3 and Equation C.4, let $N_{2,A\omega} = N_2(A_1, \omega)$ from Equation C.3 and Equation C.4 and let $N_{2,\omega} = N_2(\omega)$ from Equation C.2. Then, for every possible pair of A_1 and ω, we firstly find N_2 through $N_{2,A\omega} = N_{2,\omega}$. When such N_2 is found, then N_1 is automatically calculated by Equation C.1 with corresponding ω found in the procedure in which to find $N_{2,A\omega} = N_{2,\omega}$. The detailed algorithm is as follows.

Algorithm 1. Solving for N_1 and N_2

Initialize:

Choose appropriate range of A_1 and ω

Initialize the candidate index $i = 1$

for$_1$ the range of A_1, **do**

for$_2$ the range of ω, **do**

if$_1$ $N_{1,A} = N_{1,\omega}$

if$_2$ $N_{2,A\omega} = N_{2,\omega}$

Record Solution(i) = ($N_{1,A}$,$N_{2,\omega}$)

$i = i + 1$

end if$_2$

end if$_1$

end for$_2$

end for$_1$

REFERENCES

[1] J. H. Wall, J. S. Orr, and T. S. VanZwieten, "Space launch system implementation of adaptive augmenting control," 2014.

[2] Z. T. Dydek, A. M. Annaswamy, and E. Lavretsky, "Adaptive control and the nasa x-15-3 flight revisited," *IEEE Control Systems Magazine*, vol. 30, no. 3, pp. 32–48, 2010.

[3] J. S. Orr and C. J. Dennehy, "Analysis of the x-15 flight 3-65-97 divergent limit-cycle oscillation," *Journal of Aircraft*, pp. 135–148, 2016.

[4] A. J. Van Der Schaft and J. M. Schumacher, *An introduction to hybrid dynamical systems*. Springer London, 2000, vol. 251.

[5] W. E. Vander Velde, *Multiple-input describing functions and nonlinear system design*. McGraw-Hill, New York, 1968.

[6] J. M. Gonçalves, A. Megretski, and M. A. Dahleh, "Global analysis of piecewise linear systems using impact maps and surface lyapunov functions," *IEEE Transactions on Automatic Control*, vol. 48, no. 12, pp. 2089–2106, 2003.

[7] A. Beléndez, E Gimeno, T Beléndez, and A Hernández, "Rational harmonic balance based method for conservative nonlinear oscillators: Application to the duffing equation," *Mechanics Research Communications*, vol. 36, no. 6, pp. 728–734, 2009.

[8] J.-H. He, "Preliminary report on the energy balance for nonlinear oscillations," *Mechanics Research Communications*, vol. 29, no. 2, pp. 107–111, 2002.

[9] V. Pillai and H. Nelson, "A new algorithm for limit cycle analysis of nonlinear control systems," *ASME, Transactions, Journal of Dynamic Systems, Measurement, and Control*, vol. 110, pp. 272–277, 1988.

[10] D. H. Klyde, D. T. McRuer, and T. T. Myers, "Pilot-induced oscillation analysis and prediction with actuator rate limiting," *Journal of Guidance, Control, and Dynamics*, vol. 20, no. 1, pp. 81–89, 1997.

[11] D. Klyde, D. McRuer, and T. Myers, "Pio analysis with actuator rate limiting," in *21st Atmospheric Flight Mechanics Conference*, 1996, p. 3432.

[12] M. R. Anderson, "Pilot-induced oscillations involving multiple nonlinearities," *Journal of guidance, Control, and dynamics*, vol. 21, no. 5, pp. 786–791, 1998.

[13] G. Somieski, "An eigenvalue method for calculation of stability and limit cycles in nonlinear systems," *Nonlinear dynamics*, vol. 26, no. 1, pp. 3–22, 2001.

[14] J. M.M. S. Gonçalves, "Constructive global analysis of hybrid systems," PhD thesis, Massachusetts Institute of Technology, 2000.

[15] J. D. García-Saldaña and A. Gasull, "A theoretical basis for the harmonic balance method," *Journal of Differential Equations*, vol. 254, no. 1, pp. 67–80, 2013.

[16] S. Durmaz and M. O. Kaya, "High-order energy balance method to nonlinear oscillators," *Journal of Applied Mathematics*, vol. 2012, 2012.

[17] R. Seydel, *Practical bifurcation and stability analysis*. Springer Science & Business Media, 2009, vol. 5.

[18] F. S. Dias, L. F. Mello, *et al.*, "Hopf bifurcations and small amplitude limit cycles in rucklidge systems," *Electronic Journal of Differential Equations*, vol. 2013, no. 48, pp. 1–9, 2013.

[19] P. P. Friedmann, "Numerical methods for determining the stability and response of periodic systems with applications to helicopter rotor dynamics and aeroelasticity," *Computers & mathematics with applications*, vol. 12, no. 1, pp. 131–148, 1986.

[20] V.-M. Popov, "Absolute stability of nonlinear systems of automatic control," *Automation and Remote Control*, vol. 22, no. 8, pp. 857–875, 1962.

[21] B. Brogliato, R. Lozano, B. Maschke, and O. Egeland, "Dissipative systems analysis and control," *Theory and Applications*, vol. 2, 2007.

[22] G. Floquet, "Sur les équations différentielles linéaires à coefficients périodiques," in *Annales scientifiques de l'École normale supérieure*, vol. 12, 1883, pp. 47–88.

[23] P. J. A. Montagnier-Michau, "Dynamics and control of time-periodic mechanical systems via floquet-lyapunov theory.," 2004.

[24] P. Hartman, *Ordinary differential equations*, 2002.

[25] H. K. Khalil and J. Grizzle, *Nonlinear systems*. Prentice hall Upper Saddle River, NJ, 2002, vol. 3.

[26] L. T. Gruyitch, J.-P. Richard, P. Borne, and J.-C. Gentina, *Stability domains*. CRC Press, 2003.

[27] G. Chen, "Stability of nonlinear systems," *Wiley Encyclopedia of Electrical and Electronics Engineering*, 2001.

[28] R. Wang, "Algebraic criteria for absolute stability," *Systems & Control Letters*, vol. 47, no. 5, pp. 401–416, 2002.

[29] W. M. Haddad and D. S. Bernstein, "Explicit construction of quadratic lyapunov functions for the small gain, positivity, circle, and popov theorems and their application to robust stability. part i: Continuous-time theory," *International Journal of Robust and Nonlinear Control*, vol. 3, no. 4, pp. 313–339, 1993.

[30] M. K.-J. Johansson, *Piecewise linear control systems: a computational approach*. Springer, 2003, vol. 284.

[31] C. Heil, *Introduction to real analysis*, 2018.

[32] E. Süli and D. F. Mayers, *An introduction to numerical analysis*. Cambridge university press, 2003.

[33] C. Gear and I. G. Kevrekidis, "Computing in the past with forward integration," *Physics Letters A*, vol. 321, no. 5-6, pp. 335–343, 2004.

[34] C. W. Gear and I. G. Kevrekidis, "Projective methods for stiff differential equations: Problems with gaps in their eigenvalue spectrum," *SIAM Journal on Scientific Computing*, vol. 24, no. 4, pp. 1091–1106, 2003.

[35] J. Guckenheimer and P. J. Holmes, *Nonlinear oscillations, dynamical systems, and bifurcations of vector fields*. Springer Science & Business Media, 2013, vol. 42.

[36] Y. E. Yoon and E. N. Johnson, "Determination of limit cycle oscillation frequency in linear systems with relay feedback," in *2018 AIAA Guidance, Navigation, and Control Conference*, 2018, p. 0607.

[37] *National museum of the usaf*, `https://www.nationalmuseum.af.mil/Visit/Museum-Exhibits/Fact-Sheets/Display/Article/195777/lockheed-yf-12a/`, Accessed: 2019-03-05.

[38] S. Boyd, L. El Ghaoui, E. Feron, and V. Balakrishnan, *Linear matrix inequalities in system and control theory*. Siam, 1994, vol. 15.

[39] G. Guglieri and F. Quagliotti, "Analytical and experimental analysis of wing rock," *Nonlinear Dynamics*, vol. 24, no. 2, pp. 129–146, 2001.

[40] B. S. Liebst, "The dynamics, prediction, and control of wing rock in high–performance aircraft," *Philosophical Transactions of the Royal Society of London. Series A: Mathematical, Physical and Engineering Sciences*, vol. 356, no. 1745, pp. 2257–2276, 1998.